*ESCUELA SUPERIOR DE INGENIEROS*

UNIVERSIDAD DE SEVILLA

Departamento de Matemática Aplicada II

PROYECTO FIN DE CARRERA:

# Dynamic analysis of an automatic dynamic balancing mechanism for eccentric rotors

Realizado por:

Alberto Mendoza Muñoz

para la obtención del título de Ingeniero Industrial intensificación Mecánica–Máquinas

Director del proyecto:

Jorge Galán Vioque

Sevilla, Julio 2005

ACKNOWLEDGEMENTS
This project could not have been completed without the support and assistance of numerous people. Particularly, I would like to thank the following:

Drs Alan R. Champneys, of the University of Bristol, and Jorge Galán Vioque, of the University of Sevilla, for their support, assistance, and advice, as my supervisors over this year;

Kirk Green for his help and generosity entitling me to use some of his work;

Victor Blanco and Sebastian Carlsson for their patient during the performance of the project;

and finally my family and friends for their support.

# Contents

# List of Figures

# Chapter 1

# Introduction

## 1.1 Automatic Dynamic Balancers (ADB)

There exist several machines which are based on rotor systems, such as helicopters, jet engines, milling machines, washing machines, drills, etc. Unbalance in rotating machinery causes vibrations and generates undesirable forces. These forces are transmitted to the machine parts and may cause damage to the whole system. Generally, this unbalance is a result of unavoidable imperfections in rotor manufacture and assembly. Therefore, the balancing of rotors is clearly important and is accepted as a fundamental requirement for the normal operation of modern low and high speed rotating machines.

If the system has a fixed imbalance it is easy to balance using additional static masses. However, in a number of cases, the position of the imbalance may be free to vary in time. Therefore, it is hard to predict, a priori, where and when the imbalance will occur. This observation motivates the use of self-compensating, automatic dynamic balancers (ADB), that is, passively controlled balancing devices that require no external forces to achieve the balance.

The use of ADBs has been shown to be advantageous in a number of physical applications; for example, the balancing of optical disc drives to obtain higher operating speeds without a drop in the tracking performance [5, 13, 16, 25], and the balance of machine tools, such as, lathes, angle grinders and cutting tools [20]. By preventing vibrations and subsequently stress, the use of an ADB may lengthen the life-time of operation of such devices. In particular, using an ADB for the decrease of vibration in machine tools is of great economical value, as a balanced machine can be operated for more sustained periods of time by a single worker, without the threat of health problems such as 'Hand-arm vibration syndrome' (HAVS) [12].

## 1.2 History of ADB

An early ADB was proposed by the William Seller and Co. of Philadelphia, in 1904. This company conducted a series of tests upon an experimental steam turbine incorporating an ADB that were described by Olsen in comments on a paper by Thearle (1932) [24]. The balancer that was proposed consisted of three thin eccentric disks mounted on the shaft

with the main turbine disk. The disks were a close fit on the shaft, so there would be friction between the eccentric disks and the shaft and between the disks. As the system attained its operating speed, the eccentric disks were gradually shifted until they reached a position that brought the main disk and themselves into balance.

Between the time of this early investigation and the present, several patents were granted for various types of ADB devices that were intended for a wide range of applications. A list of U.S. patents is included in the study by Lee and Van Moorhen [18]. Both the apparatus and method for dynamically balancing such inventions are extremely similar. The key idea of an ADB is to deploy two or more masses that are free to travel around a race, filled with a viscous fluid, at a fixed distance from the centre of rotation of the rotor; see Fig.1.1. This simple arrangement motivated the theoretical studies by Sharp [21], Bövik and Högfors [3], and Majewski [19]. Another common feature of these devices is the almost complete lack of detailed theoretical and experimental investigations into their operation, until recently.

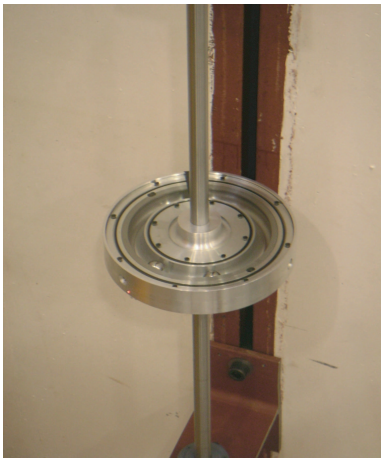

Figure 1.1: Picture of an ADB mechanism with two balls used in an experimental test.

Thearle (1932) [24] and Den Hartog (1956) [11] discussed why such devices would not work if a fluid was used in place of the solid weights. Alexander (1964) [2] presented the results of a theoretical analysis of an ADB concept. The configuration consisted of $n$ series of counterweights in the form of spherical bearing mounted in races that were located in a long slender dynamically unbalanced spinning body. In his simulations, the system was initially at rest and was brought to its final spin rate by the application of a torque. The lateral forces due to dynamic unbalance increase until the final spin rate is reached, and then it decayed due to the action of the counterweights. However, it was not stated how the counterweights move and how the motion is related to that of the long slender body. Cade (1965) [4] suggested the requirements for operation of a ADB, but the source of these suggestions is not clear.

## 1.3 Previous modelling work

The equations of motion of the balls in an ADB were derived using Lagrange's method [7, 18]. In particular, Chung and Ro [7] carried out a linear stability analysis using perturbation methods and identified stability regions of the full nonlinear problem using a scatter-gun approach. Adolfsson [1] applied a similar linear stability analysis and identified regions of stable, balanced operation by considering the largest real eigenvalue. Numerical simulation has also been employed to verify the stability of the ADB. However, due to the highly nonlinear nature of the problem, these studies have shown that the ADB mechanism may make things catastrophically worse at some parameter values [7] and, therefore, there has only been a limited, successful commercial application of the ADB mechanism [23]. Moreover, a linear stability analysis is an inadequate tool for understanding such nonlinear behaviour. Finally, we note that some experimental studies have been carried out to verify the validity of the mathematical models; see Refs.[13, 18]. Very recently, the first detailed nonlinear bifurcation analysis of the dynamics of the ADB with two balls using numerical continuation tools was presented in Green [9]. This study highlighted the importance of transient effects, which were further studied in [10].

## 1.4 Aims of the project

The purpose of this project is to compare and contrast the dynamic stability and behaviour of the automatic dynamic balancing mechanism (ADB) with two, three, and four correction masses. We undertake a bifurcation and a transient analysis of these systems, using the equations of motion which model the mechanism. Through these results, we provide the design requirements for the ADBs to achieve balance of the system, and study the effects of the damping and initial positions of the balls on the transient response. Thus, we find optimal initial positions from which the balls should be launched to make sure that balance is attained, and that transient vibrations are as small as possible.

Using the obtained results from each case (two, three, and four balls), we make comparison between them. Thus, since other studies have been already performed for the ADB with two balls, the main aim of this project is to notice any similarities between the three cases, and to highlight any improvements or detrimental effects for the ADB with three and four balls compared with the behaviour of the system with two balls.

A side result of our project is to test `MATCONT`, the continuation package built on `Matlab`, with which the bifurcation analysis has been carried out. In [9] a detailed bifurcation analysis was performed for the ADB with two balls by using `AUTO`. Hence, we can compare our results in the case of two balls with those in [9], to be sure of the computation executed by `MATCONT`. Therefore, we show that `MATCONT` gives good results, and we assert that it could be used for bifurcation analysis in other projects.

## 1.5 Outline

The project is organised as follows. In Chapter 2 we derive the equations of motion for the ADB with a generic number of balls $n$. Specifically, in Section 2.1 we formulate a Lagrangian description of the system; we then derive a dimensionless form in Section 2.2. In Section

2.3 the equations of motion are rewritten in a rotating frame of reference to produce a time-independent, autonomous form. In Chapter 3 steady state solutions are found and various conditions governing their existence are identified. Continuation techniques are employed in Chapter 4 to perform a bifurcation analysis of the ADB with two balls (Section 4.1), three balls (Section 4.2), and four balls (Section 4.3). Thus, we investigate what effect varying physical parameters in the system has on the stability of the steady state solutions, while we highlight the differences between each system. A transient analysis is carried out in Chapter 5, in which we investigate the transient dynamics of solutions using numerical simulation. In Section 5.1 we analyse the sensitivity of the response of the system to the initial conditions. Thus, first we show some numerical results for different initial positions and velocities of the centre of rotation in Subsection 5.1.1. In Subsection 5.1.2 we study the bevahiour of the system for different initial position of the balls, and we try to find out the optimal position from which the balls should be launched to obtain the best transient responses. Finally in Subsection 5.1.3, we discuss the effect of balls starting initially stationary within an external fixed frame. In Section 5.2 the effects of the parameter set are studied. Firstly, in Subsection 5.2.1 we compare numerical simulations results with the bifurcation diagrams obtained in Chapter 4; in Subsection 5.2.2 we study how the damping affects the behaviour of the systems, and in Subsection 5.2.3 several results are shown for a range of velocity and eccentricity of the rotor values. Finally, in Chapter 6 we draw conclusions and discuss future work. Here all the similarities and differences between the three studied cases (ADB with two, three, and four balls) found in the bifurcation and transient analyses, are enumerated. We also give some recommendations for practical applications of the ADB mechanism.

# Chapter 2

# Equations of motion

Our object of study is an eccentric rotating disc together with an automatic dynamic balancing mechanism (ADB) consisting of two or more balls free to move in a race filled with a viscous fluid and positioned at a fixed distance from the centre of rotation of the disc. This set-up is shown schematically in Figure 2.1. The point $W$ represents the centre of mass of the disc (without the balancing balls) and is located a distance $\epsilon$ from the centre of rotation, point $C$. Note that this model assumes that the disc is attached to a non-flexible shaft through the point $C$. For the study of an eccentric rotor with a flexible shaft see, for example, Ref. [6].

In the following section we will derive the equations of motion of an ADB using Lagrange's method, where we make the assumption that all motion is confined to the two-dimensional $(X, Y)$-plane. We also assume that there are no interactions between the balls. This assumption is valid provided the balls are in an equilibrium state. Note that neglecting impacts between the balls can be considered as a model of a multiple ball races mounted at different axial positions, with each ball moving in its own race [14]. The following analysis holds for either single or multiple race models, provided each race is assumed to be at the same radial distance from the rotor spindle. Our analysis initially follows a Lagrangian description first considered in Ref.[18]. In addition, we develop a dimensionless model in a rotating frame; see, for example, Ref.[1].

## 2.1 Lagrangian description

The equations of motion describing an ADB with $n$ balls can be derived from Lagrange's equation

$$\frac{d}{dt}\left(\frac{\partial T}{\partial \dot{q}_k} - \frac{\partial V}{\partial \dot{q}_k}\right) - \frac{\partial T}{\partial q_k} + \frac{\partial V}{\partial q_k} = Q_k, \tag{2.1}$$

with $k = 1, \ldots, 3 + n$, where $T$ is the kinetic energy, $V$ is the potential energy, $q_k$ are the generalised coordinates and $Q_k$ are the generalised forces acting on the system. Assuming the disc is constrained to move in the $(X, Y)$-plane, the generalised coordinates are given as

$$\mathbf{q} = (X, Y, \psi, \phi_i), \tag{2.2}$$

where $X$ and $Y$ define the position of the centre of rotation $C$ within an external fixed frame, $\psi$ describes the angular motion of the rotating disc, and $\phi_i$ (with $i = 1, \ldots, n$) rep-

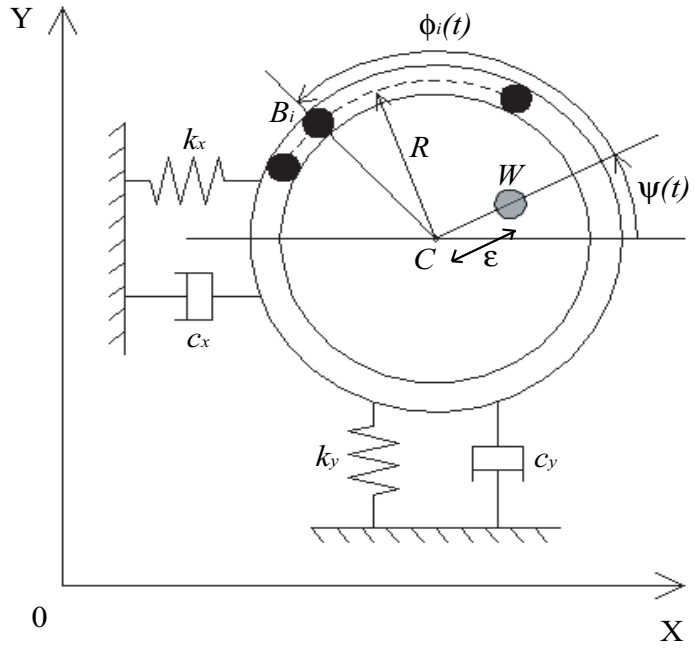


Figure 2.1: Schematic diagram of an automatic dynamic balancer, see text for definitions of the variables.

resents the angular position with respect the centre of mass $W$ of the $i$th ball.

The position vector of the centre of mass $W$ of the disc is

$$\mathbf{r}_{OG} = (X + \epsilon\cos\psi)\mathbf{i} + (Y + \epsilon\sin\psi)\mathbf{j}, \tag{2.3}$$

and the position vector of the $i$th ball is

$$\mathbf{r}_{OB_i} = (X + R\cos(\psi + \phi_i))\mathbf{i} + (Y + R\sin(\psi + \phi_i))\mathbf{j}. \tag{2.4}$$

Moreover, the respective velocities are given as

$$\dot{\mathbf{r}}_{OG} = (\dot{X} - \epsilon\dot{\psi}\sin\psi)\mathbf{i} + (\dot{Y} + \epsilon\dot{\psi}\cos\psi)\mathbf{j}, \tag{2.5}$$

$$\dot{\mathbf{r}}_{OB_i} = (\dot{X} - R(\dot{\psi} + \dot{\phi}_i)\sin(\psi + \phi_i))\mathbf{i} + (\dot{Y} + R(\dot{\psi} + \dot{\phi}_i)\cos(\psi + \phi_i))\mathbf{j}. \tag{2.6}$$

The total kinetic energy of the system is given by

$$T = \frac{1}{2}I_z\dot{\psi}^2 + \frac{1}{2}M(\dot{\mathbf{r}}_{OG}\cdot\dot{\mathbf{r}}_{OG}) + \frac{1}{2}\sum_{i=1}^{n} m_i(\dot{\mathbf{r}}_{OB_i}\cdot\dot{\mathbf{r}}_{OB_i}), \tag{2.7}$$

where $M$ is the mass of the disc, $m_i$ is the mass of the $i$th ball and $I_z$ is the moment of inertia of the rotor about $C$. The potential energy of the system is given by

$$V = \frac{1}{2}k_X X^2 + \frac{1}{2}k_Y Y^2 + Mg(Y + \epsilon\sin\psi) + \sum_{i=1}^{n} m_i g(Y + R\sin(\psi + \phi_i)), \tag{2.8}$$

where $g$ is the acceleration due to gravity, and $k_X$ and $k_Y$ are linear spring constants acting on the rotor in the $X$ and $Y$ directions, respectively.

Finally, the generalised forces, that is, forces not arising from a potential, are modelled by simple viscous damping terms

$$\mathbf{Q} = -\frac{\partial F}{\partial \dot{q}_k} = (-c_X\dot{X}, -c_Y\dot{Y}, \tilde{M}, -D_i\dot{\phi}_i), \tag{2.9}$$

where $c_X$ and $c_Y$ are linear damping constants acting on the rotor in the $X$ and $Y$ directions, respectively, $F$ is Rayleigh's dissipation function and $\tilde{M}$ is the moment (torque) driving the system.

Substituting (2.7), (2.8) and (2.9) into (2.1) yields the nonlinear equations of motion. The equations of motion of the centre of rotation are

$$\begin{aligned} &M\ddot{X} - M\epsilon\dot{\psi}^2\cos\psi - M\epsilon\ddot{\psi}\sin\psi + \sum_{i=1}^{n} m_i\Big\{\ddot{X} - R(\ddot{\psi}+\ddot{\phi}_i)\sin(\psi+\phi_i) \\ &-R(\dot{\psi}+\dot{\phi}_i)^2\cos(\psi+\phi_i)\Big\} + k_X X = -c_X\dot{X}, \end{aligned} \tag{2.10}$$

and

$$\begin{aligned} &M\ddot{Y} - M\epsilon\dot{\psi}^2\sin\psi + M\epsilon\ddot{\psi}\cos\psi + \sum_{i=1}^{n} m_i\Big\{\ddot{Y} + R(\ddot{\psi}+\ddot{\phi}_i)\cos(\psi+\phi_i) \\ &-R(\dot{\psi}+\dot{\phi}_i)^2\sin(\psi+\phi_i)\Big\} + k_Y Y + Mg + \sum_{i=1}^{n} m_i g = -c_Y\dot{Y}. \end{aligned} \tag{2.11}$$

The equation of motion of the rotation about that centre is

$$\begin{aligned} &I_z\ddot{\psi} - M\epsilon\ddot{X}\sin\psi + M\epsilon\ddot{Y}\cos\psi + M\epsilon^2\ddot{\psi} - \sum_{i=1}^{n} m_i\Big\{R\Big[\ddot{X}\sin(\psi+\phi_i) - \\ &\ddot{Y}\cos(\psi+\phi_i)\Big] - R^2(\ddot{\psi}+\ddot{\phi}_i)\Big\} + Mg\epsilon\cos\psi + \sum_{i=1}^{n} m_i gR\cos(\psi+\phi_i) = \tilde{M}, \end{aligned} \tag{2.12}$$

and, finally, the equation of motion of the $i$th ball is

$$\begin{aligned} &-m_i R\left[\ddot{X}\sin(\psi+\phi_i) - \ddot{Y}\cos(\psi+\phi_i)\right] + m_i R^2(\ddot{\psi}+\ddot{\phi}_i) \\ &+m_i gR\cos(\psi+\phi_i) = -D_i\dot{\phi}_i, \end{aligned} \tag{2.13}$$

where $i = 1 \ldots n$.

Equations (2.10)-(2.13) can be simplified by assuming that all balls in the balancer have equal mass $m$, exert equal viscous drag $D$, and that the system is controlled not by a torsional load, but is forced to rotate at a constant angular velocity $\omega$, that is,

$$m_i = m, \quad D_i = D, \quad \dot{\psi} = \omega. \tag{2.14}$$

where $i = 1 \ldots n$. In this project, we will study an ADB mechanism which verifies these assumptions, so we will use (2.14) to simplify the equations of motion of the system.

## 2.2 Non-dimensionalisation

Equations (2.10)-(2.13) can be written in dimensionless form by considering the non-dimensional states $\bar{X}$ and $\bar{Y}$, and the non-dimensional time $\bar{t}$, given by

$$\bar{X} = \frac{X}{R}, \quad \bar{Y} = \frac{Y}{R}, \quad \bar{t} = \omega_n t, \tag{2.15}$$

together with the dimensionless parameters

$$\mu = \frac{m}{M}, \quad \Omega = \frac{\omega}{\omega_n}, \quad \delta = \frac{\epsilon}{R}, \quad G = \frac{g}{\epsilon\omega_n^2}, \tag{2.16}$$

where $\omega_n$ is the natural frequency of the harmonic oscillation found by the mass of the rotating disc and the suspension spring of the rotor, given by

$$\omega_n = \sqrt{\frac{k}{M}}. \tag{2.17}$$

Note that, to obtain this form for $\omega_n$, and in the ensuing analysis, we will assume isotropic suspension of the rotor, that is,

$$\{c, k\} = \{c_X, k_X\} = \{c_Y, k_Y\}. \tag{2.18}$$

Furthermore, we introduce the following dimensionless parameters

$$\zeta = \frac{c}{2\sqrt{kM}}, \quad \beta = \frac{D}{mR^2\omega_n}, \tag{2.19}$$

describing the damping ratio of the rotor system $\zeta$, and the non-dimensional viscous damping acting on the balls in the balancer $\beta$. Note that all the parameters are assumed to be positive. This is without loss of generality since negative $\epsilon$ implies an eccentric centre of mass on the negative axis, which can be mapped back to the positive axis by a simple change of coordinate frame.

Consequently, assuming (2.14), the rate equations (2.10),(2.11) and (2.13) can be written in the following dimensionless form

$$\begin{aligned}&(1+n\mu)\ddot{X} + 2\zeta\dot{X} + X = \delta\Omega^2\cos\Omega t \\ &+\mu\sum_{i=1}^{n}\left[\ddot{\phi}_i\sin(\Omega t+\phi_i) + (\Omega+\dot{\phi}_i)^2\cos(\Omega t+\phi_i)\right],\end{aligned} \tag{2.20}$$

$$\begin{aligned}&(1+n\mu)\ddot{Y} + 2\zeta\dot{Y} + Y = \delta\Omega^2\sin\Omega t \\ &-\mu\sum_{i=1}^{n}\left[\ddot{\phi}_i\cos(\Omega t+\phi_i) - (\Omega+\dot{\phi}_i)^2\sin(\Omega t+\phi_i)\right] - G(1+n\mu),\end{aligned} \tag{2.21}$$

$$\ddot{\phi}_i - \ddot{X}\sin(\Omega t+\phi_i) + \ddot{Y}\cos(\Omega t+\phi_i) + \delta G\cos(\Omega t+\phi_i) = -\beta\dot{\phi}_i. \tag{2.22}$$

Note that, for simplicity, we drop the 'bar' notation used in (2.15). Furthermore, as we are not interested in the variation of the torque $\tilde{M}$, necessary to drive the system at a constant angular velocity $\omega$, we do not consider the third equation of motion (2.12).

## 2.3 Autonomous equations in the rotating frame

The final part of our formulation converts the non-dimensional equations (2.20)-(2.22) to autonomous equations in a rotating frame, see [7, 1]. To this end, we consider the following substitutions

$$X = x\cos\Omega t - y\sin\Omega t, \tag{2.23}$$
$$Y = x\sin\Omega t + y\cos\Omega t. \tag{2.24}$$

Furthermore, we ignore the effects of gravity, that is, set $G$=0 in (2.22). This assumption is justified because, in practice and for high rotation speeds, the centrifugal forces are much greater than the gravitational effect on the balls. Gravity can also be neglected if the rotor is held in a horizontal position. Considering these assumption results in the following autonomous dynamical system

$$\begin{aligned}
&\begin{pmatrix} 1+n\mu & 0 \\ 0 & 1+n\mu \end{pmatrix}\begin{pmatrix} \ddot{x} \\ \ddot{y} \end{pmatrix} + \begin{pmatrix} 2\zeta & -2\Omega(1+n\mu) \\ 2\Omega(1+n\mu) & 2\zeta \end{pmatrix}\begin{pmatrix} \dot{x} \\ \dot{y} \end{pmatrix} \\
&+\begin{pmatrix} K & -2\Omega\zeta \\ 2\Omega\zeta & K \end{pmatrix}\begin{pmatrix} x \\ y \end{pmatrix} \\
&= \begin{pmatrix} \delta\Omega^2 \\ 0 \end{pmatrix} + \mu\sum_{i=1}^{n}\begin{pmatrix} (\Omega+\dot{\phi}_i)^2 & \ddot{\phi}_i \\ -\ddot{\phi}_i & (\Omega+\dot{\phi}_i)^2 \end{pmatrix}\begin{pmatrix} \cos\phi_i \\ \sin\phi_i \end{pmatrix},
\end{aligned} \tag{2.25}$$

and

$$\ddot{\phi}_i + \beta\dot{\phi}_i = (\ddot{x} - \Omega^2 x - 2\Omega\dot{y})\sin\phi_i - (\ddot{y} - \Omega^2 y + 2\Omega\dot{x})\cos\phi_i, \tag{2.26}$$

where $i = 1, ..., n$ and

$$K = 1 - \Omega^2(1+n\mu). \tag{2.27}$$

We note that by setting the right-hand side of (2.25) to zero we recover the equations of motion of a damped, isotropic rotor in the rotating frame. Similarly, setting $\mu = 0$, reduces (2.25) to the equations of motion for the Jeffcott rotor [15]. The consequence of the ADB is to add extra forcing terms provided by the motion of the balls. The forcing though is coupled to the motion of the centre of mass of the rotor, thus resulting in a fully coupled nonlinear system. In the case that $\mu$ is small, the coupling may be small, but the nonlinearity is not weak since, due to geometric effects, the full sine nonlinearity is involved in the coupling terms.

# Chapter 3

# Steady state solutions

To obtain the equilibrium states of the system, it is necessary to set all time derivatives terms in (2.25) and (2.26) to zero. Thus we have

$$\begin{pmatrix} K & -2\Omega\zeta \\ 2\Omega\zeta & K \end{pmatrix} \begin{pmatrix} x \\ y \end{pmatrix} = \begin{pmatrix} \delta\Omega^2 \\ 0 \end{pmatrix} + \mu \sum_{i=1}^{n} \begin{pmatrix} \Omega^2 & 0 \\ 0 & \Omega^2 \end{pmatrix} \begin{pmatrix} \cos\phi_i \\ \sin\phi_i \end{pmatrix}, \tag{3.1}$$

and

$$0 = (-\Omega^2 x)\sin\phi_i - (-\Omega^2 y)\cos\phi_i, \tag{3.2}$$

where the index $i = 1, \ldots, n$.

Rewriting these equations we get

$$Kx - 2\Omega\zeta y - \delta\Omega^2 - \mu \sum_{i=1}^{n} \Omega^2 \cos\phi_i = 0, \tag{3.3}$$

$$2\Omega\zeta x + Ky - \mu \sum_{i=1}^{n} \Omega^2 \sin\phi_i = 0, \tag{3.4}$$

$$x\sin\phi_i - y\cos\phi_i = 0, \quad i = 1, \ldots, n. \tag{3.5}$$

Let us now discuss two different kinds of solutions to these equations: *balanced* and *unbalanced*.

A balanced steady state occurs when the centre of rotation of the system $C$ is at the origin, so we set $x$ and $y$ in (3.3)-(3.5) to zero. After that, (3.5) is verified by any set of values for $\phi_i$, $i = 1...n$ , so we would have only two equations with $n$ unknown variables. That is, in this balanced steady state, there are $n-2$ degrees of freedom, and the following constraints have to be satisfied:

$$\begin{aligned} &x = y = 0, \\ &\sum_{i=1}^{n} \cos\phi_i = -\frac{\delta}{\mu}, \\ &\sum_{i=1}^{n} \sin\phi_i = 0. \end{aligned} \tag{3.6}$$

Due to this, there exist infinitely many balanced steady states when $n > 2$. In what follows, we will refer to (3.6) as the set of balanced states **1**.

Now let us turn to unbalanced steady states, for which $x, y \neq 0$. In this case, (3.5) gives us

$$\frac{y}{x} = \tan\phi_i, \quad i = 1, \dots n, \tag{3.7}$$

that is, all the angles $\phi_i$ have the same tangent. Due to this, the coordinates $\phi_i$ have to satisfy

$$\phi_i = \phi_1 + k_i\pi, \quad i = 2 \dots n, \tag{3.8}$$

where $k_i$ is any whole number, without loss of generality 0 or 1. When $k_i = 0$, the coordinate $\phi_i$ is coincident with the coordinate $\phi_1$, that is, the balls 1 and $i$ coincide (recall that we do not model collisions or interaction between the balls). When $k_i = 1$ the balls 1 and $i$ are on opposite sides, and in line with the centre of rotation $C$. Now we differentiate two kinds of equilibria which are out of balance:

- Out of balance steady states in which all the balls are coincident. In this case $\phi_1 = \phi_2 = \ldots = \phi_n$. Solving (3.3) and (3.4) we can obtain expressions for $x$ and y in terms of $\phi_1$, and hence an expression for $\phi_1$ from (3.5). Specifically we get

$$\begin{aligned}
x &= \frac{K\Omega^2(n\mu\cos\phi_1 + \delta) + 2n\mu\Omega^3\zeta\sin\phi_1}{K^2 + (2\Omega\zeta)^2}, \\
y &= \frac{nK\mu\Omega^2\sin\phi_1 - 2\Omega\zeta(\delta\Omega^2 + n\mu\Omega^2\cos\phi_1)}{K^2 + (2\Omega\zeta)^2}, \\
\phi_1 &= \pm\arccos\left(\frac{-2n\mu\zeta\Omega}{\sqrt{(2\Omega\zeta\delta)^2 + (K\delta)^2}}\right) - \arctan\left(\frac{-K}{2\Omega\zeta}\right), \\
\phi_1 &= \phi_2 = \ldots = \phi_n.
\end{aligned} \tag{3.9}$$

  In what follows, we will refer to (3.9) as the coincident states **2**$\pm$, with the sign depending on the sign that is taken for the arccosine in the expression for $\phi_1$.

- Out of balance steady states in which there are $m$ coincident balls and ($n$-$m$) balls on the opposite side and in line with the centre of rotation $C$. Solving in this case (3.3) and (3.4), we obtain the following equilibrium:

$$\begin{aligned}
x &= \frac{K\Omega^2((2m-n)\mu\cos\phi_1 + \delta) + 2(2m-n)\mu\Omega^3\zeta\sin\phi_1}{K^2 + (2\Omega\zeta)^2}, \\
y &= \frac{(2m-n)K\mu\Omega^2\sin\phi_1 - 2\Omega\zeta(\delta\Omega^2 + (2m-n)\mu\Omega^2\cos\phi_1)}{K^2 + (2\Omega\zeta)^2}, \\
\phi_1 &= \pm\arccos\left(\frac{-2(2m-n)\mu\zeta\Omega}{\sqrt{(2\Omega\zeta\delta)^2 + (K\delta)^2}}\right) - \arctan\left(\frac{-K}{2\Omega\zeta}\right), \\
\phi_i &= \phi_1, \quad i = 1, 2, \ldots, m, \\
\phi_j &= \phi_1 + \pi, \quad j = m+1, \ldots, n.
\end{aligned} \tag{3.10}$$

In what follows, we will refer to (3.10) as the $(n-m)$ in-line states **3(n-m)**$\pm$. That is, the steady state for the ADB system with $n$ balls in which there are $m$ coincident balls at the position $\phi_1$, and the other $(n-m)$ balls are on the opposite side and in line with the centre of rotation $C$. The sign depends on the sign that is taken for the arccosine in the expression for $\phi_1$.

Initially, in an ADB system with $n$ balls, there would exist $2(n-1)$ different in-line states **3(n-m)**$\pm$. However, some of them are physically the same. Thus, let us investigate how many in-line states exist for the ADB system with two, three and four balls. In the case $n=2$, the only possible value for $m$ is 1. Although there should be two different in-line states, **3(2-1)+** and **3(2-1)-**, we will demonstrate that they, in fact, they are the same. After setting $m$ in the expression for $\phi_1$ in (3.10) to 1, we have

$$\phi_{1_{3(2-1)+}} = \frac{\pi}{2} - \arctan\left(\frac{-K}{2\Omega\zeta}\right), \tag{3.11}$$

for the state **3(2-1)+**, and

$$\phi_{1_{3(2-1)-}} = -\frac{\pi}{2} - \arctan\left(\frac{-K}{2\Omega\zeta}\right), \tag{3.12}$$

for the state **3(2-1)-**. Note that the difference between (3.11) and (3.12) is equal to $\pi$, so the coordinate $\phi_2$ for the in-line state **3(2-1)-** is the same as the coordinate $\phi_1$ for the in-line state **3(2-1)+**,

$$\phi_{2_{3(2-1)-}} = \phi_{1_{3(2-1)-}} + \pi = \frac{\pi}{2} - \arctan\left(\frac{-K}{2\Omega\zeta}\right) = \phi_{1_3(2-1)+}. \tag{3.13}$$

Therefore, since $\phi_1$ and $\phi_2$ are in-line, the coordinate $\phi_2$ for the state **3(2-1)+** is the same as the coordinate $\phi_1$ for the state **3(2-1)-**. Hence, the state **3(2-1)+** is equivalent to the state **3(2-1)-** (and vice versa), obtained by exchanging $\phi_1$ and $\phi_2$. However, physically these correspond to the same state since the balls are assumed identical, and, hence, one can consider these steady states to be unique by assuming without loss of generality that $-\pi \leq \phi_2 \leq \phi_1 \leq \pi$. Consequently, when $n=2$, there exists a single in-line state called **3**.

In the case $n=3$, there are two possibilities for the number of coincident balls, $m=1$ or $m=2$. However, both of these states are the same in the sense that we can obtain one state from the other simply changing $\phi_1$ with $\phi_3$. That is, since the three balls are identical, it is physically the same if the two coincident balls are $\phi_2$ and $\phi_3$ (case $m=1$) as if the two coincident balls are $\phi_1$ and $\phi_2$ (case $m=2$). Hence, we will refer the in-line states for the ADB with three balls as **3**$\pm$, with the sign depending on the sign that is chosen for the arccosine in the expression for $\phi_1$ in (3.10). For $n=4$, the number of coincident balls could be $m=1$, 2 or 3. The cases $m=1$ and $m=3$ are equivalent for the same reason just mentioned in the ADB system with three balls. That is, since the four balls are identical, it is the same if the three coincident balls are $\phi_2$, $\phi_3$ and $\phi_4$ (case $m=1$), as if they are $\phi_1$, $\phi_2$ and $\phi_3$ (case $m=3$). Therefore, we will call in-line states **3B**$\pm$ to these equivalent states **3(4-1)**$\pm$ and **3(4-3)**$\pm$. The same situation that for the states **3(2-1)**$\pm$ happens for the in-line states **3(4-2)**$\pm$. Thus, the state **3(4-2)+** is equivalent to the state **3(4-2)-**, and in the following we will refer them as the in-line state **3A**.

To sum up, for $n = 2$ balls we have a unique in-line state called state **3**, for $n = 3$ we consider two in-line states **3+** and **3-**, and for $n = 4$ there exist an in-line state with two coincident balls called **3A**, and two with three coincident balls called **3B+** and **3B-**.

Let us study when the steady states can exist. Note that there are various conditions governing the existence of the different steady state solutions. In the case of the balanced states **1** given by (3.6), its second equation implies that the ratio $\delta/\mu$ has a limit. That is, due to $|\cos\phi_i| \leq 1$, the modulus of the sum of the $\cos\phi_i$ must always be less or equal to $n$. Hence the modulus of the ratio $\delta/\mu$ cannot be more than $n$ in order for the balanced state to exist. Therefore we get $\frac{\delta}{\mu} \leq n$, which implies that a necessary condition for the balanced state to exist is

$$\mu \geq \mu_c := \frac{\delta}{n}. \tag{3.14}$$

Physically, this means that, in order to achieve dynamic balance, the mass of the balls must be large enough to cope with the dimensionless eccentricity $\delta$. When equality is reached in (3.14), the balanced state **1** becomes one of the coincident state **2**$\pm$ for $\phi_i = \pi, \forall i$. On varying $\mu$ through $n$ this corresponds to a pitchfork bifurcation between the state **1** and one of the coincident states **2**$\pm$ as we will see in Chapter 4. Note that the condition (3.14) is only valid for the ADB system with two balls, and for the ADB with $n$ balls when the $n-2$ free balls are on the opposite side to the centre of mass $W$ and in line with the centre of rotation $C$ (that is, $\phi_i = \pi$ for $i = 3, ..., n$). In other cases, a balanced state might not exist even if the condition (3.14) is satisfied.

The two coincident states **2**$\pm$ exist provided the modulus of the argument in the arccosine of the expression for $\phi_1$ in (3.9) is less than 1. Thus, it is necessary to satisfy

$$\sqrt{(2\Omega\zeta\delta)^2 + (K\delta)^2} \geq 2n\mu\zeta\Omega. \tag{3.15}$$

Rewriting this expression, we have

$$K^2 \geq (2\Omega\zeta)^2 \left( \left( \frac{n\mu}{\delta} \right)^2 - 1 \right) = (2\Omega\zeta)^2 \left( \left( \frac{\mu}{\mu_c} \right)^2 - 1 \right). \tag{3.16}$$

When $\mu < \mu_c$ the right-hand side of (3.16) is always negative, so the coincident states **2**$\pm$ always exist. If $\mu > \mu_c$ we would have to do a more detailed study to know when the coincident states **2**$\pm$ could exist. As an example, we will fix the $\mu$, $\delta$ and $\zeta$ parameters and the number of balls $n$ in (3.16) to know for which $\Omega$ values the condition would be satisfied. If we fix $\mu = 0.05$, $\delta = 0.01$, $\zeta = 0.01$, and $n = 3$, we can see in Figure 3.1 that the inequality (3.16) is satisfied in a range of $\Omega$ values: for $\Omega < \Omega_{c1}$ and $\Omega > \Omega_{c2}$. However, there exists an intermediary range of $\Omega$ values in which the discriminant is negative ($\Omega_{c1} < \Omega < \Omega_{c2}$). Hence we have existence of the two coincident states **2**$\pm$ for small $\Omega$ which meet and disappear at some value $\Omega_{c1}$, only to reappear at some higher $\Omega_{c2}$. This is typical of a saddle-node bifurcation, and is confirmed as such in the next chapter. The values $\Omega_{c1,c2}$ depend on $\delta$, $\zeta$, $\mu$, and $n$ in a nontrivial way. In this example $\Omega_{c1} = 0.8114$ and $\Omega_{c2} = 1.0717$.

Now we consider the states **3(n-m)**$\pm$. These will exist only if the modulus of the argument in the arccosine of the expression for $\phi_1$ in (3.10) is less than 1. That is,

$$\sqrt{(2\Omega\zeta\delta)^2 + (K\delta)^2} \geq 2(2m - n)\mu\zeta\Omega. \tag{3.17}$$

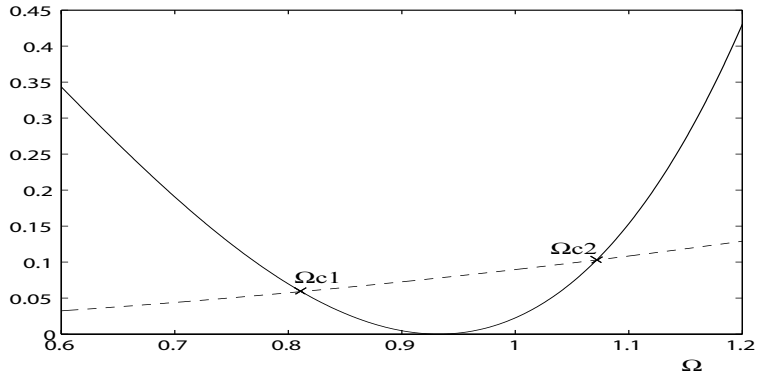


Figure 3.1: Representation of the functions $K^2$ (solid line) and $(2\Omega\zeta)^2\left(\left(\frac{n\mu}{\delta}\right)^2-1\right)$ (broken line) for the fixed values $\mu=0.05$, $\delta=0.01$, $\zeta=0.01$, and $n=3$ balls. The intersection points ($\Omega_{c1}=0.8114$ and $\Omega_{c2}=1.0717$) define the $\Omega$ range in which the coincident states **2**$\pm$ do not exist, that is, when $K^2$ is less than $(2\Omega\zeta)^2\left(\left(\frac{n\mu}{\delta}\right)^2-1\right)$.

Rewriting this expression, we have

$$K^2 > (2\Omega\zeta)^2\left(\left(\frac{(2m-n)\mu}{\delta}\right)^2-1\right). \tag{3.18}$$

For the ADB system with two balls ($n=2$), the only possible value for $m$ is 1, and in that case the inequality (3.18) is always satisfied. Therefore, when $n=2$ the in-line state **3** exists for all values of the physical parameters. For the ADB system with more than two correction masses ($n>2$), when $\mu<\delta/(2m-n)$ the states **3(n-m)**$\pm$ always exist, because the right-hand side of (3.18) is negative, so the inequality is satisfied. If $\mu>\delta/(2m-n)$ we need a more detailed analysis to know when the states **3(n-m)**$\pm$ exist. Now we will see a case similar to the above case of **2**$\pm$. Here however, only two balls are coincident, and the third ball is on the opposite side. Thus, we can see in Figure 3.2 that similarly to the states **2**$\pm$ there also exists a region of mid-range $\Omega$-values for which the inequality (3.18) is not satisfied. This region is delimited by $\Omega_{c1}$ and $\Omega_{c2}$, which in this example are 0.8909 and 0.9761 respectively. In conclusion, the states **3(n-m)**$\pm$ will exist for $\Omega<\Omega_{c1}$ and $\Omega>\Omega_{c2}$.

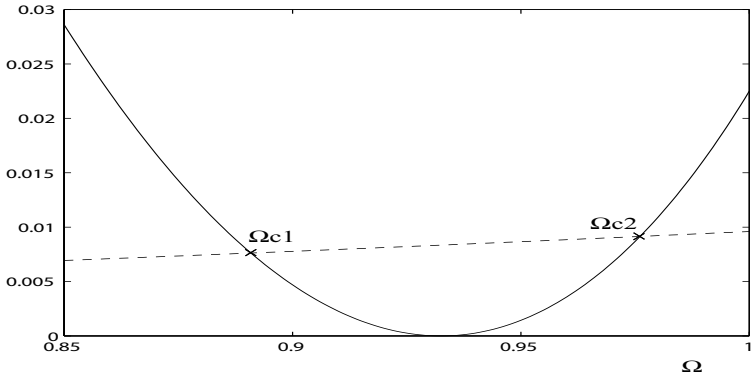


Figure 3.2: Representation of the functions $K^2$ (solid line) and $(2\Omega\zeta)^2\left(\left(\frac{(2m-n)\mu}{\delta}\right)^2-1\right)$ (broken line) for the fixed values $\mu = 0.05$, $\delta = 0.01$, $\zeta = 0.01$, $n = 3$ and $m = 2$. The intersection points ($\Omega_{c1} = 0.8909$ and $\Omega_{c2} = 0.9761$) define the $\Omega$ range in which the in-line states **3(n-m)**$\pm$ do not exist, that is, when $K^2$ is less than $(2\Omega\zeta)^2\left(\left(\frac{(2m-n)\mu}{\delta}\right)^2-1\right)$.

# Chapter 4

# Bifurcation analysis of the ADB system

In this chapter, we perform a numerical bifurcation analysis for the ADB system with two, three and four correction masses, that is, setting $n = 2$, $n = 3$ and $n = 4$ in (2.25). The computation has been carried out using `MATCONT` [8], a continuation package built on `Matlab`, to compute bifurcation diagrams showing boundaries of stability in various parameter planes. In [9] a detailed studied was performed for the ADB with two balls. In that case the results were obtained with `AUTO`, so the work made in this case for $n = 2$ is useful to be sure of the computation executed by `MATCONT`, and to check that the equations were written in a correct way (see Appendix A). The results for three and four balls are entirely new. Moreover, we try to notice any similarities between the three cases and to highlight any improvements or detrimental effects compared with the behaviour of the system with two balls.

The main object of interest of the bifurcation analysis performed in this chapter is to identify the stability region of the balanced steady state in different parameter planes, that is, to find under what parameter sets it is possible to balance the system. We also use numerical bifurcation theory to generate bifurcation curves in two-parameter planes, and to depict steady state solutions and bifurcation points in one-parameter planes. For the studied system, we identify three kinds of bifurcations:

- *Saddle-node bifurcation*, which is characterised by the fact that on one side of the bifurcation two equilibria exist, while on the other side of the bifurcation these two equilibria have disappeared. The moment of bifurcation can be thought of as the moment where the two equilibria collide. The saddle-node bifurcation can take place in any system and is, in fact, a very typical bifurcation to happen when a parameter is varied.

- *Pitchfork bifurcation*, which happens when the system has an equilibrium that exists for all values of the parameter and can never be destroyed; when this equilibrium collides with another equilibrium, the two equilibria exchange their stabilities properties, but continue to exist both before and after the bifurcation. This bifurcation only exists when there is a reflectional symmetry present in the system.

- *Hopf bifurcation*, which is characterised by the appearance of a periodic orbit or limit cycle. The equilibrium exist on either side of the bifurcation, but might change its

stability. The amplitude of the periodic orbit is 0 at the moment of the bifurcation and grows as the parameter increases. The frequency of the periodic orbit, at the onset of the bifurcation, is equal to the absolute value of the imaginary part of the eigenvalue of the equilibrium point.

Static bifurcations (either saddle-node bifurcations or pitchfork bifurcations) occur when a real eigenvalue passes through zero, and oscillatory bifurcations (Hopf bifurcations) occur when a pair of pure eigenvalues cross the imaginary axis; see, for example, Ref. [22, 17] for further details about bifurcation theory.

Let us explain the nomenclature used in the bifurcation diagrams represented along this chapter. Saddle-node bifurcations are identified by SN, pitchfork bifurcations by PF, and Hopf bifurcations by H. The bifurcating steady states are indicated by numbers. Specifically, in two-parameter bifurcation diagrams, broken lines correspond to bifurcation curves of the in-line states **3(n-m)**$\pm$, and solid lines to curves of balanced and coincident states **1** and **2**$\pm$. Moreover, we identify regions in which steady states are stable. Thus, dark shading corresponds to the region of stability of a balanced steady state, light shading to the region of stability of a coincident steady state, and no shading to a region where there are no stable steady state solutions. As we will see in next sections, the in-line steady states are always found to be unstable. In the one-parameter bifurcation diagrams, which are obtained fixing one more parameter in the two-parameter bifurcation diagrams, the stable steady states are drawn as solid lines, and the unstable as broken lines. Pitchfork bifurcations PF and saddle-node bifurcations SN are marked by a ($\times$), and Hopf bifurcations H are marked by a ($*$).

## 4.1 Numerical bifurcation diagrams for ADB with two balls

In this section, we obtain two-parameter bifurcation diagrams for the ADB system with $n = 2$ balls, with which we will be able to see how the variation of the parameters can affect the stability of the steady state solutions. We also show one-parameter bifurcation diagrams corresponding to vertical and horizontal transitions through the two-parameter bifurcation diagrams. In the case of the ADB system with two balls, there is a unique balanced equilibrium, which is the solution of (3.6) setting $n = 2$. We will call it state **1**. For the coincident states there exist two states **2**$\pm$, whose sign corresponds to the sign of the arccosine in the expression for $\phi_1$ in (3.9). Finally, as was said in Chapter 3, there is a unique in-line state called state **3**.

Figure 4.1 shows the results of a two-parameter bifurcation analysis upon variation of the dimensionless parameters $\Omega$ and $\mu$, while considering the fixed parameters $\zeta = \beta = \delta = 0.01$. Physically, this corresponds to a small eccentricity and low damping in the suspension and balancing systems. In panel (b) it is represented a zoom of panel (a) for small values of $\mu$, and in that, the letters $s$ and $u$ indicate which steady states are 'stable' and 'unstable', respectively. We can see that for $\mu < \mu_c := \delta/n = 0.01/2 = 0.005$, the only stable steady state is the coincident state **2-**. This solution is unstable inside the region bounded by the Hopf bifurcation H2-. The coincident state **2+** exists, but is always unstable for $\mu < \mu_c$; see Fig.4.1(b). The same thing happens for the in-line state **3**, which always exists for $\mu < \mu_c$ but is unstable. As was said in Chapter 3, when the ball mass parameter $\mu$ is smaller

than $\mu_c$, the balancing mass is not large enough to offset the imbalance produced by the eccentricity in the rotor. Hence, for $\mu < \mu_c$, the balanced equilibrium does not exist.

For $\mu > \mu_c$ the balanced state **1** always exists. Figure 4.1(b) shows that for small values of $\Omega$ the coincident state **2-** is stable while the coincident state **2+** is unstable. These coincident steady states are born in a saddle-node bifurcation at the left-most boundary of the wedge-shaped region bounded by the curves SN2+-. Inside this region the coincident states **2**$\pm$ do not exist, and the only steady state are the balanced state **1** and the in-line state **3**, which are unstable. The coincident states **2**$\pm$ appear again at the saddle-node bifurcation SN2+- found on the right-most boundary of this wedge. In this case, both states **2**$\pm$ are unstable. Note that the left and right boundaries of the wedge-shaped region correspond, respectively, to the critical points $\Omega_{c1}$ and $\Omega_{c2}$ identified at the end of Chapter 3. For increasing values of $\Omega$, the unstable coincident state **2-** undergoes a further Hopf bifurcation at the curve H2-. Finally, for large values of $\Omega$ the balanced state **1** stabilises in a Hopf bifurcation H1. Note that, for sufficiently large values of $\mu$ there are also a pair of Hopf bifurcations H1 that stabilise the balanced state **1** around the *critical rotation speed* $\Omega = 1$. The in-line state **3** for $\mu > \mu_c$ has the same properties than for $\mu < \mu_c$, that is, it always exists but is unstable.

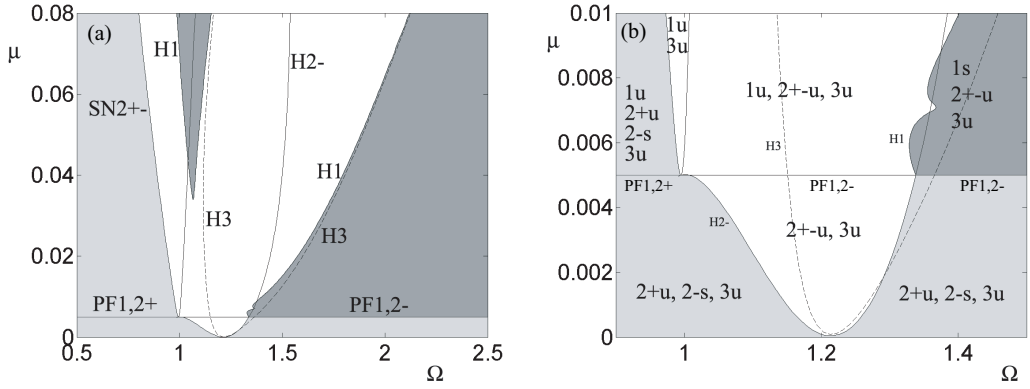


Figure 4.1: Two-parameter bifurcation diagram of steady state solutions of the ADB system with two balls in the $(\Omega, \mu)$-plane for $\zeta = \beta = \delta = 0.01$. Here SN stands for saddle-node bifurcation, PF for pitchfork bifurcation, and H for Hopf bifurcation. The numbers indicate which steady states are bifurcating. Broken lines correspond to bifurcation curves of the state **3**, and solid lines to states **1** and **2**$\pm$. Dark shading corresponds to the region of stability of the balanced state **1**, and light shading to the region of stability of the coincident state **2-**. Panel (b) shows a zoom of (a) for small values of $\mu$. The labels correspond to which of the states **1**, **2**$\pm$ or **3** exist, and letters $s$ and $u$ correspond to 'stable' and 'unstable' respectively.

Panel (b) of Fig.4.1 shows that the curve of Hopf bifurcations H2- terminates at the low-$\Omega$ end in a codimension-two pitchfork-Hopf point which is given precisely by

$$(\mu, \Omega) = (\mu_c, \Omega_c) := (\delta/2, 1/\sqrt{1+2\mu}) = (0.005, 0.9950372). \tag{4.1}$$

The point $\Omega_c$ also marks the tip of the wedge-shaped region bounded by the curves SN2+-, that is, where the critical points $\Omega_{c1}$ and $\Omega_{c2}$ come together. Moreover, $\Omega_c$ is defined by $K = 0$ which is the analogue of the critical rotation speed $\Omega = 1$ in the case without the balancing mechanism ($\mu = 0$). For increasing values of $\Omega$, the curve H2- meets the curve PF1,2-

again, at another codimension-two pitchfork-Hopf point given by $(\mu, \Omega) = (\mu_c, 1.338096)$; see Fig.4.1(b).

As it has already been mentioned, for the parameter values under consideration, the in-line state **3** was always found to be unstable and therefore of little physical interest. It does undergo a Hopf bifurcation that cuts through the middle of the parameter region in question, but does not interact with any other bifurcation curve, as it is shown in Fig.4.1 with broken line. However, as the steady state undergoing the bifurcation is already unstable (with one unstable eigenvalue), so is the bifurcating periodic solution.

Figure 4.2 shows one-parameter bifurcation diagrams corresponding to horizontal transitions through Fig.4.1(a) for $\mu = 0.05$ and $\mu = 0.0025$, respectively. Here we can see the result of increasing $\Omega$ for $\mu > \mu_c$ and $\mu < \mu_c$, respectively. In the first case (see panel (a)), it is shown how the coincident states **2**$\pm$ are born in the saddle-node bifurcations SN2+-. For $\Omega$-values to the left of the left-most saddle-node bifurcation point, the state **2-** is stable, while to the right of the right-most saddle-node bifurcation point, both **2-** and **2+** are unstable. The state **2-** undergoes another Hopf bifurcation when $\Omega$ increases, but its stability does not change. In panel (b) it is possible to see that the saddle-node bifurcations SN2+- disappear for $\mu < \mu_c$ and the states **2**$\pm$ do not coincide in any point. While the state **2+** is unstable in all the $\Omega$-range, the state **2-** is only unstable between the two Hopf bifurcation points H2-. The balanced state **1** does not exist for $\mu < \mu_c$, so it does not appear in Fig.4.2(b). In Fig.4.2(a) it is shown that this state has two regions of stability, one for large $\Omega$-values after a Hopf bifurcation point, and another between two Hopf bifurcation points around the critical rotation speed. This last stability region only exists for large enough values of $\mu$, as it is possible to see in Fig.4.1(a). Comparing the equilibrium curves of state **3** in Figs.4.2(a) and (b), we note that its behaviour is the same for $\mu < \mu_c$ as for $\mu > \mu_c$. That is, it is always unstable and it has two Hopf bifurcation points. We can also notice that for low and high $\Omega$-values this state **3** becomes close to the coincident state **2+**.

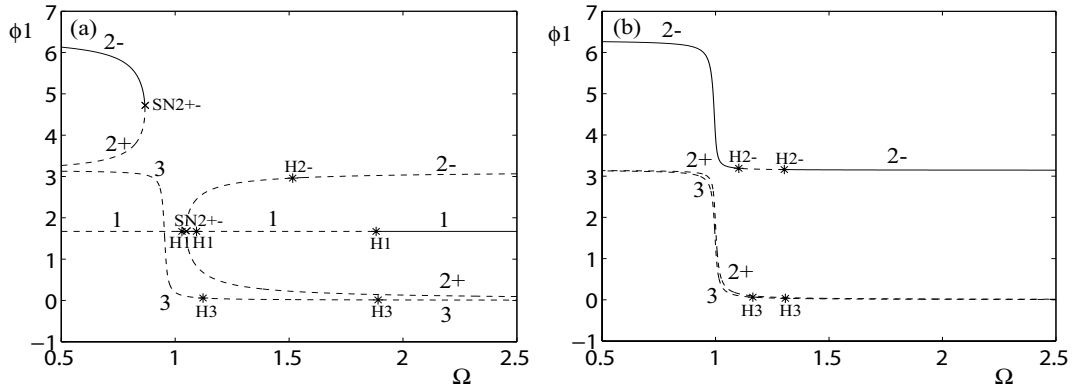


Figure 4.2: One-parameter bifurcation diagrams of steady state solutions of the ADB system with two balls. Panels (a) and (b) show diagrams in $\Omega$ for $\mu = 0.05$ and 0.0025, respectively. The solid lines correspond to stable states, and broken lines to unstable ones. Saddle-node (SN) bifurcations are marked by a ($\times$), and Hopf (H) bifurcations by a ($*$). The numbers indicate which steady states are bifurcating.

Let us comment the position of the coincident balls for the stable state **2-**. As we see in Fig.4.2, for low Ω-values, the state **2-** positions the balls around $\phi_1 = 2\pi$. That means the balls are near the imbalance, so the vibration in the rotor is increased comparing with the case without balls. In contrast, for larger Ω-values, to the right of the right-most saddle-node bifurcation point, the balls turn being positioned around $\phi_1 = \pi$, that is, at the other side that the imbalance. Hence, in this case, the balls help to offset the imbalance, and although it is not possible to reach the balance of the system, the vibration is decreased with respect to the rotor without ADB. Therefore, when Ω is large enough, the stable coincident state **2-** helps to decrease the vibration of the rotor in the case in which the balls mass is not large enough to reach the balance ($\mu < \mu_c$). However, for small Ω, the state **2-** makes worse the behaviour of the rotor. We will confirm these affirmations with simulation results in Chapter 5.

Figure 4.3 shows one-parameter bifurcation diagrams corresponding to vertical transitions through Fig.4.1(a) for $\Omega = 0.5$ and $\Omega = 1.5$, respectively. Here we can see the result of increasing $\mu$ through $\mu_c$ for $\Omega < \Omega_c$ and $\Omega > \Omega_c$, respectively. In both cases, the balanced state **1** is born in a pitchfork bifurcation PF from one of the coincident states **2**±. Note that the two copies of the balanced state **1** which are born in this bifurcation come from taking $\phi_1 \leftrightarrow \phi_2$. For $\Omega < \Omega_c$ (see panel (a)), it is the unstable coincident state **2+** that is involved, creating an unstable balanced state **1**. As Ω is increased through $\Omega_c$ the roles of the coincident states **2-** and **2+** are reversed, but the balanced state **1** created is still unstable. As Ω is increased further through the second codimension-two pitchfork-Hopf bifurcation at $\Omega = 1.338096$, the pitchfork bifurcation PF changes in character again; see panel (b). It becomes supercritical so that the coincident state **2-** and the bifurcating balanced state **1** are both stable. The balanced state **1** becomes unstable again once it reaches the Hopf bifurcation H1. This state remains stable up to large values of Ω in our region of interest.

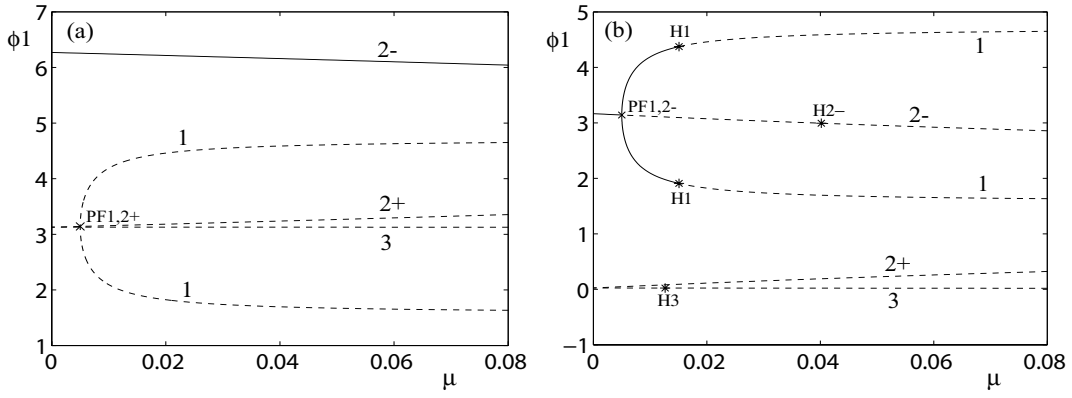


Figure 4.3: One-parameter bifurcation diagrams of steady state solutions of the ADB system with two balls. Panels (a) and (b) show diagrams in $\mu$ for $\Omega = 0.5$ and 1.5, respectively. The solid lines correspond to stable states, and broken lines to unstable ones. Pitchfork (PF) bifurcations are marked by a ($\times$), and Hopf (H) bifurcations by a ($*$). The numbers indicate which steady states are bifurcating.

Now let us consider some stability diagrams akin to Fig.4.4 in which we vary the other dimensionless parameters $\delta$, $\zeta$, and $\beta$. Henceforth, we shall assume that $\mu \geq \mu_c$ so that

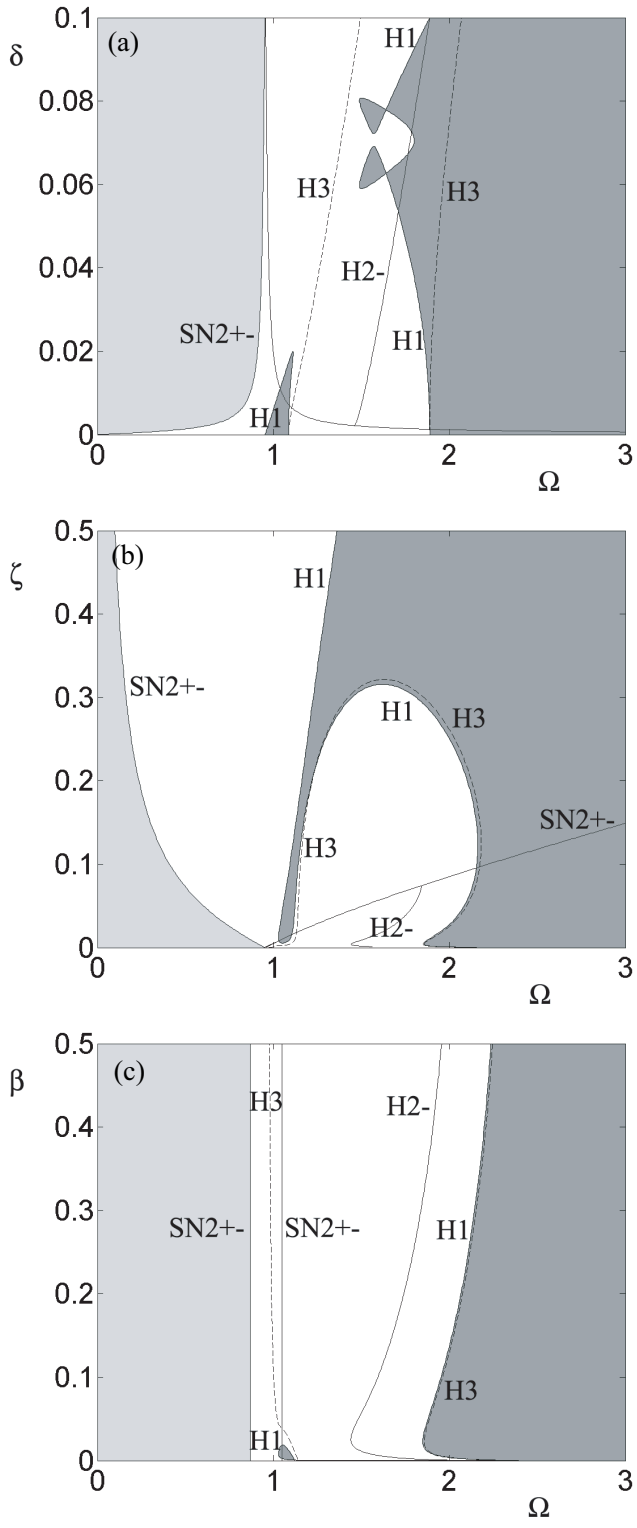


Figure 4.4: Two-parameter bifurcation diagrams of steady state solutions of the ADB system with two balls. Here SN stands for saddle-node bifurcation, PF for pitchfork bifurcation, and H for Hopf bifurcation. The numbers indicate which steady states are bifurcating. Broken lines correspond to bifurcation curves of the state **3**, and solid lines to states **1** and **2**±. Dark shaded regions correspond to a stable balanced state **1** and light shaded regions to a stable unbalanced coincident state **2-**.In each panel the fixed parameters are $\mu = 0.05$, and $\beta = \delta = \zeta = 0.01$. The varying parameters are $\delta$ versus $\Omega$ (a), $\zeta$ versus $\Omega$ (b), and $\beta$ versus $\Omega$ (c).

the condition needed for balance is satisfied. This condition means $\delta \leq n\mu$, because we define the critical ball mass as $\mu_c := \delta/n$. Therefore, we will only consider the $\delta$-range $0 \leq \delta \leq n\mu = 2 \cdot 0.05 = 0.1$. Figure 4.4 shows further two-parameter bifurcation analyses upon variation of other, physically relevant parameters. Specifically, Figs.4.4(a), (b) and (c) show dependence of stability boundaries upon variation of the dimensionless parameters controlling the eccentricity $\delta$, the damping ratio of the rotor $\zeta$, and the damping of the balls $\beta$, respectively, as the rotation speed $\Omega$ is increased. In each case, the onset of instability of the coincident state **2-** appears in a saddle-node bifurcation SN2+-, and the stability of the balanced state **1** in a Hopf bifurcation H1. The same broad trends as in Fig.4.1 are observed, namely that the coincident state **2-** is stable for low enough values of $\Omega$, whereas the balanced state **1** is stable for sufficiently large rotation speeds. In between there is a region of instability where neither state is stable. Significantly, the onset of stability of the balanced state **1** is weakly sensitive to each of the system parameters, however it is always stable for $\Omega > 2.5$. Moreover, we note, from Figs.4.4(a) and (b), that the details of what happens for intermediate values of $\Omega$ (between approximately 1.0 and 2.0) can be quite complex. To sum up, as conclusion we can say that for $\mu \geq \mu_c$ (that means $\delta \leq n\mu = 2\mu$), the balanced state **1** is stable for large enough $\Omega$, independently of $\zeta$ and $\beta$ values. When the rotation speed of the rotor is small, the stable steady state is the coincident state **2-**.

## 4.2 Numerical bifurcation diagrams for ADB with three balls

In this section, we obtain two-parameter bifurcation diagrams similarly as in the last section, but now we analyse the case with three balls. We also show one-parameter bifurcation diagrams corresponding to vertical and horizontal transitions through the two-parameter bifurcation diagrams for specified fixed parameter. We will comment all the diagrams, and will highlight the differences with respect to the diagrams of the ADB system with two balls. Now for $n = 3$ balls, there are infinitely many balanced steady states due to the fact that there is a degree of freedom in the balance equations (3.6). To undertake the bifurcation analysis of the system, we will only consider one balanced equilibrium in which the third ball is fixed in the position $\phi_3 = \pi$. This balanced steady state will be identify as state **1**. For the coincident states there exist two states **2**$\pm$, whose sign corresponds to the sign of the arccosine in (3.9). For the in-line states there are two possibilities for the number of coincident balls, $m = 1$ and $m = 2$. However, as was explained in Chapter 3, these cases are equivalent because we are assuming that all the balls are identical. Hence, we will have two in-line steady states, and we will refer them as states **3**$\pm$, whose sign corresponds to the sign of the arccosine in (3.10).

Figure 4.5 shows a two-parameter bifurcation diagram for the ADB system with three balls upon variation of the dimensionless parameters $\Omega$ and $\mu$, while considering the fixed parameters $\zeta = \beta = \delta = 0.01$. Comparing its panel (b) with Fig.4.1(b), we can observe that now the pitchfork bifurcation curve PF1,2+ is positioned at a lower $\mu$ value. Effectively, this curve PF1,2+ appear for $\mu = \mu_c$, and in this case for three balls $\mu_c := \delta/n = 0.01/3 = 0.003333$, while in the case for two balls we have $\mu_c := \delta/n = 0.01/2 = 0.005$. Like for $n = 2$ balls, when $\mu < \mu_c$ the balanced state **1** does not exist, and when $\mu > \mu_c$ it always exists. Now for $n = 3$ balls, **1** achieves the stability only for high $\Omega$ values, that is, to the right of last Hopf bifurcation curves H1. Note the difference with respect to $n = 2$ balls. Now there does not exist a second region of stability bounded by a Hopf bifurcation curve

H1 for intermediate $\Omega$ values. Instead of that, there is an intersection between two Hopf bifurcation curves H1. These curves define the unique region of stability for the balanced state **1**. The coincident states **2**$\pm$ are born in saddle-node bifurcations SN2+- again. They have the same broad trends as for ADB with two balls. For $\mu < \mu_c$, the coincident state **2-** is always stable except inside a region bounded by a Hopf bifurcation curve H2-. For $\mu > \mu_c$, the onset of stability of **2-** appears for $\Omega$ values to the left of the left-most boundary of the wedge-shaped region bounded by the curves SN2+-. Inside this region, both states **2**$\pm$ do not exist. The stability of the state **2+** is never reached.

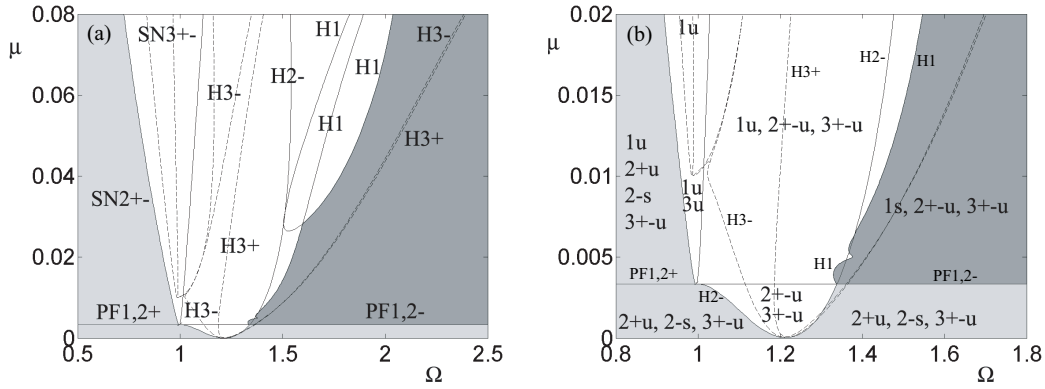


Figure 4.5: Two-parameter bifurcation diagram of steady state solutions of the ADB system with three balls in the $(\Omega, \mu)$-plane for $\zeta = \beta = \delta = 0.01$. Here SN stands for saddle-node bifurcation, PF for pitchfork bifurcation, and H for Hopf bifurcation. The numbers indicate which steady states are bifurcating. Broken lines correspond to bifurcation curves of the in-line states **3**$\pm$, and solid lines to states **1** and **2**$\pm$. Dark shading corresponds to the region of stability of the balanced state **1**, and light shading to the region of stability of the coincident state **2-**. Panel (b) shows a zoom of (a) for small values of $\mu$. The labels correspond to which of the states **1**,**2**$\pm$ or **3**$\pm$ exist, and letters $s$ and $u$ correspond to 'stable' and 'unstable' respectively.

Figure 4.5(b) shows that, as in the last section, the Hopf bifurcation curve H2- terminates at its low-$\Omega$ end in a codimension-two pitchfork-Hopf point. This point also marks the tip of the wedge-shaped region bounded by the curves SN2+-, that is, where the critical points $\Omega_{c1}$ and $\Omega_{c2}$ come together. Therefore, we can obtain this point analytically if we transform the inequality (3.16) into an equation in term of $\Omega$. Setting $\mu = \mu_c$ in this equation, it is shown that this first codimension-two pitchfork-Hopf point is defined by $K = 0$. Hence, we get

$$(\mu, \Omega) = (\mu_c, \Omega_c) := (\delta/n, 1/\sqrt{1 + n\mu_c}) = (\delta/n, 1/\sqrt{1 + \delta}) = (0.0033333, 0.9950372) \quad (4.2)$$

Note that the $\Omega_c$ value is in this case the same as for $n = 2$. That is, since $n\mu_c = \delta$, the expression for $\Omega_c$ does not depend on the number of balls $n$, so it is the same as for the ADB system with two balls, considering that we take the same eccentricity $\delta = 0.01$ in both cases. The second codimension-two pitchfork-Hopf point for which curve H2- meets the curve PF1,2- again is $(\mu, \Omega) = (\mu_c, 1.338096)$, that is, the same $\Omega$ value as for $n = 2$; see Fig.4.5(b).

The bifurcation curves of the in-line states **3**$\pm$ are the most different with respect to $n = 2$. Now there exist two saddle-node curves SN3+- where they are born. Inside the

region defined by these curves, the in-line states **3**± do not exist. We can see in Fig.4.5(b) that these curves SN3+- come together for $\mu = 0.01$, and that for $\mu < 0.01$ both in-line states **3**± always exist. This fact coincides with the existence conditions for states **3**± found at the end of Chapter 3. Effectively, there we saw that for $\mu < \delta/(2m-n)$ the in-line states **3**± always exist. Setting $\delta = 0.01$, $m = 2$, and $n = 3$ for this case, we have $\delta/(2m-n) = 0.01$, in agreement with the $\mu$ value obtained by numerical bifurcation. Another curve of Hopf bifurcations H3- terminates at the low-$\Omega$ end in the tip of the wedge-shaped region bounded by curves SN3+-. This point is defined by $K = 0$, and can be obtained from inequality (3.18) by setting $\mu = \delta/(2m-n)$. The coordinates of the point are

$$(\mu, \Omega) = (\delta/(2m-n), 1/\sqrt{1+n\mu}) = (0.01, 0.9853293). \tag{4.3}$$

The last thing we should mention about Fig.4.5 is the existence of other two Hopf bifurcation curves H3+ and H3-. They cross the middle of the parameter region, and become very close as $\Omega$ is increased.

Figure 4.6 shows one-parameter bifurcation diagrams corresponding to horizontal transitions through Fig.4.5(a) for $\mu = 0.05$, 0.005, and 0.0025. Here we can see the result of increasing $\Omega$ for different values of $\mu$. In the bifurcation diagram shown in panel (a) the horizontal transition is through $\mu = 0.05$, that is, $\mu > \mu_c := \delta/n = 0.0033333$, and $\mu > \delta/(2m-n) = 0.01$. In this case, since $\mu > \mu_c$ we can see that the balanced state **1** exists, and that the coincident states **2**± and the in-line states **3**± are both born in saddle-node bifurcation points SN2+- and SN3+-, respectively. The stability of the steady states are as it has already been commented in Fig.4.5. Namely, the balanced state **1** is stable for $\Omega$ values to the right of the last Hopf bifurcation point H1, and the coincident state **2-** for $\Omega$ values to the left of the first saddle-node bifurcation point SN2+-. The other states are always unstable.

In Fig.4.6(b) the value of the chosen fixed parameter is $\mu = 0.005$. In this case, because $\mu > \mu_c$, the balanced state **1** still exists, and the coincident states **2**± are still born in the saddle-node bifurcation points SN2+-. However, since $\mu < \delta/(2m-n)$, the saddle-node bifurcation points SN3+- have disappeared. Hence, the in-line states **3**± exist now for all the $\Omega$-range. The stability of the states is the same as that for $\mu = 0.05$. In Fig.4.6(c) the $\Omega$-bifurcation diagram is depicted for $\mu = 0.0025$, for which $\mu < \mu_c$ and $\mu < \delta/(2m-n)$. Therefore, in this picture it is possible to see that the balanced state **1** does not exist, and that there are no saddle-node points for coincident states **2**± or in-line states **3**±. Now, both coincident and in-line steady states exist for all $\Omega$-values, but the unique stable steady state is the coincident **2-**, which loses its stability between the two Hopf bifurcation points in the middle of the $\Omega$-range. The last thing to be mentioned about Fig.4.6(c) is that for small and high $\Omega$-values, the states **2-** and **3-** come together. The same fact happens for the states **2+** and **3+**.

Figure 4.7 shows one-parameter bifurcation diagrams corresponding to vertical transitions through Fig.4.5(a) for $\Omega = 0.5$, 1.25 and 1.5. Here we can see how the pitchfork bifurcation point character changes as $\Omega$ is increased. For $\Omega = 0.5 < \Omega_c$ (see panel (a)) the states bifurcating in the pitchfork bifurcation point PF1,2+ are **1** and **2+**, both unstable. When $\Omega$ becomes larger than $\Omega_c$, the states bifurcating are **1** and **2-**, so the state **2+** is changed to the state **2-**, that is, PF1,2+ turns being PF1,2-. At the beginning, both states **1** and **2-** bifurcating are still unstable as it is shown in panel (b). However, when $\Omega$

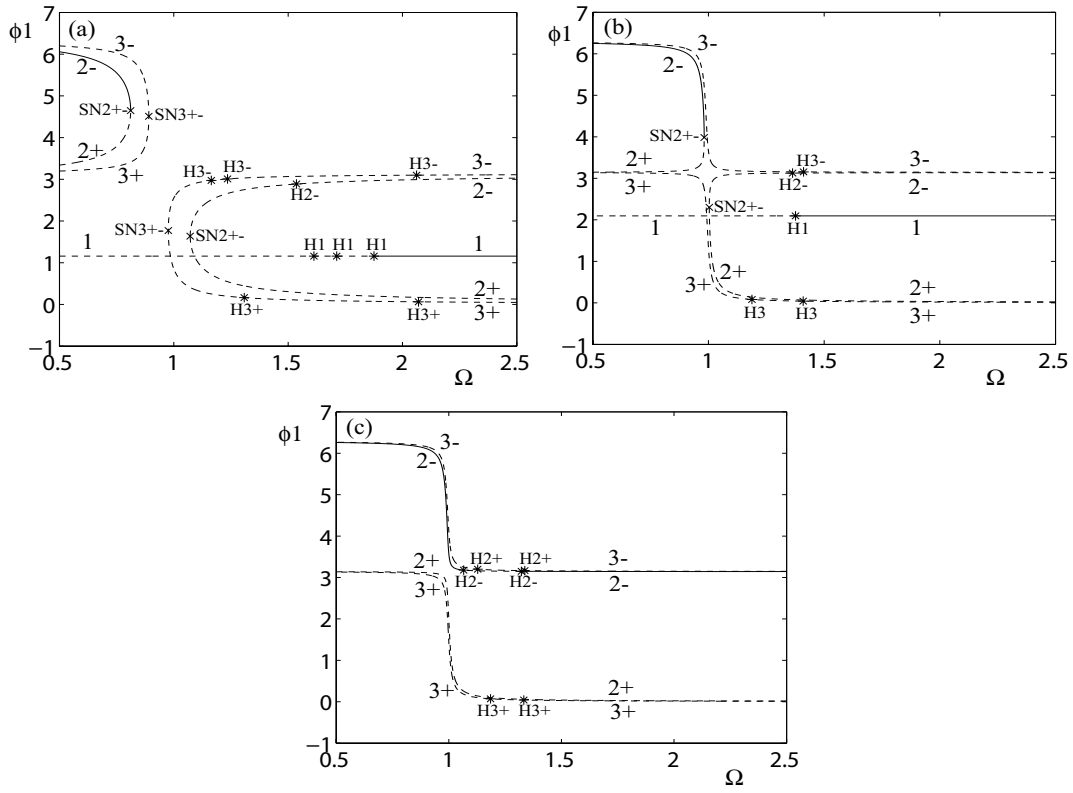


Figure 4.6: One-parameter bifurcation diagrams of steady state solutions of the ADB system with three balls. Panels (a), (b) and (c) show diagrams in $\Omega$ for $\mu = 0.05$, 0.005 and 0.0025, respectively. The solid lines correspond to stable states, and broken lines to unstable ones. Saddle-node (SN) bifurcations are marked by a ($\times$), and Hopf (H) bifurcations by a ($*$). The numbers indicate which steady states are bifurcating.

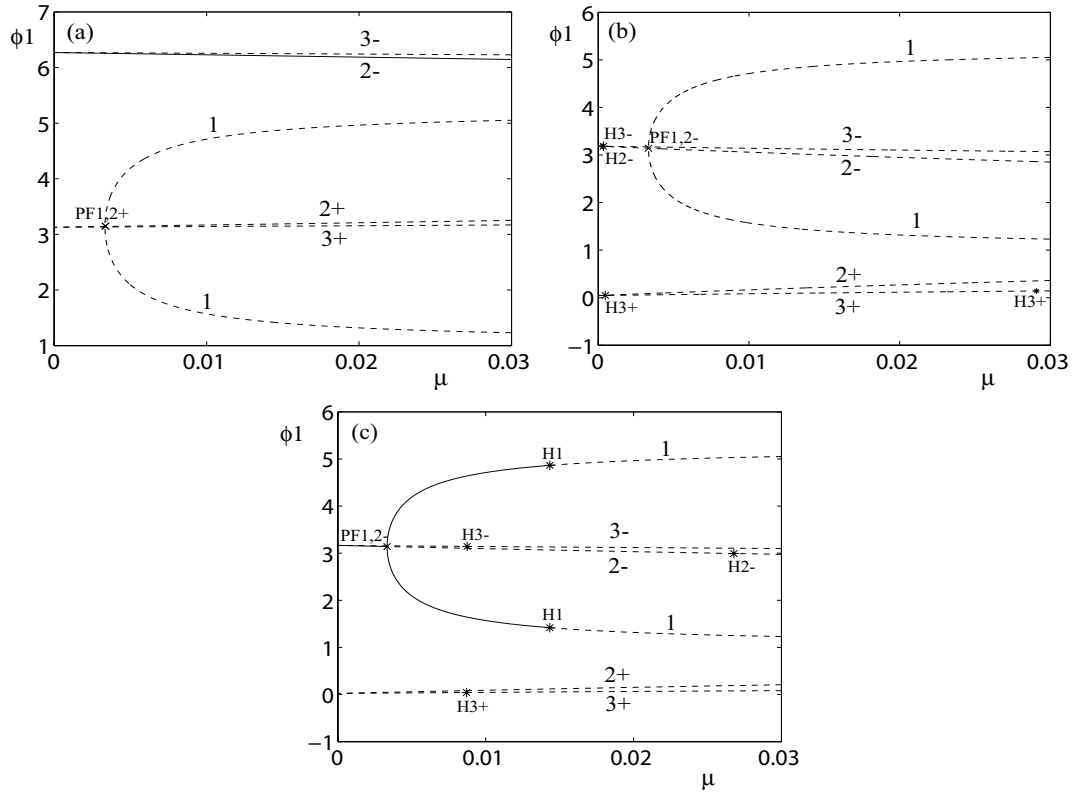


Figure 4.7: One-parameter bifurcation diagrams of steady state solutions of the ADB system with three balls. Panels (a), (b) and (c) show diagrams in $\mu$ for $\Omega = 0.5$, 1.25 and 1.5, respectively. The solid lines correspond to stable states, and broken lines to unstable ones. Pitchfork (PF) bifurcations are marked by a ($\times$), and Hopf (H) bifurcations by a ($*$). The numbers indicate which steady states are bifurcating.

goes over the second codimension-two pitchfork-Hopf point, the pitchfork bifurcation point changes its character again. It becomes supercritical so that the coincident state **2-** and the bifurcating balanced state **1** are both stable, as it is shown in panel (c). This same fact happened in the previous section, with the ADB system with two balls. Fig.4.7(a) also shows that the coincident state **2-** is always stable for small $\Omega$ values. In Figs.4.7 (b) and (c) in which $\Omega$ is larger, the stability of the coincident state **2-** is delimited by a Hopf bifurcation point H2-, and by a pitchfork bifurcation point PF1,2-, respectively. Fig.4.7 also shows that states **2-** and **3-** come together while $\mu$ is decreasing, as it was already shown in Fig.4.6(c). The same fact happens between the states **2+** and **3+**.

Let us now consider other two-parameter bifurcation analyses for the ADB with three balls. In Figure 4.8 we can see the two-parameter bifurcation diagrams in the $(\Omega, \delta)$-plane in panel (a), in the $(\Omega, \zeta)$-plane in (b), and in the $(\Omega, \beta)$-plane in (c). The parameters which do not vary in these diagrams are fixed at $\mu = 0.05$, and $\zeta = \beta = \delta = 0.01$. In Fig.4.8(a), we depict the range of $\delta$-values in which the balanced steady state exists, namely $0 \leq \delta \leq n\mu = 0.15$. In fact, for $\delta > n\mu$ the eccentricity is too large, and the ball masses are not big enough to balance the system ($\mu < \mu_c$). We can see in this panel (a) that the onset of stability of the states **1** and **2-** are similar to the ADB with two balls. The coincident state **2-** is stable for $\Omega$-values to the left of the left-most boundary of the wedge-shaped region bounded by SN2+-. For larger $\Omega$-values, that is, to the right of right-most Hopf bifurcation curves H1, the balanced steady state is stable. The stability of these steady states are hardly sensitive to $\delta$, the exception being for very low $\delta$-values, for which **2-** loses its stability.

The two-parameter bifurcation diagram in the $(\Omega, \zeta)$-plane which is shown in Fig.4.8(b), presents a big difference to the ADB system with two balls. In Fig.4.4(b) we saw that the balanced steady state stability for the case with two balls was approximately insensitive within $\zeta$ for $\Omega > 2.5$. That is, state **1** was found to be stable for the whole $\zeta$-range when $\Omega > 2.5$. However, Fig.4.8(b) shows that for the ADB with three balls, the state **1** is stable for large $\Omega$, but only for low $\zeta$-values. For example, we can see that for $\Omega = 3$, the balanced steady state is stable only for $\zeta < 0.02$. Therefore, an important conclusion we can extract is that the ADB system with three balls cannot offset the imbalance when the rotor damping $\zeta$ is too high. Finally, Fig.4.8(c) shows that the stability of **1** and **2-** in the $(\Omega, \beta)$-plane has the same broad trends as in the $(\Omega, \delta)$-plane as for the ADB with two balls (see Fig.4.4(c)). The only difference is that for very small ball damping $\beta$, steady state **1** becomes unstable.

Another point to note is that for intermediate values of $\Omega$ (between approximately 1.0 and 2.0), there are also several Hopf bifurcation curves of coincident and in-line steady states, and the saddle-node curves for the in-line steady states, which were already seen in the $(\Omega, \mu)$-plane (see Fig.4.5). For example, notice that in Fig.4.8(a), the SN3+- curves come together at $\delta = 0.05$, and they do not exist for larger $\delta$ values. Really, for $\delta > 0.05$ we have $\mu < \delta/(2m - n)$, and for these $\mu$ values we saw in Fig.4.5 that the saddle-node curves SN3+- disappeared. In Fig.4.8(b), the meeting point between the SN3+- curves is for $\zeta = 0$. In contrast, for Fig.4.8(c), the SN3+- curves are parallel, and they never meet each other. As in Fig.4.5, we can see in Fig.4.8(a) and (b) that a Hopf curve H3+- terminates in its low-$\Omega$ end at the top of the wedge-shaped region bounded by SN3+- curves. Definitively, we can see that there are big differences with the curves shown in Figs.4.4 for the case with two balls. However, since there is no change in stability of the steady states, they are not

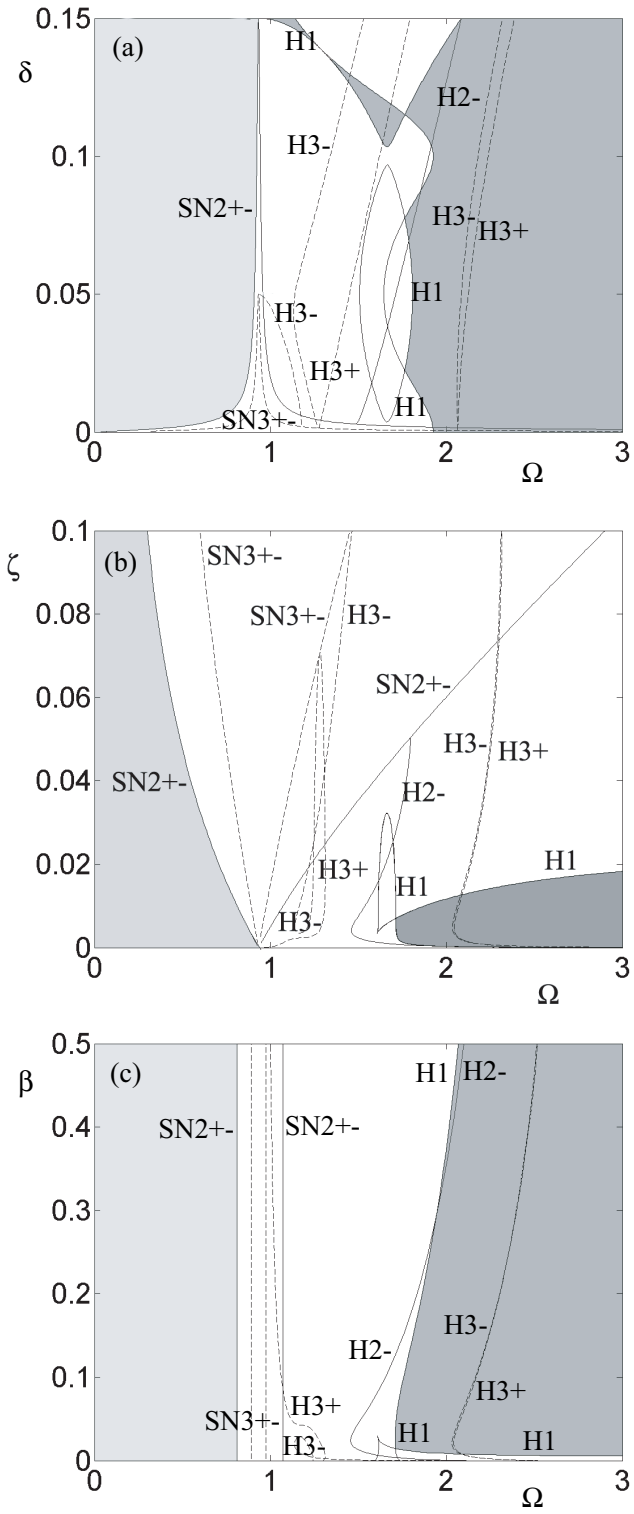


Figure 4.8: Two-parameter bifurcation diagrams of steady state solutions of the ADB system with three balls. Here SN stands for saddle-node bifurcation, PF for pitchfork bifurcation, and H for Hopf bifurcation. The numbers indicate which steady states are bifurcating. Broken lines correspond to bifurcation curves of the state **3**±, and solid lines to states **1** and **2**±. Dark shaded regions correspond to a stable balanced state **1** and light shaded regions to a stable unbalanced coincident state **2-**.In each panel the fixed parameters are $\mu = 0.05$, and $\beta = \delta = \zeta = 0.01$. The varying parameters are $\delta$ versus $\Omega$ (a), $\zeta$ versus $\Omega$ (b), and $\beta$ versus $\Omega$ (c).

important as they do not provide any modification to the stability behaviour of the system.

Let us study more deeply the loss of stability of the balanced state **1** which we have just seen in the $(\Omega, \zeta)$-bifurcation diagram (Fig.4.8(b)). We saw that the $\zeta$-range in which the balanced steady state is stable was very small. In Figure 4.9 we analyse how $\beta$ affects the stability of **1**. Panel (a) shows a two-parameter bifurcation diagram in the $(\zeta, \beta)$-plane, for $\Omega = 4$, $\delta = 0.01$, and $\mu = 0.05$. Here, it is shown that the $\zeta$-range in which **1** is stable grows linearly as $\beta$ increases. Thus, approximately for $\beta > 0.25$ the balanced state **1** is found to be stable in the whole represented range $0 < \zeta < 0.5$. As in Fig.4.8(c), the saddle-node curves SN2+- and SN3+- are vertical. That means that the coincident states **2**±, and the in-line states **3**± have little sensitivity to $\beta$. In fact, we note that $\beta$ does not appear in the analytic expression for the states **2**± and **3**± (see (3.9), and (3.10), respectively). In Fig.4.8(b) we depict another two-parameter bifurcation diagram in the $(\Omega, \zeta)$-plane, for an increased ball damping $\beta = 0.25$, and the values fixed $\delta = 0.01$, and $\mu = 0.05$. We can reassert that, for a higher $\beta$-value, the region of stability of the balanced state **1** is much larger (compare with Fig.4.8(b) in which $\beta = 0.01$). Now, for $\Omega = 3$, the state **1** is stable approximately for $\zeta < 0.5$. We can also see that, unlike for the ADB with two balls, for the ADB with three balls this stability region grows when $\Omega$ is increased. Finally, we can conclude that, in practical applications of the ADB with three balls, we will obtain better results (that is, the balance will be reached more often) if we take a high ball damping. We will demonstrate this with the help of simulation results in Chapter 5.

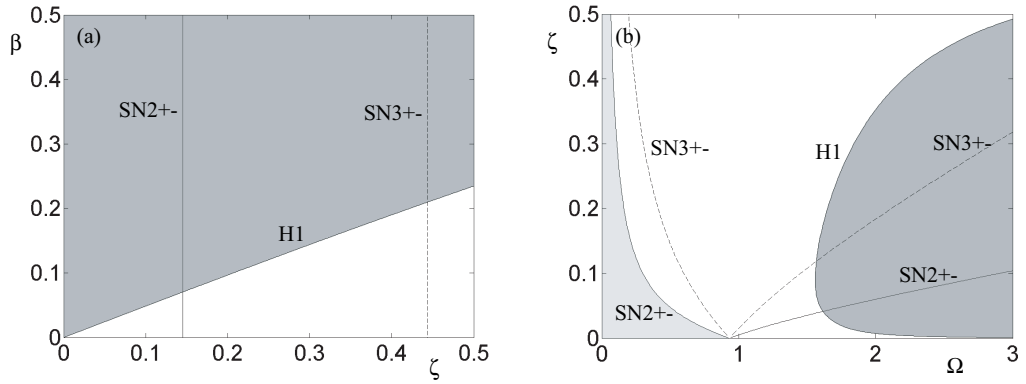


Figure 4.9: Two-parameter bifurcation diagrams of steady state solutions of the ADB system with three balls. Panel (a) shows a $(\zeta, \beta)$-plane diagram, with $\Omega = 4$, $\delta = 0.01$, and $\mu = 0.05$. Panel (b) shows a $(\Omega, \zeta)$-plane diagram, with $\beta = 0.25$, $\delta = 0.01$, and $\mu = 0.05$. Here SN stands for saddle-node bifurcation, and H for Hopf bifurcation. The numbers indicate which steady states are bifurcating. Broken lines correspond to bifurcation curves of the state **3**±, and solid lines to states **1** and **2**±. Dark shaded regions correspond to a stable balanced state **1** and light shaded regions to a stable unbalanced coincident state **2-**.

## 4.3 Numerical bifurcation diagrams for ADB with four balls

In this section we obtain some bifurcation diagrams, in one-parameter and in two-parameter planes, for the ADB system with four balls. We will highlight the differences with respect to the bifurcation diagrams for the cases with two and three balls. In the case of the ADB

system with four balls, as for the ADB with three balls, there are infinitely many balanced steady states due to the fact that there are two degrees of freedom in the balance conditions (3.6). To perform the bifurcation analysis of the system, we will only consider one balanced steady state in which the third and the fourth balls are fixed at the position $\phi_3 = \pi$ and $\phi_4 = -\pi$. We will call it state **1**. For the coincident steady states, there exist two states **2**$\pm$, whose sign corresponds to the sign of the arccosine in (3.9). For the in-line states there are three possible values for the number of coincident balls, $m = 1$, $m = 2$ and $m = 3$. However, as was explained in Chapter 3, the cases with $m = 1$ and $m = 3$ are equivalent because we are assuming that all the balls are identical. Moreover, in the case $m = 2$, the state 3(4-2)+ is physically the same as the state 3(4-2)-. Therefore, we will have an in-line state with two coincident balls, called **3A**, and two in-line states with three coincident balls, called **3B**$\pm$, whose sign corresponds to the sign of the arccosine in (3.10).

Figure 4.10 shows a two-parameter bifurcation diagram for the ADB system with four balls upon variation of the dimensionless parameters $\Omega$ and $\mu$, while considering the fixed parameters $\zeta = \beta = \delta = 0.01$. To avoid confusion in the diagram, bifurcation curves of the in-line state **3A** are drawn with dotted lines, curves of the in-line states **3B**$\pm$ are drawn with broken lines, and bifurcation curves of the balanced state **1** and of the coincident states **2**$\pm$ with solid lines.

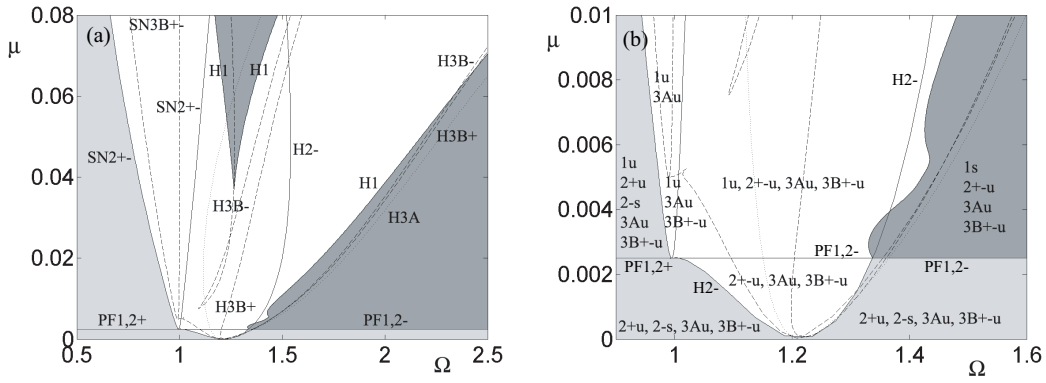


Figure 4.10: Two-parameter bifurcation diagram of steady state solutions of the ADB system with four balls in the $(\Omega, \mu)$-plane for $\zeta = \beta = \delta = 0.01$. Here SN stands for saddle-node bifurcation, PF for pitchfork bifurcation, and H for Hopf bifurcation. The numbers indicate which steady states are bifurcating. Dotted lines correspond to Hopf bifurcation curves of the state **3A**, dashed lines correspond to bifurcation curves of the state **3B**$\pm$, and solid lines to states **1** and **2**$\pm$. Dark shading corresponds to the region of stability of the balanced state **1**, and light shading to the region of stability of the coincident state **2-**. Panel (b) shows a zoom of (a) for small values of $\mu$. The labels correspond to which of the states **1**, **2**$\pm$, **3A** or **3B**$\pm$ exist, and letters $s$ and $u$ correspond to 'stable' and 'unstable' respectively.

For the ADB with four balls, the critical ball mass is less than for two and three balls, when the eccentricity $\delta$ is fixed at the same value for the three cases. For the given fixed parameters we get $\mu_c := \delta/n = 0.01/4 = 0.0025$. Thus, we can see in Fig.4.10(b) that for $\mu < \mu_c = 0.0025$ the balanced state **1** does not exist. Hence, to offset the imbalance produced by a fixed eccentricity $\delta$, the ADB system with four balls would need smaller balls

(that is, lower $\mu$ values) than the ADB with two and three balls. From another point of view, we could say that, if we had balls with a specific mass, the ADB with four balls would be able to balance the system with a larger eccentricity $\delta$, which could not be balanced by an ADB with two or three balls.

Considering the region of stability of the balanced state **1**, we can observe in Fig.4.10 that is the same as with two balls (see Fig.4.1). There exist two different regions, one for large $\Omega$-values to the right of the right-most Hopf bifurcation curve H1, and another inside the region bounded by the curve H1 for intermediate $\Omega$-values. However, as we saw in Fig.4.5 for $n = 3$, this stability region for intermediate $\Omega$-values disappears in the case for three balls.

The coincident states **2**$\pm$ for four balls have similar bifurcation curves as the ADB with two and three balls, but with a different $\mu$ scale. In fact, if we represented these curves in the $(\Omega, n\mu)$-plane, the bifurcation curves of the coincident states would be the same for two, three, and four balls. That means that the bifurcation analysis of the coincident state is the same for ADB with different numbers of balls, if the total ball mass $n\mu$ is the same in all the systems. Effectively, a coincident steady state for the ADB with $n$ balls consists in $n$ balls coinciding in the same position; this state is physically equivalent to an out of balance equilibrium for an ADB with one ball with mass equal to $n\mu$. Hence, all the ADB system with similar total ball mass $n\mu$ have equivalent coincident steady states. As we can see in Fig.4.10, there exists again a Hopf curve H2- which collides with the pitchfork bifurcation curve PF1,2- in two codimension-two pitchfork-Hopf points. The $\Omega$-coordinates of these points are the same as for two and three balls, although now the $\mu$-coordinates are smaller. Effectively, the $\mu$-coordinate of these points coincides with $\mu_c$, so now for $n = 4$ we have $\mu_c = \delta/n = 0.0025$, which is smaller than for two balls (0.005), and than for three balls (0.003333). We can also observe that the stability region of the states **2**$\pm$ is similar as for two and three balls. State **2-** is stable for $\mu < \mu_c$ and for $\Omega$-values to the left of the left-most boundary of the wedge-shaped region bounded by curves SN2+-, while the state **2+** is always unstable.

Let us now consider the bifurcation curves of the in-line states. The dotted line in Fig.4.10 represents the unique Hopf curve for the state **3A**. This curve is similar to the Hopf curve H3 of the state **3** for two balls (see Fig.4.1). Furthermore, if we represent $n\mu$ instead of $\mu$, these both curves would be the same. Really, the state **3A** consists in two balls which coincide in a specific position, while the other two balls are coincident at the opposite side of the disc. Since we are assuming identical balls, this state is physically the same that an in-line state for two balls with larger mass (exactly the double). Hence, we can say that the in-line state **3A** for an ADB with four balls is equivalent to the in-line state **3** for an ADB with two balls with double mass. The dashed lines in Fig.4.10 correspond with the bifurcation curves of the states **3B**$\pm$. For these steady states, there are three balls coinciding in the same position, and the other ball is positioned in line with the centre of rotation. This equilibrium is similar to an in-line steady state for two balls with different masses. This same fact happen to the in-line states **3**$\pm$ for three balls, which is also similar to an in-line state for two different balls. Therefore, there is a similitude between the states **3B**$\pm$ for four balls, and the states **3**$\pm$ for three balls, as we can see comparing Fig.4.10 with Fig.4.5. Effectively, as for the state **3**$\pm$ for three balls, there exist two saddle-node curves SN3B+- for states **3B**$\pm$ for four balls. These curves come together

at $\mu = \delta/(2m-n) = 0.01/(2\cdot 3-4) = 0.005$. Besides these curves, there exist other Hopf bifurcation curves H3B+ and H3B- in the middle of the $(\Omega,\mu)$-plane. One of the H3B- curves terminates in its low-$\Omega$ end in the tip of the region bounded by SN3B+- curves, at a $\Omega$ value defined by $K = 0$. Specifically we get

$$(\mu,\Omega) = (\frac{\delta}{2m-n}, 1/\sqrt{1+n\mu}) = (0.005, 0.9901). \tag{4.4}$$

The in-lines states **3A** and **3B**$\pm$ are all unstable in the whole $(\Omega,\mu)$-plane.

Figure 4.11 shows one-parameter bifurcation diagrams corresponding to horizontal transitions through Fig.4.10(a). In panels (a) and (b) we take the fixed parameter $\mu = 0.05$, and 0.004, respectively, which satisfy $\mu > \mu_c = 0.0025$. In panel (c) we take $\mu = 0.002$, that is, $\mu < \mu_c$. States **1** and **2**$\pm$ are found to be similar as for two balls (see Fig.4.2) and three balls (see Fig.4.6). In panels (a) and (b) in which $\mu > \mu_c$ the coincident states **2**$\pm$ are born in two saddle-node points SN2+-, and the balanced state **1** exist for all the $\Omega$-range. However, for $\mu < \mu_c$ (see panel (c)), the saddle-node points SN2+- disappear, and the balanced state **1** does not exist.

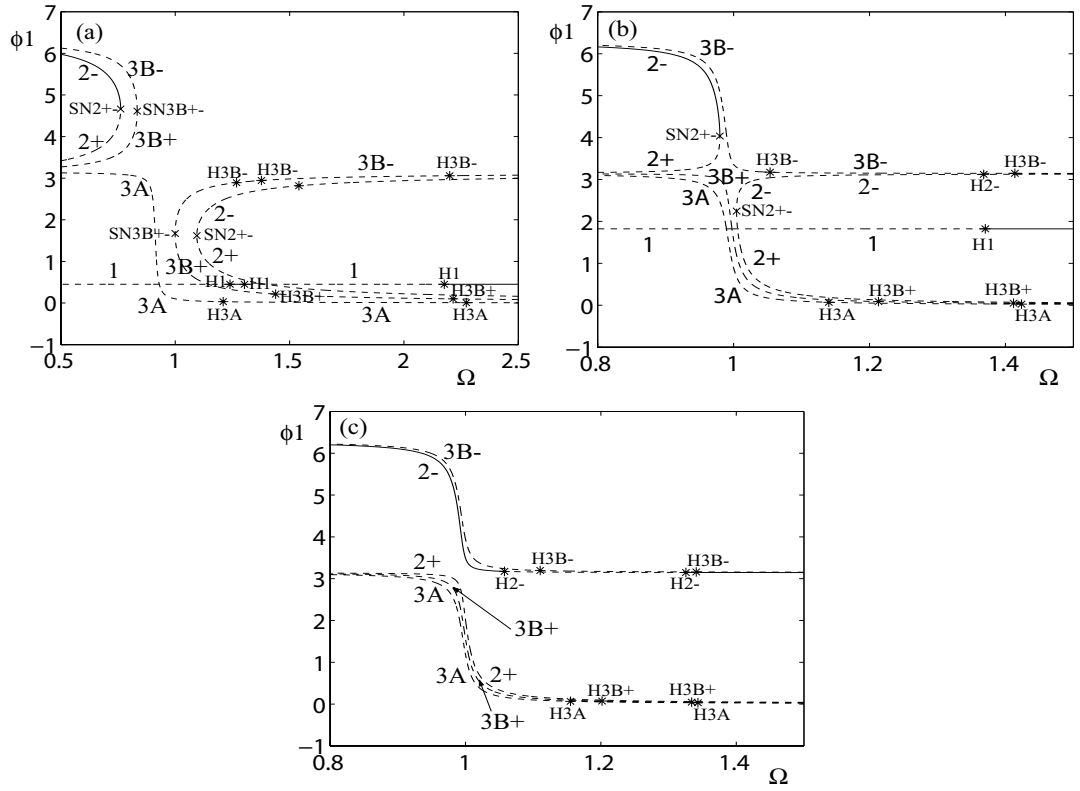


Figure 4.11: One-parameter bifurcation diagrams of steady state solutions of the ADB system with four balls. Panels (a), (b) and (c) show diagrams in $\Omega$ for $\mu = 0.05$, 0.004 and 0.002, respectively. The solid lines correspond to stable states, and broken lines to unstable ones. Saddle-node (SN) bifurcations are marked by a ($\times$), and Hopf (H) bifurcations by a ($*$). The numbers indicate which steady states are bifurcating.

As we have already commented in a previous paragraph, we can see in Fig.4.11 that the in-line state **3A** is similar to the state **3** for the ADB with two balls depicted in Fig.4.2. It exists for all the $\Omega$-range. Effectively, for this in-line state we have $m = 2$ coincident balls (with $n = 4$), so $\delta/(2m - n) \to \infty$, and the existence condition for the in-line states (3.18) is always satisfied. As we also said, Fig.4.11 shows that the states **3B**$\pm$ are similar to the in-line states **3**$\pm$ for the ADB with three balls (see Fig.4.6). Now $m = 3$, so $\delta/(2m-n) = 0.005$. Hence, in panel (a) in where $\mu = 0.05 > \delta/(2m-n)$ the states **3B**$\pm$ are born in the saddle-node points SN3B+-, and in panels (b) and (c) in where $\mu = 0.004$ and 0.002, respectively, which satisfy $\mu < \delta/(2m - n)$, the points SN3B+- disappear. Finally, we can observe that for small $\mu$ (see panels (b) and (c)), the coincident state **2-**, and the in-line state **3B-** come together to the imbalance side ($\phi_1 = 2\pi$) while decreasing $\Omega$, and for increasing $\Omega$ they come together to the balance side ($\phi_1 = \pi$). The same fact is found for the coincident state **2+**, and the in-line states **3A** and **3B+**, but now for large $\Omega$ the balls come to the imbalance, and for small $\Omega$ the balls come to the balance side. Therefore, we can suggest that for high $\Omega$ values the states **2-** and **3B-** cause a smaller radial vibration than the rotor without the ADB mechanism, and for low $\Omega$ values the reduction of the vibration is produced by the states **2+** and **3B+**. We cannot say anything about the state **3A**, because when two of the balls stand near the imbalance, the other two would stand at the opposite side, that is, the balance side.

Figure 4.12 shows one-parameter bifurcation diagrams corresponding to vertical transitions through Fig.4.10(a) for $\Omega = 0.5$, 1.25, and 1.5, respectively. In these, we can observe that, as happened for two and three balls, the pitchfork bifurcation point changes its character when $\Omega$ is increased. Thus, for $\Omega = 0.5 < \Omega_c$ the bifurcating states are **1**, and **2-**, while when $\Omega$ becomes larger than $\Omega_c$, the state **2-** is changed by the state **2+**. Hence, we can see that from panel (a) to panels (b) and (c), the pitchfork bifurcation points changes from PF1,2+ to PF1,2-. The other character change is experimented from panel (b) to (c). Effectively, we can see that in Fig.4.12(b) both bifurcating states are unstable, while in Fig.4.12(c) they become stable. The balanced state **1** is always born in this pitchfork bifurcation point, but it only becomes stable when $\Omega$ is to the right of the second codimension-two pitchfork-Hopf point. Thus, we can see in panel (c) in which $\Omega = 1.5$ that the state **1** is stable between PF1,2- and H1. Fig.4.12 also shows that the coincident state **2-** is stable for all $\mu$ values when $\Omega$ is small (panel (a) in which $\Omega = 0.5$). For $\Omega > \Omega_c$, the region of stability of **2-** becomes smaller, delimited by the curve H2- in panel (b), and for the curve PF1,2- in panel (c). Finally, with Fig.4.12 we can corroborate what we said in last paragraph. Really, we see that in panel (a) in which $\Omega < \Omega_c$ the states **2-** and **3B-** come near the imbalance, that is, $\phi_1 \approx 2\pi$, and that in panels (b) and (c) in which $\Omega > \Omega_c$ they come at the balance side ($\phi_1 \approx \pi$). In contrast, the states **2+**, **3A**, and **3B+** come near the imbalance when $\Omega > \Omega_c$ (in panels (b) and (c)), and they come at the balance side when $\Omega < \Omega_c$ (panel (a)).

As we made for the ADB with two balls, and for the ADB with three balls, we now analyse the stability of the steady state solutions for other varying dimensionless parameters. Figure 4.13(a) shows a two-parameter bifurcation diagram in the $(\Omega, \delta)$-plane. We represent the $\delta$-range in which the balanced steady state exists, that is, $\delta < 0.2$. Effectively, for $\delta > 0.2$ we have $\mu_c > 0.05$, and therefore the fixed $\mu = 0.05$ does not satisfy $\mu > \mu_c$, which is the ball mass condition necessary for the balanced steady state to exist. The stability of the steady states in this $(\Omega, \delta)$-plane is similar to the stability for ADB with two balls (see Fig.4.4(a)) and for ADB with three balls (see Fig.4.8(a)). Thus, the coincident

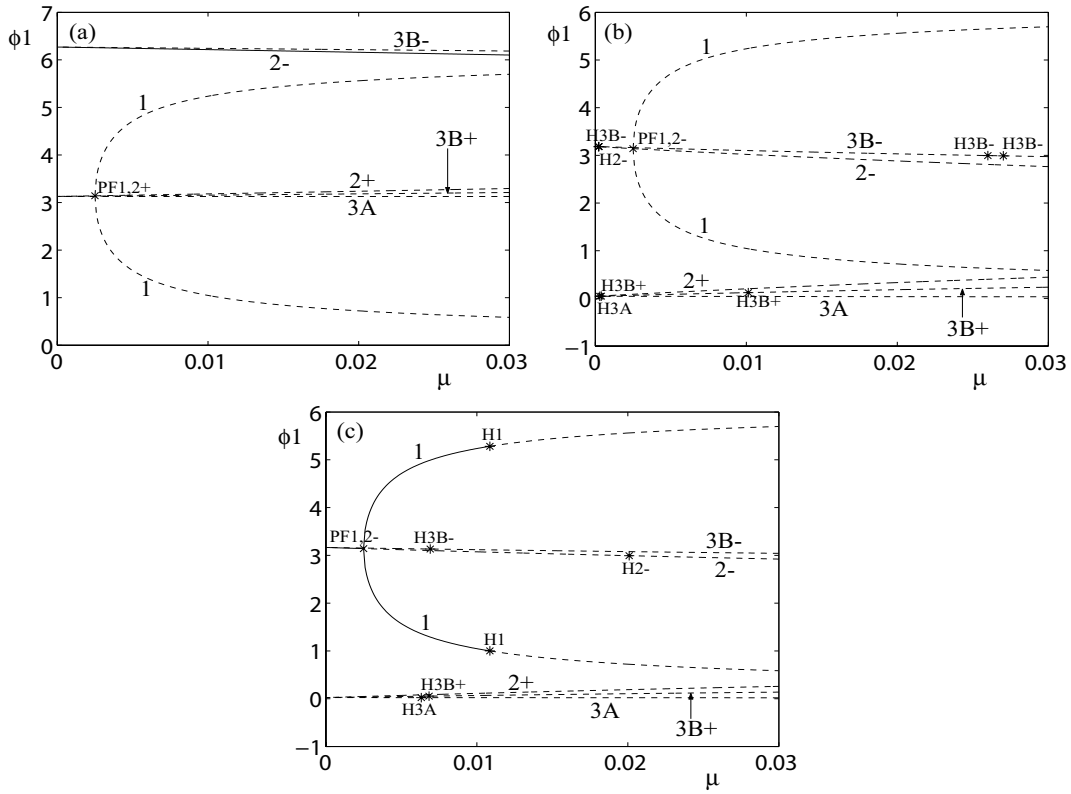


Figure 4.12: One-parameter bifurcation diagrams of steady state solutions of the ADB system with four balls. Panels (a), (b) and (c) show diagrams in $\mu$ for $\Omega = 0.5$, 1.25 and 1.5, respectively. The solid lines correspond to stable states, and broken lines to unstable ones. Pitchfork (PF) bifurcations are marked by a ($\times$), and Hopf (H) bifurcations by a ($*$). The numbers indicate which steady states are bifurcating.

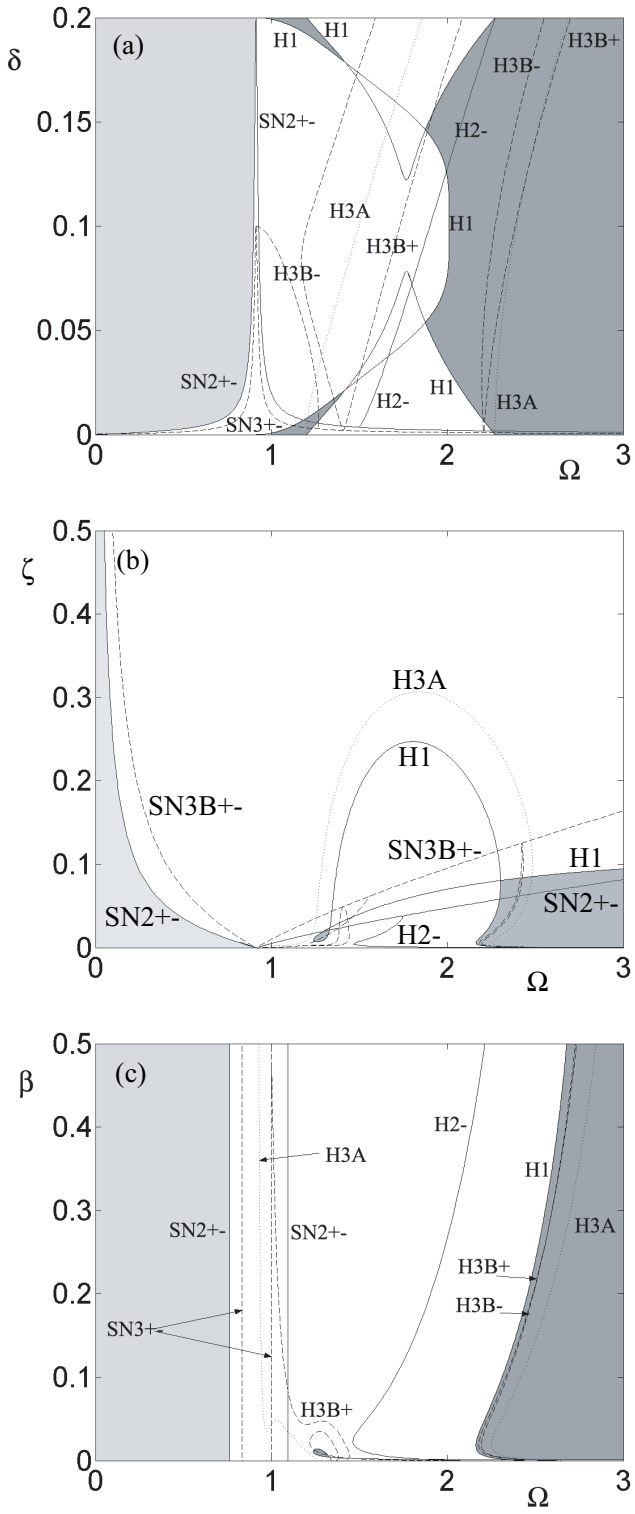


Figure 4.13: Two-parameter bifurcation diagrams of steady state solutions of the ADB system with four balls. Here SN stands for saddle-node bifurcation, PF for pitchfork bifurcation, and H for Hopf bifurcation. The numbers indicate which steady states are bifurcating. Dotted lines correspond to Hopf bifurcation curves of the state **3A**, dashed lines correspond to bifurcation curves of the states **3B**$\pm$, and solid lines to states **1** and **2**$\pm$. Dark shaded regions correspond to a stable balanced state **1** and light shaded regions to a stable unbalanced coincident state **2-**. In each panel the fixed parameters are $\mu = 0.05$, and $\beta = \delta = \zeta = 0.01$. The varying parameters are $\delta$ versus $\Omega$ (a), $\zeta$ versus $\Omega$ (b), and $\beta$ versus $\Omega$ (c).

state **2-** is stable for small $\Omega$, to the left of the left-most boundary of the region bounded by the curves SN2+-. The balanced state **1** is stable for the represented $\delta$-range for large $\Omega$, approximately when it is larger than 2.5. There exists another small region of stability of **1** for intermediate $\Omega$-values, and small and large $\delta$. In Fig.4.13(b) we can see that, like for ADB with three balls, the region of stability of the balanced state **1** in the $(\Omega, \zeta)$-plane is smaller than for ADB with two balls. Thus, state **1** is stable when $\Omega$ is large, but only for low $\zeta$-values. For example, when $\Omega = 3$, **1** is only stable for $\zeta < 0.1$. Comparing with ADB with three balls (see Fig.4.8(b)), the reduction of the stability region of **1** is now less. The region of stability of the coincident state **2-** is found to be similar as the region for two and three balls. The stability diagram in the $(\Omega, \beta)$-plane shown in Fig.4.13(c) is found to be very similar as for ADB with two balls, and as for ADB with three balls. The coincident state **2-** is stable, like in the other diagrams, for small $\Omega$, to the left of the left-most saddle-node curve SN2+-. This region of stability is not sensitive to $\beta$, as shows the fact that the curves SN2+- are vertical. The region of stability of the balanced state **1** has little sensitivity to $\beta$, and we can affirm that approximately for $\Omega > 2.5$ **1** is stable for all $\beta$ values.

Besides the regions of stability of the steady states **1** and **2-**, the bifurcation diagrams akin to Fig.4.13 show the bifurcation curves of all the steady states. The dotted line corresponds to the Hopf bifurcation curve H3A of the in-line state **3A**. The saddle-node curves SN3B+-, and the Hopf curves H3B+ and H3B-, are depicted by dashed lines. Besides the curves SN2+-, the coincident state **2-** has a Hopf bifurcation curve H2- represented by filled line. These curves are not important in the sense that they do not change the stability of the bifurcating states, so they do not require more comments.

Figure 4.14 analyses the effect of the ball damping $\beta$ on the stability of the balanced state **1** for the ADB system with four balls. In panel (a), we can see a stability diagram in the $(\zeta, \beta)$-plane, while fixed $\Omega = 4$, $\delta = 0.01$, and $\mu = 0.05$. We observe qualitatively similar results as for the ADB with three balls (see Fig.4.9(a)), that is, the $\zeta$-range for which **1** is stable grows linearly while $\beta$ increases. However, now for the ADB with four balls, the region of stability of **1** is larger than for ADB with three balls. Thus, when $\beta$ is approximately larger than 0.05, **1** is stable for all the values of the represented $\zeta$-range $(0 < \zeta < 0.5)$, while for the ADB with three balls, this $\beta$-value is higher (approximately 0.2).

Fig.4.14(b) depicts a $(\Omega, \zeta)$-bifurcation diagram for an increased ball damping $\beta = 0.25$, and for the fixed $\delta = 0.01$ and $\mu = 0.05$. It is found that the region of stability of the balanced state **1** is much larger than for $\beta = 0.01$ (compare with Fig.4.13(b)). Comparing with the ADB with three balls (see Fig.4.9(b)), we see again that this region is larger for the ADB with four balls. In summary, we conclude that, like for the ADB with three balls, a large ball damping $\beta$ makes the balanced state **1** to be stable in a larger $\zeta$-range. Finally, we can recommend that to secure the stability of the balanced state **1** for the ADB mechanism with four balls, it should be taken a small rotor damping $\zeta$, and a large ball damping $\beta$.

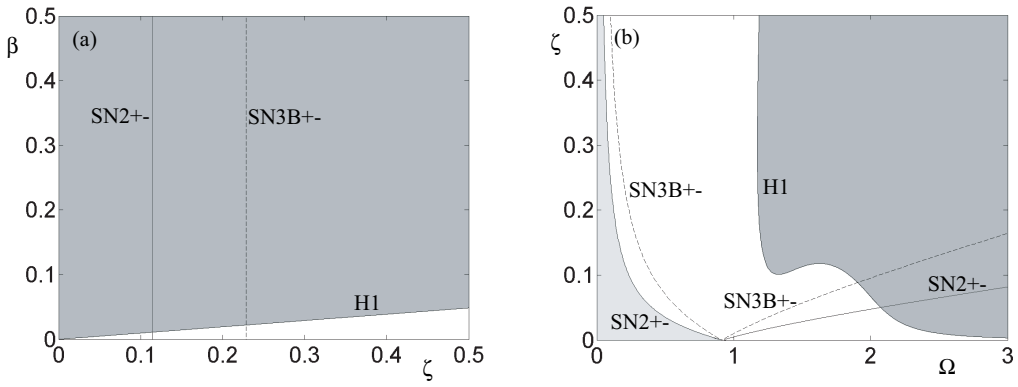


Figure 4.14: Two-parameter bifurcation diagrams of steady state solutions of the ADB system with four balls. Panel (a) shows a $(\zeta, \beta)$-plane diagram, with $\Omega = 4$, $\delta = 0.01$, and $\mu = 0.05$. Panel (b) shows a $(\Omega, \zeta)$-plane diagram, with $\beta = 0.25$, $\delta = 0.01$, and $\mu = 0.05$. Here SN stands for saddle-node bifurcation, PF for pitchfork bifurcation, and H for Hopf bifurcation. The numbers indicate which steady states are bifurcating. Broken lines correspond to bifurcation curves of the state **3B**$\pm$, and solid lines to states **1** and **2**$\pm$. Dark shaded regions correspond to a stable balanced state **1** and light shaded regions to a stable unbalanced coincident state **2-**.

# Chapter 5

# Transient analysis of the ADB system

In this chapter we carry out a transient analysis of the ADB system with two, three, and four balls. We show results obtained by direct numerical integration of the governing equations (2.25) and (2.26) derived in Chapter 2. In our experiments, we use the `Matlab` routine `ode45`.

The chapter is divided into two sections. In one of them we study how the initial conditions affect the transient response of the system and the stability of the balanced state. For that, we undertake several numerical runs, for a specific parameter set, and compare the results obtained for different initial conditions. Firstly, we study the effect of the initial position and velocity of the centre of rotation. After that, different initial positions of the balls are studied, and we try to obtain an optimal configuration to apply in practical applications of the ADB mechanism. Finally, we see what differences appear when the balls are initially held fixed in an external, rather than rotating reference frame. In each case, we analyse the possible differences between the ADB with two, three, and four balls, for similar ball mass $\mu$. In the second section of the chapter, we study the effects of parameter variation. We make numerical runs with specific initial conditions for two, three and four balls, and we compare the obtained results for each system. A detailed study is performed to analyse the effects of both ball and rotor damping on the system, following the highlighted sensitivity to these parameters in the previous chapter. As a final point, we represent the maximum amplitude of the radial vibration, and the transient length in an $\Omega$ and a $\delta$-ranges, for random initial positions of the balls. These graphs could be useful to know approximately which results will be useful in practical experiments.

## 5.1 Effects of the initial conditions

We will discuss how the initial conditions affect the response of the system. For that, a large number of numerical runs were conducted for many different initial conditions values, and for the parameter set

$$\Omega = 4, \quad \zeta = \delta = \beta = 0.01, \quad \mu = 0.05. \tag{5.1}$$

This particular value of parameter was chosen since in [9] a coexistence between the stable balanced state **1** and a stable limit cycle oscillation was identified in the ADB system with two balls. The main points to consider in the response of the system are the maximum amplitude of the radial vibration, how long the transient is, and which the dynamic attraction is (that is, if the system goes to a steady state or to another dynamic behaviour as limit cycle or chaotic motion).

### 5.1.1 Initial position and velocity of the centre of rotation

In Figures 5.1, 5.2 and 5.3, both the amplitude of the radial vibration ($r = \sqrt{x^2 + y^2}$) and the position of the balls ($\phi_i$) are plotted against the dimensionless time, for the ADB system with two balls, three balls, and four balls, respectively. A statistical normal variable with $\mu_s = 0$ and $\sigma_s = 0.1$ was used to choose the initial position of the centre of rotation of the system and its initial velocity ($x(0)$, $y(0)$, $\dot{x}(0)$, $\dot{y}(0)$): (-0.0433, 0.0125, -0.1666, 0.0288) in panels (a1)-(a2), (-0.1146, 0.1189, 0.1191, -0.0038) in panels (b1)-(b2) , (0.0327, -0.0187, 0.0175, 0.0726) in panels (c1)-(c2) and (-0.0588, -0.0136, 0.2183, 0.0114) in panels (d1)-(d2). The initial positions of the balls were fixed at $\phi_1(0) = \pi/2$ and $\phi_2(0) = -\pi/2$ for ADB with two balls (Figure 5.1), $\phi_1(0) = \pi/2$, $\phi_2(0) = -\pi/2$ and $\phi_3(0) = \pi$ for ADB with three balls (Figure 5.2), and $\phi_1(0) = \pi/2$, $\phi_2(0) = -\pi/2$, $\phi_3(0) = \pi$ and $\phi_4(0) = 0$ for ADB with four balls (Figure 5.3). In all the cases the initial velocity of the balls was set to zero, that is, $\dot{\phi}_i(0) = 0$ for $i = 1, \ldots, n$.

Figure 5.1 shows that the responses in the ADB with two balls for the different values of $x(0)$, $y(0)$, $\dot{x}(0)$ and $\dot{y}(0)$ are very similar. In all the cases the system achieves the balance in a similar time, more or less when $t = 600$. There is a small difference in the maximum amplitude of the radial vibration between the different panels, but they always have the same order of magnitude. For the ADB system with three balls (see Figure 5.2), there are also similarities in all its panels in the time in which the balance is achieved, and in the order of magnitude of the maximum amplitude of the radial vibration during the transient. However, now the balls achieve different positions in each panel after the transient is finished. The reason is that when the ADB has more than two balls, there are infinitely many configurations which are able to reach the balance of the system. In Figure 5.3 it is possible to see these same facts for the ADB system with four balls.

We notice that in the three Figures 5.1, 5.2 and 5.3, (b1) is the panel in which the maximum amplitude of the radial vibration is largest. This panel corresponds with the highest initial radial vibration value. Hence, we can say that the initial position of the centre of rotation and its velocity can affect the maximum amplitude of the radial vibration during the transient. However, as a conclusion, it has been demonstrated that the response of the system has little sensitivity to $x(0)$, $y(0)$, $\dot{x}(0)$ and $\dot{y}(0)$, in the sense that the same dynamic attraction (the balanced steady state in this case) always is achieved , and that the decay time does not vary significantly. Therefore, in the following we will always consider $x(0) = y(0) = \dot{x}(0) = \dot{y}(0) = 0$.

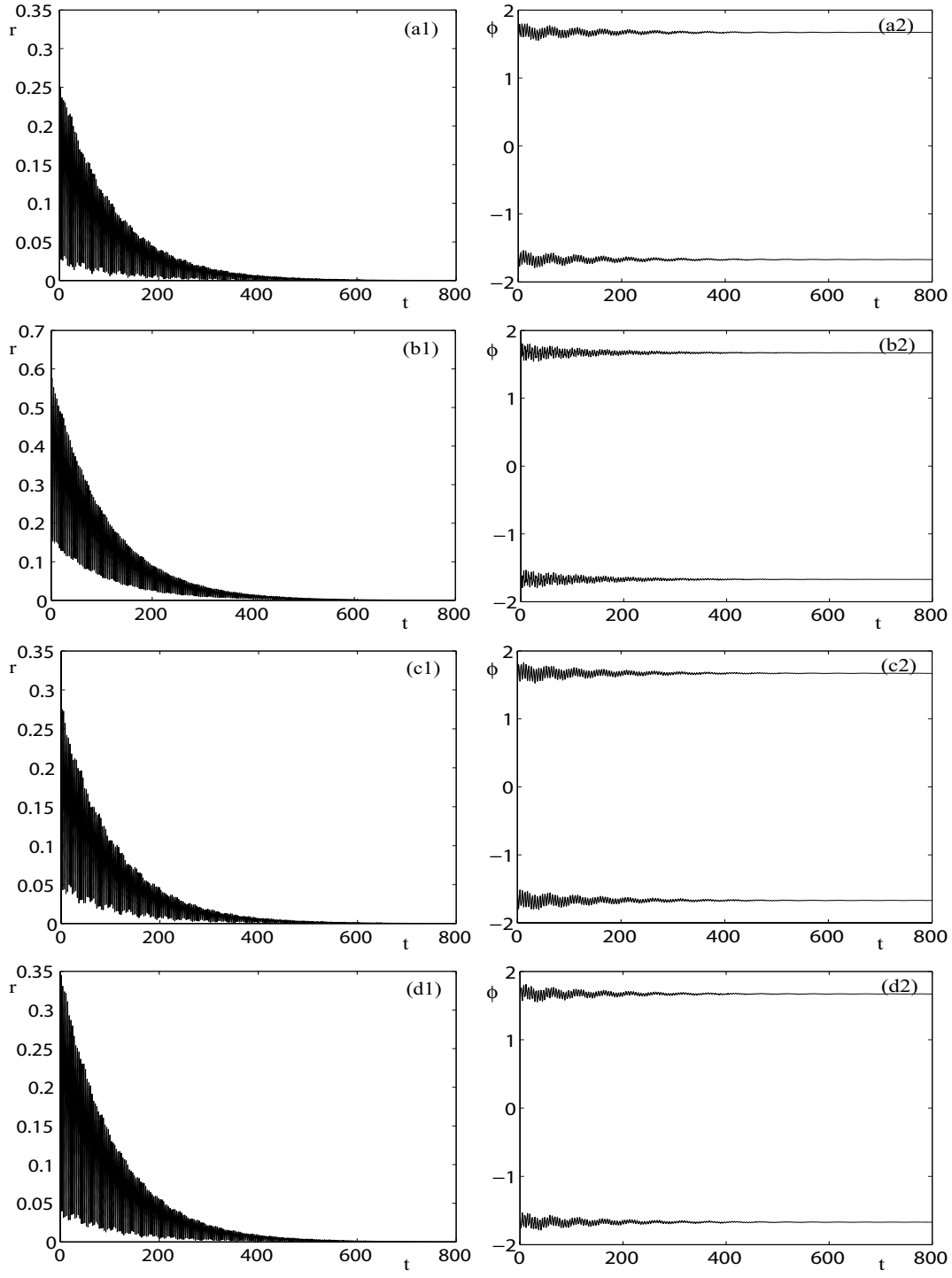


Figure 5.1: Numerical simulations of the ADB system with two balls for the parameter set $\Omega = 4.0$, $\zeta = 0.01$, $\beta = 0.01$, $\delta = 0.01$, and $\mu = 0.05$, with random initial conditions. The initial position of the centre of rotation and its velocity $(x(0), y(0), \dot{x}(0), \dot{y}(0))$ were chosen randomly with a statistical normal variable with $\mu_s = 0$ and $\sigma_s = 0.1$; their values were $(-0.0433, 0.0125, -0.1666, 0.0288)$ for panels (a1)-(a2), $(-0.1146, 0.1189, 0.1191, -0.0038)$ for panels (b1)-(b2) , $(0.0327, -0.0187, 0.0175, 0.0726)$ for panels (c1)-(c2), and $(-0.0588, -0.0136, 0.2183, 0.0114)$ for panels (d1)-(d2). The initial position of the balls and their respective velocities were fixed at $\phi_1(0) = \pi/2$, $\phi_2(0) = -\pi/2$ and $\dot{\phi}_1(0) = \dot{\phi}_2(0) = 0$ in all the panels. Both the amplitude of the radial vibration $r = \sqrt{x^2 + y^2}$ (panels (a1), (b1), (c1) and (d1)) and the position of the balls $\phi_1$ and $\phi_2$ (panels (a2), (b2), (c2) and (d2)) are plotted against the dimensionless time $t$.

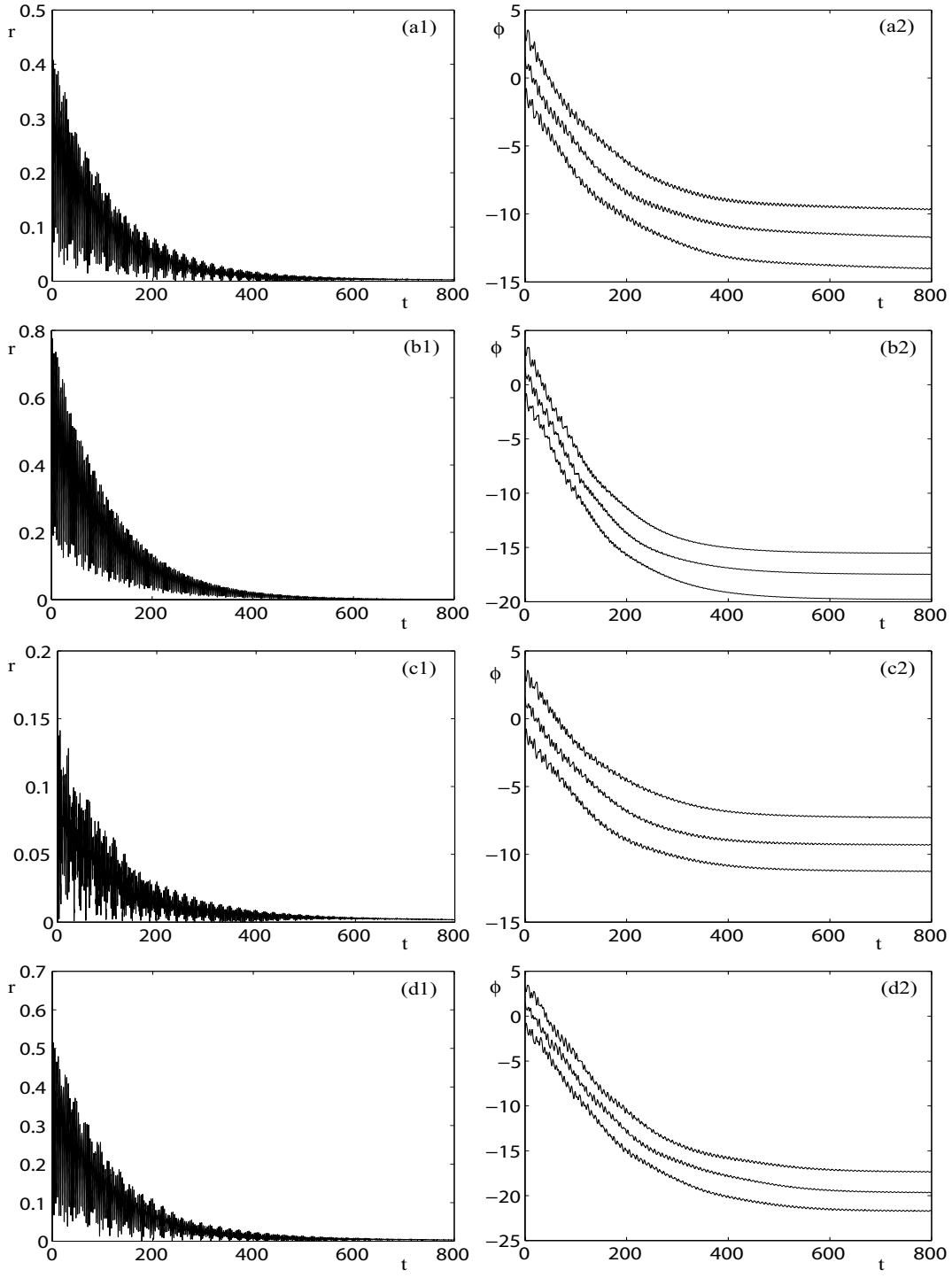


Figure 5.2: Numerical simulations of the ADB system with three balls for the parameter set $\Omega = 4.0$, $\zeta = 0.01$, $\beta = 0.01$, $\delta = 0.01$, and $\mu = 0.05$, with random initial conditions. The initial position of the centre of rotation and its velocity $(x(0), y(0), \dot{x}(0), \dot{y}(0))$ were chosen randomly with a statistical normal variable with $\mu_s = 0$ and $\sigma_s = 0.1$; their values were $(-0.0433, 0.0125, -0.1666, 0.0288)$ for panels (a1)-(a2), $(-0.1146, 0.1189, 0.1191, -0.0038)$ for panels (b1)-(b2) , $(0.0327, -0.0187, 0.0175, 0.0726)$ for panels (c1)-(c2), and $(-0.0588, -0.0136, 0.2183, 0.0114)$ for panels (d1)-(d2). The initial position of the balls and their respective velocities were fixed at $\phi_1(0) = \pi/2$, $\phi_2(0) = -\pi/2$, $\phi_3(0) = \pi$ and $\dot{\phi}_1(0) = \dot{\phi}_2(0) = \dot{\phi}_3(0) = 0$ in all the panels. Both the amplitude of the radial vibration $r = \sqrt{x^2 + y^2}$ (panels (a1), (b1), (c1) and (d1)) and the position of the balls $\phi_1$, $\phi_2$ and $\phi_3$ (panels (a2), (b2), (c2) and (d2)) are plotted against the dimensionless time $t$.

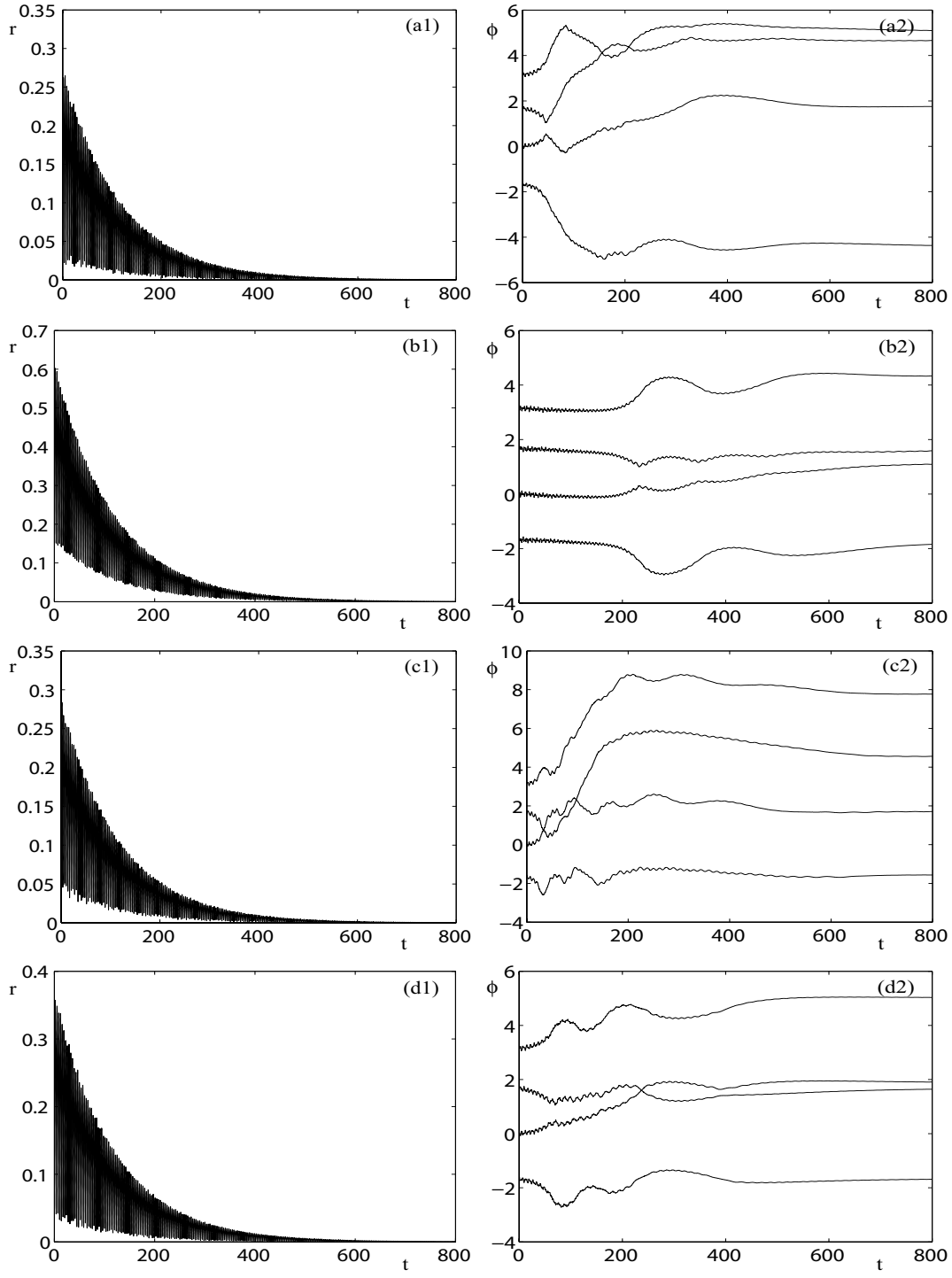


Figure 5.3: Numerical simulations of the ADB system with four balls for the parameter set $\Omega = 4.0$, $\zeta = 0.01$, $\beta = 0.01$, $\delta = 0.01$, and $\mu = 0.05$, with random initial conditions. The initial position of the centre of rotation and its velocity $(x(0), y(0), \dot{x}(0), \dot{y}(0))$ were chosen randomly with a statistical normal variable with $\mu_s = 0$ and $\sigma_s = 0.1$; their values were $(-0.0433, 0.0125, -0.1666, 0.0288)$ for panels (a1)-(a2), $(-0.1146, 0.1189, 0.1191, -0.0038)$ for panels (b1)-(b2) , $(0.0327, -0.0187, 0.0175, 0.0726)$ for panels (c1)-(c2), and $(-0.0588, -0.0136, 0.2183, 0.0114)$ for panels (d1)-(d2). The initial position of the balls and their respective velocities were fixed at $\phi_1(0) = \pi/2$, $\phi_2(0) = -\pi/2$, $\phi_3(0) = \pi$, $\phi_4(0) = 0$ and $\dot{\phi}_1(0) = \dot{\phi}_2(0) = \dot{\phi}_3(0) = \dot{\phi}_4(0) = 0$ in all the panels. Both the amplitude of the radial vibration $r = \sqrt{x^2 + y^2}$ (panels (a1), (b1), (c1) and (d1)) and the position of the balls $\phi_1$, $\phi_2$, $\phi_3$ and $\phi_4$ (panels (a2), (b2), (c2) and (d2)) are plotted against the dimensionless time $t$.

### 5.1.2 Initial position of the balls

Let us now study the effect of the initial position of the balls, considering that they are initially stationary within the rotating frame, that is, $\dot{\phi}_i(0) = 0$, $i = 1 \ldots, n$. In Figure 5.4, both the amplitude of the radial vibration $r$ and the position of the balls $\phi_1$ and $\phi_2$ of the ADB with two balls, are plotted against the dimensionless time $t$, for the parameter set shown in (5.1), and for four different specific initial positions of the balls: $\phi_1(0) = \pi/2$ and $\phi_2(0) = -\pi/2$ in panels (a1)-(a2), $\phi_1(0) = \pi/4$ and $\phi_2(0) = -\pi/4$ in (b1)-(b2), $\phi_1(0) = 3\pi/4$ and $\phi_2(0) = -3\pi/4$ in (c1)-(c2), and $\phi_1(0) = 0$ and $\phi_2(0) = \pi$ in (d1)-(d2). The initial position of the centre of rotation and its velocity are chosen equal to zero: $x(0) = y(0) = \dot{x}(0) = \dot{y}(0) = 0$. The balance is achieved in all the panels of Fig.5.4 except in (b1)-(b2), in which the system reaches a stable limit cycle. In this case, the amplitude of the radial vibration $r$ takes higher values during the transient response than in the other cases. Moreover, after transient decays, $r$ keeps vibrating around a high value. For that, this limit cycle behaviour is strongly undesirable in practical applications of the ADB mechanism, and it would be necessary to investigate further in which cases it is possible to reach it. The balance reached in panels (a2), (c2), and (d2) is given by setting $n = 2$ in the expression of the balanced steady state (3.6). Specifically we get

$$\begin{aligned} \phi_1 &= \arccos \frac{\delta}{2\mu} = \arccos \frac{0.01}{2 \cdot 0.05} = 1.67096374795646, \\ \phi_2 &= -\phi_1 = -1.67096374795646, \end{aligned} \tag{5.2}$$

for the parameter set shown in (5.1). If we consider that the balance is achieved when $r < 10^{-3}$, then the dimensionless transient decay times $t_{dec}$ are 462.42, 745.02, and 549.93 in panels (a1), (c1), and (d1), respectively. The maximum amplitudes of the radial vibration during the transient $r_{max}$ are 0.0483, 0.2878, and 0.0478 in panels (a1), (c1), and (d1), respectively. We can note that $t_{dec}$ and $r_{max}$ are in panel (c1) much larger than in panels (a1) and (d1). Moreover, in that case, we can see in (c2) that before arriving to the balance, the balls go around the rotor some times, while in (a2) and (d2) the balls go directly to vibrate around the unique balanced position. Hence, we can suppose that, when the balance is achieved, the transient response is determined by the way the balls take around the rotor before they stop. Thus, while the number of laps that the balls go around the rotor increases, the $r_{max}$ and $t_{dec}$ values grow. Since these movements of the balls depend on their initial positions (as we can see comparing panels (a2), (c2), and (d2)), these positions from which the balls start affect the $r_{max}$ and $t_{dec}$ values during the transient. Let us discuss more deeply this fact in the next paragraph.

Figure 5.5 shows the maximum amplitude of the radial vibration $r_{max}$ against the initial position of one ball, $\phi_1(0)$, while $\phi_2(0) = -\phi_1(0)$ in panel (a), and $\phi_2(0) = \phi_1(0) + \pi$ in panel (b). The points marked by '$\times$' are the cases in which the balance is not achieved, and in the points marked by '$\cdot$' the system attains a balanced equilibrium. In Fig.5.5(a) we can see that there exist a $\phi_1(0)$ value for which $r_{max}$ is equal to zero. This initial position of the balls coincides with the balanced equilibrium position (5.2). The $r_{max}$ increases until high values ($r_{max} \approx 0.5$) as the balls come away from this balanced position , and there exist some cases in which the system achieves a limit cycle. These points are marked in Fig.5.5(a) by '$\times$'. In Fig.5.5(b) we can see that $r_{max}$ does not vary practically with the initial position of the balls. If we compare these $r_{max}$ values with the ones in Fig.5.5(a), we notice that these are much lower in general. Another difference for this configuration is

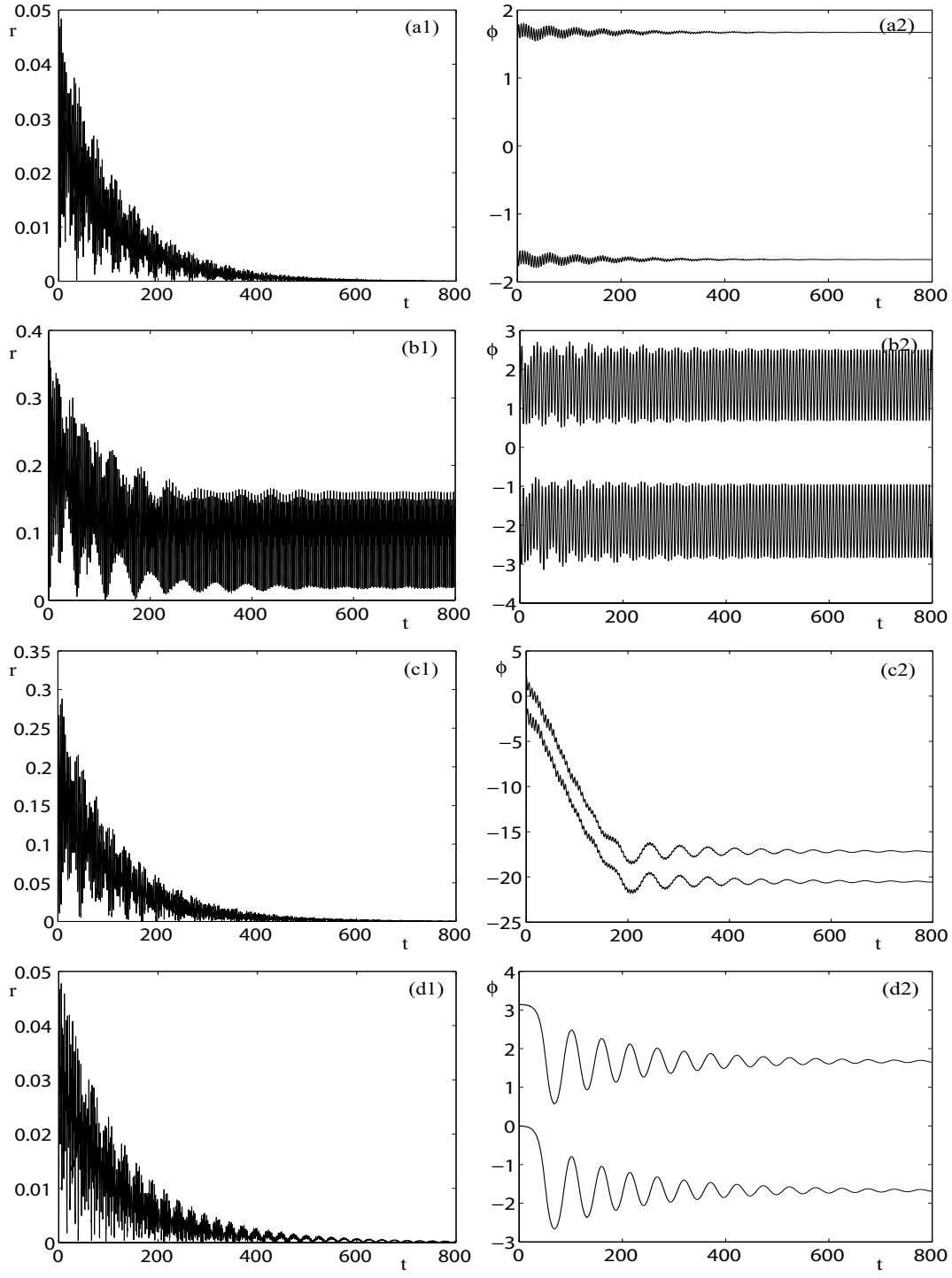


Figure 5.4: Numerical simulations of the ADB system with two balls for the parameter set $\Omega = 4.0$, $\zeta = 0.01$, $\beta = 0.01$, $\delta = 0.01$, and $\mu = 0.05$. The initial position of the centre of rotation and its velocity, and the velocity of the balls are fixed at zero ($x(0) = y(0) = \dot{x}(0) = \dot{y}(0) = \dot{\phi}_1(0) = \dot{\phi}_2(0) = 0$) in all the panels. The initial position of the balls are fixed at $\phi_1(0) = \pi/2$ and $\phi_2(0) = -\pi/2$ in panels (a1)-(a2), $\phi_1(0) = \pi/4$ and $\phi_2(0) = -\pi/4$ in (b1)-(b2), $\phi_1(0) = 3\pi/4$ and $\phi_2(0) = -3\pi/4$ in (c1)-(c2), and $\phi_1(0) = 0$ and $\phi_2(0) = \pi$ in (d1)-(d2). Both the amplitude of the radial vibration $r = \sqrt{x^2 + y^2}$ (panels (a1), (b1), (c1) and (d1)) and the position of the balls $\phi_1$ and $\phi_2$ (panels (a2), (b2), (c2) and (d2)) are plotted against the dimensionless time $t$.

that now any limit cycle is never achieved. Therefore, we can conclude that when the balls start at opposites sides and in line with the centre of rotation ($\phi_2(0) = \phi_1(0) + \pi$), it is easier to obtain the balance than when the balls start from an opposite position within the $x$-axis ($\phi_2(0) = -\phi_1(0)$), because in the first case we never reach a limit cycle. Moreover, the transient response is softer ($r_{max}$ values are lower) in the first case than in the second case almost every time, except when the balls start very close to the balanced position. We can confirm these affirmations with the Figure 5.4. As it has already been said, in Figs.5.4(a1) and (d1), $r_{max}$ is smaller than in Figs.5.4(b1) and (c1), and precisely those panels(a1), (d1) correspond to $\phi_2(0) = \phi_1(0) + \pi$, while these panels (b1) and (c1) correspond to $\phi_2(0) = -\phi_1(0)$. In conclusion, in practical applications of the ADB mechanism with two balls, it would be better to launch the balls at an in line initial position which satisfies $\phi_2(0) = \phi_1(0) + \pi$.

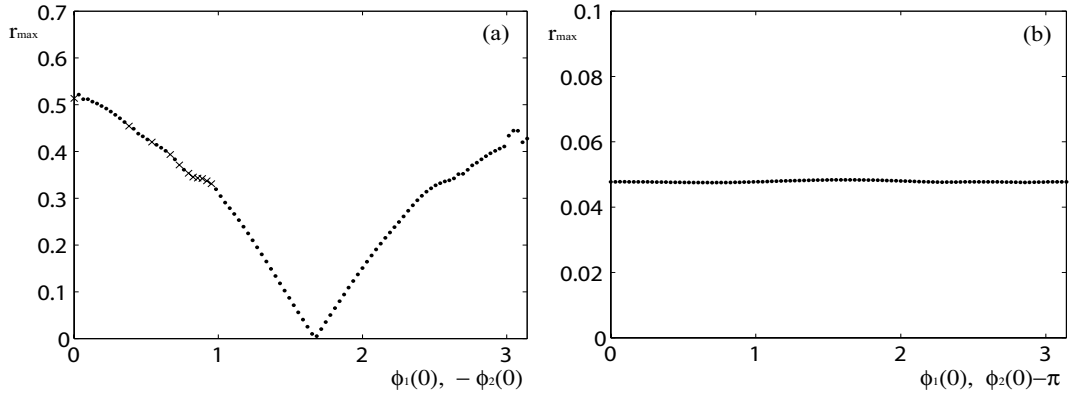


Figure 5.5: Maximum amplitude of the radial vibration $r_{max}$ against $\phi_1(0)$, while $\phi_2(0) = -\phi_1(0)$ in (a), and $\phi_2(0) = \phi_1(0) + \pi$ in (b), for the ADB system with two balls. The rest of the initial conditions are chosen to equal zero ($x(0) = y(0) = \dot{x}(0) = \dot{y}(0) = \dot{\phi}_1(0) = \dot{\phi}_2(0) = 0$), and the parameter set taken is $\Omega = 4$, $\zeta = \beta = \delta = 0.01$ and $\mu = 0.05$. The points marked by '$\cdot$' refers to balanced states, and points marked by '$\times$' refers to limit cycles.

In Figure 5.6 $r$, $\phi_1$, $\phi_2$ and $\phi_3$ are plotted against $t$ for the ADB system with three balls, for the parameter set shown in (5.1), and $x(0) = y(0) = \dot{x}(0) = \dot{y}(0) = \dot{\phi}_1(0) = \dot{\phi}_2(0) = \dot{\phi}_3(0) = 0$, for four specific initial positions of the balls: $\phi_1(0) = \pi/2$, $\phi_2(0) = -\pi/2$ and $\phi_3(0) = \pi$ in panels (a1)-(a2), $\phi_1(0) = \pi/4$, $\phi_2(0) = -\pi/4$ and $\phi_3(0) = \pi$ in panels (b1)-(b2), $\phi_1(0) = 3\pi/4$, $\phi_2(0) = -3\pi/4$ and $\phi_3(0) = 0$ in panels (c1)-(c2), and $\phi_1(0) = 0$, $\phi_2(0) = \pi$ and $\phi_3(0) = \pi/2$ in panels (d1)-(d2). Figs.5.6 (a1), (b1), (c1) and (d1) show that in all the depicted cases, $r$ goes to zero while $t \to \infty$, that is, the balance of the system is always achieved. However, we can see in Figs.5.6 (a2), (b2), (c2) and (d2) that now the final relative positions of the balls are different in each case. As was said in Chapter 3, when the ADB mechanism have more than two balls, there exist infinitely many relative positions of the balls which reach the balance of the system. We can check in each represented case, that all these final positions of the balls satisfy the balance conditions (3.6) for $n = 3$, so it is proved that the balanced equilibrium is reached in each case. Figs.5.6 (a1), (b1), (c1) and (d1) also show that there exist quite big differences in the $r_{max}$ values, and in the transient decay times $t_{dec}$ between each panel. Thus, the $r_{max}$ values are (0.1806, 0.1285, 0.0450, 0.2278), respectively, and if we consider the transient finishes when $r < 10^{-3}$, then the $t_{dec}$

values are (1090.40, 714.47, 901.88, 1330.20), respectively. Hence, the importance of the initial position of the balls on the transient response is confirmed. In Figs.5.6 (a2), (b2), (c2) and (d2) we can see that, in addition to the fact that the final relative positions of the balls are not the same in each case, the trajectories followed by the balls are different as well. Moreover, it is possible to observe that there is a correlation between the movements of the balls before they stop, and the $r_{max}$ values. Thus, the bigger number of laps given by the balls around the rotor are in panels (d2), (a2), (b2) and (c2), respectively, which coincides with the highest $r_{max}$ values (panels (d1), (a1), (b1) and (c1), respectively). Therefore, as was suggested for the ADB with two balls, we can reassert that the initial position of the balls determines their trajectories during the transient, and these movements of the balls around the rotor have a direct influence in the radial vibration values before the balance is reached.

In Figure 5.7 the maximum amplitude of the radial vibration $r_{max}$ is plotted against the initial position of the first ball $\phi_1(0)$ in the ADB system with three ball for the parameter set shown in (5.1), and with the rest of the initial conditions equal to zero. The points marked by '$\cdot$' refers to balanced states, and points marked by '$\times$' refers to cases in which the balance is not achieved. Panels (a1)-(a2) show that, when two of the balls are launched symmetrically opposite to each other such that the line joining them is orthogonal to $x$-axis of eccentricity ($\phi_2(0) = -\phi_1(0)$) , $r_{max}$ takes zero value in a specific position of the balls, and grows as it comes away from this initial position. This specific initial position of the balls coincides with a balanced equilibrium position, as we can check setting $n = 3$ in the conditions for the balanced steady state (3.6). Effectively, in (a1), in which the third ball starts from the unbalanced side ($\phi_3(0) = 0$), the balanced equilibrium position is $\phi_1 = 2.21429743558818$, $\phi_2 = -2.21429743558818$, and $\phi_3 = 0$; in (a2), in which the third ball is launched from the balanced side ($\phi_3(0) = \pi$), the balance is at $\phi_1 = 1.15927948072741$, $\phi_2 = -1.15927948072741$, and $\phi_3 = \pi$.

Figs.5.7(b1)-(b2) show that, when two of the balls start at opposite sides and in line with the centre of rotation, the $r_{max}$ varies very little with $\phi_1(0)$. The $r_{max}$ values are higher when the third ball is fixed at $\phi_3(0) = 0$ (panel (b1)) than when is fixed at $\phi_3(0) = \pi$ (panel (b2)). This fact may be because in the first case the third ball starts from the unbalanced side ($\phi_3(0) = 0$), and it would have to go over a larger trajectory in order to balance the system, than if it starts from the balanced side ($\phi_3(0) = \pi$). In general, the $r_{max}$ value is lower in (b1)-(b2) than in (a1)-(a2), but now this difference is not as big as in Fig.5.5 for ADB with two balls. Hence, now we can not assert that an in-line initial position of the balls is better than an opposite initial position of the balls, because Figs.5.7(a1)-(a2) ($\phi_2(0) = -\phi_1(0)$) show a large $\phi_1(0)$-range in which the $r_{max}$ value is lower than in Figs.5.7(b1)-(b2) ($\phi_2(0) = \phi_1(0) + \pi$). Finally, in panel (c), the balls are launched equidistantly, that is, the initial position of the second and the third balls vary as $\phi_2(0) = \phi_1(0)+\pi/3$ and $\phi_3(0) = \phi_1(0)-\pi/3$. Like in (b1) and (b2), $r_{max}$ is almost constant. In this case, we can see that $r_{max}$ takes lower values than in Figs.5.7(b1)-(b2), and they are in general lower than in Figs.5.7(a1)-(a2) except for few points close to $r_{max} = 0$. Hence, the best relative initial position of the balls for ADB with three balls is such that the three balls start equidistantly.

One difference with respect to the ADB system with two balls is that now, Fig.5.7 shows only a few cases in which the balance is not achieved. Let us discuss these points. The whole

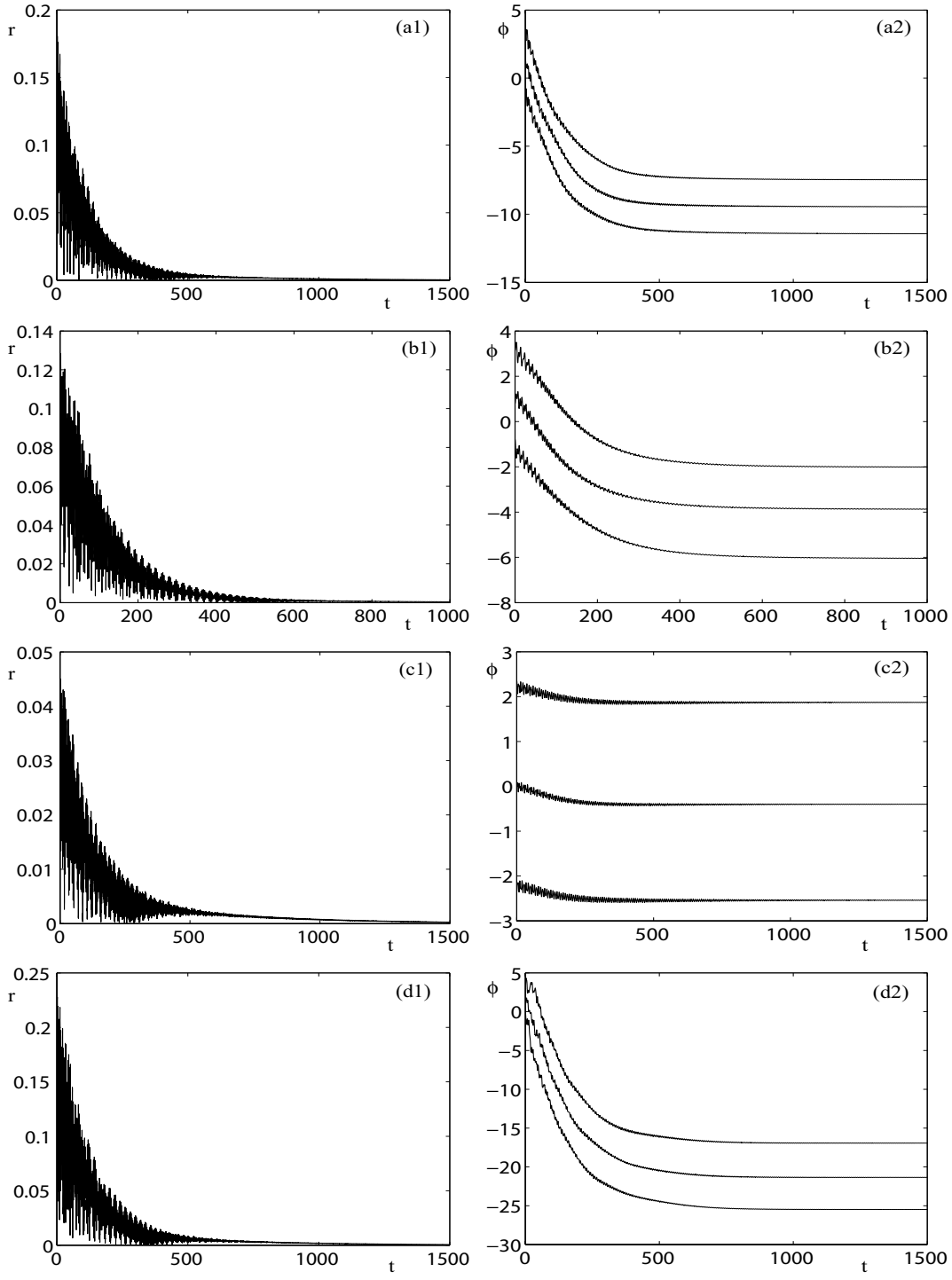


Figure 5.6: Numerical simulations of the ADB system with three balls for the parameter set $\Omega = 4.0$, $\zeta = 0.01$, $\beta = 0.01$, $\delta = 0.01$, and $\mu = 0.05$. The initial position of the centre of rotation and its velocity, and the velocity of the balls are fixed at zero ($x(0) = y(0) = \dot{x}(0) = \dot{y}(0) = \dot{\phi}_1(0) = \dot{\phi}_2(0) = \dot{\phi}_3(0) = 0$) in all the panels. The initial position of the balls are fixed at $\phi_1(0) = \pi/2$, $\phi_2(0) = -\pi/2$ and $\phi_3(0) = \pi$ in panels (a1)-(a2), $\phi_1(0) = \pi/4$, $\phi_2(0) = -\pi/4$ and $\phi_3(0) = \pi$ in (b1)-(b2), $\phi_1(0) = 3\pi/4$, $\phi_2(0) = -3\pi/4$ and $\phi_3(0) = 0$ in (c1)-(c2), and $\phi_1(0) = 0$, $\phi_2(0) = \pi$ and $\phi_3(0) = \pi/2$ in (d1)-(d2). Both the amplitude of the radial vibration $r = \sqrt{x^2 + y^2}$ (panels (a1), (b1), (c1) and (d1)) and the position of the balls $\phi_1$, $\phi_2$ and $\phi_3$ (panels (a2), (b2), (c2) and (d2)) are plotted against the dimensionless time $t$.

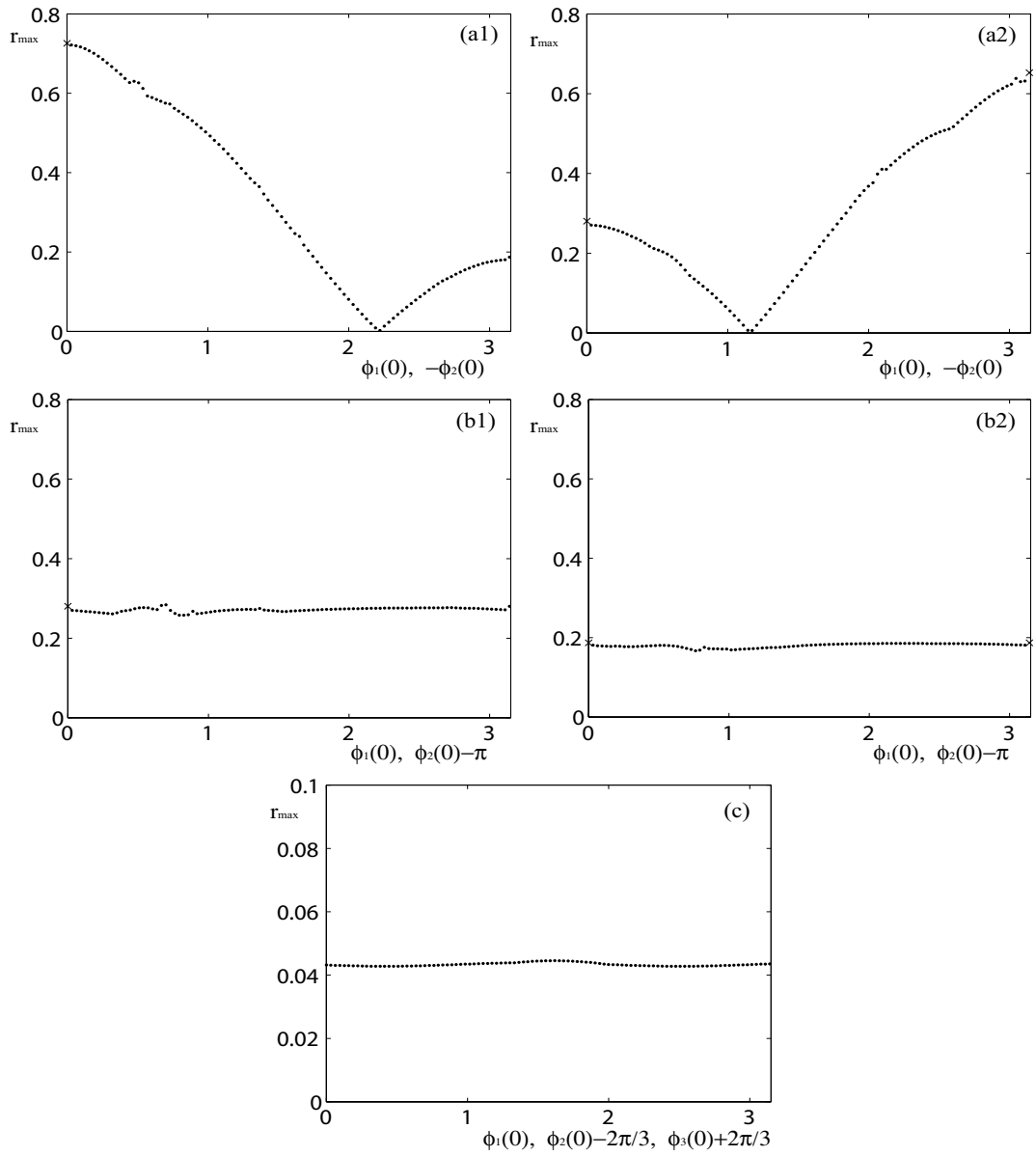


Figure 5.7: Maximum amplitude of the radial vibration $r_{max}$ against $\phi_1(0)$ for ADB with three balls. In panels (a1)-(a2) $\phi_2(0) = -\phi_1(0)$ while $\phi_3(0) = 0$ in (a1), and $\phi_3(0) = \pi$ in (a2). In panels (b1)-(b2) $\phi_2(0) = \phi_1(0) + \pi$ while $\phi_3(0) = 0$ in (b1), and $\phi_3(0) = \pi$ in (b2). In panel (c) $\phi_2(0) = \phi_1(0) + \pi/3$, and $\phi_3(0) = \phi_1(0) - \pi/3$. The rest of the initial conditions are chosen to equal zero ($x(0) = y(0) = \dot{x}(0) = \dot{y}(0) = \dot{\phi}_1(0) = \dot{\phi}_2(0) = \dot{\phi}_3(0) = 0$), and the taken parameter set is $\Omega = 4$, $\zeta = \beta = \delta = 0.01$ and $\mu = 0.05$. The points marked by '$\cdot$' refers to balanced states, and points marked by '$\times$' refers to cases in which the balance is not achieved.

number of points marked by '×' in Fig.5.7 is six, but they can be summarized in four because all the balls are similar, and the initial positions $\phi_1(0) = \phi_2(0) = 0, \phi_3(0) = \pi$ and $\phi_1(0) = 0, \phi_2(0) = \phi_3(0) = \pi$ are equivalent to the initial positions $\phi_1(0) = \phi_3(0) = 0, \phi_2(0) = \pi$ and $\phi_1(0) = \phi_3(0) = \pi, \phi_2(0) = 0$, respectively. After making simulation for these four initial position of the balls, we find that one of them corresponds with a limit cycle, and the other three with unbalanced equilibria. In fact, when $\phi_1(0) = \phi_2(0) = \phi_3(0) = 0$, the system goes to a limit cycle. When $\phi_1(0) = \phi_2(0) = \phi_3(0) = \pi$, the three balls do not separate during all the time, and after the transient finishes, the system achieves an equilibrium which corresponds with the coincident steady state solution **2-** given by (3.9) for $n = 3$ and for the parameter set (5.1): $x = 0.1285$, $y = -0.0083$, and $\phi_i = 3.0772$ for $i = 1, 2, 3$. When the balls start from $\phi_1(0) = \phi_2(0) = 0, \phi_3(0) = \pi$, and $\phi_1(0) = 0, \phi_2(0) = \phi_3(0) = \pi$, the two balls which start from a coincident initial position do no separate during all their trajectory along the time. In these both cases, the system achieves the in-line steady states **3(3-2)-** and **3(3-1)+**, which are the same considering that all the balls are similar: $x = 0.0368$, $y = -0.0007$, $\phi_1 = \phi_2 = -3.16$ and $\phi_3 = -0.0184$.

Let us discuss the response of the ADB system with four balls for four specific initial positions of the balls. In Figure 5.8, $r$ and $\phi_i$ (for $i = 1, 2, 3, 4$) are plotted against $t$ for the ADB with four balls with the parameter set (5.1), and $x(0) = y(0) = \dot{x}(0) = \dot{y}(0) = \dot{\phi}_1(0) = \dot{\phi}_2(0) = \dot{\phi}_3(0) = \dot{\phi}_4(0) = 0$. The taken initial positions of the balls were $\phi_1(0) = \pi/2$, $\phi_2(0) = -\pi/2$, $\phi_3(0) = \pi$ and $\phi_4(0) = 0$ in panels (a1)-(a2), $\phi_1(0) = \pi/4$, $\phi_2(0) = -\pi/4$, $\phi_3(0) = \phi_4(0) = \pi$ in panels (b1)-(b2), $\phi_1(0) = 3\pi/4$, $\phi_2(0) = -3\pi/4$, $\phi_3(0) = \phi_4(0) = 0$ in panels (c1)-(c2), and $\phi_1(0) = \pi/4$, $\phi_2(0) = -\pi/4$, $\phi_3(0) = 3\pi/4$ and $\phi_4(0) = -3\pi/4$ in panels (d1)-(d2). Figs.5.8(a1),(b1),(c1) and (d1) show that for all the taken initial positions of the balls, the balance of the system is achieved, as it happened for the ADB with three balls. That is, $r \to 0$ when $t \to \infty$. Effectively, in panels (a2), (b2), (c2) and (d2) we can see that the balls end at final relative positions which satisfy the balance conditions shown in (3.6) for $n = 4$ balls. Like in ADB with three balls, these final relative positions are different in each panel, because for $n > 2$ there exist infinitely many balanced equilibrium positions. The maximum amplitude of the radial vibration $r_{max}$ is 0.0444 in (a1), 0.0810 in (b1), 0.1768 in (c1) and 0.0444 in (d1). If we consider the transient is finished when $r < 10^{-3}$, then the transient decay time is 495.87 in (a1), 567.48 in (b1), 708.36 in (c1) and 485.04 in (d1). Again, there exist some important differences in the transient response between each initial position. Hence, we will try to find optimal initial positions of the balls to obtain as soft transient response as possible. Figs.5.8(a2), (d2) show that the balls go over soft trajectories. In fact, the high frequency oscillations correspond to small amplitudes, and the high amplitude oscillations have low frequency. Figs.5.8(b2), (c2) show that the balls which start coincidently (from $\phi(0) = \pi$ and $\phi(0) = 0$) also make similar soft movements without separating each other during all their trajectories. Unlike, the other two balls make sudden movements, that is, their high frequency oscillations have medium amplitude values ( 2 radians). These brusque movements of the balls make the $r$ values in (b1) and (c1) to be larger than in (a1) and (d1). Again it is confirmed that the movements of the balls before they stop determine the $r$ values during the transient. In both cases (a1)-(a2) and (d1)-(d2), the balls are launched equidistantly. In the next paragraph, we will check that, in general, when the initial conditions have equidistant balls, $r_{max}$ is smaller than when the initial conditions have two of the balls in the same position.

We will try to deduce which configuration for the initial position of the balls would be

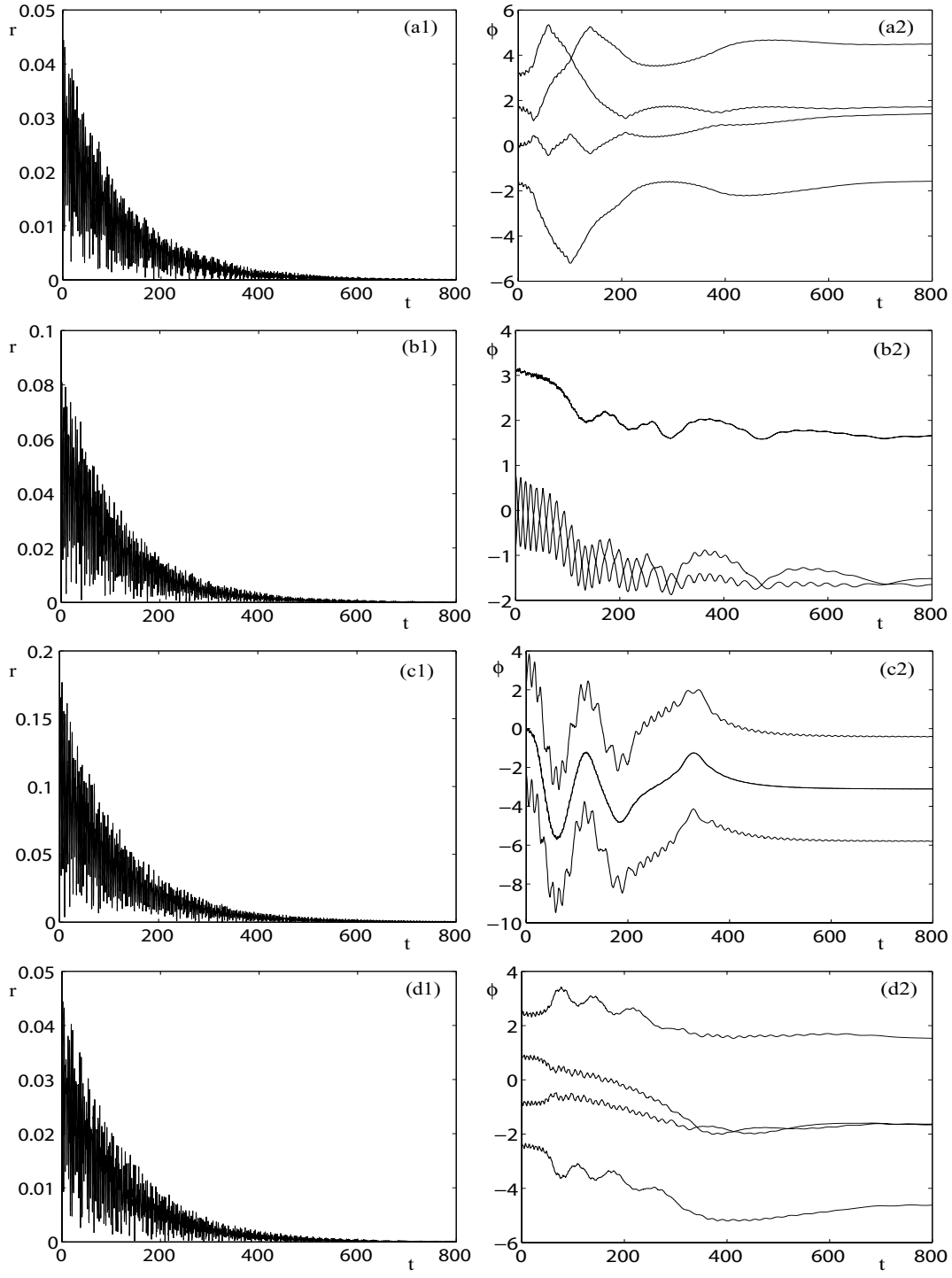


Figure 5.8: Numerical simulations of the ADB system with four balls for the parameter set $\Omega = 4.0$, $\zeta = 0.01$, $\beta = 0.01$, $\delta = 0.01$, and $\mu = 0.05$. The initial position of the centre of rotation and its velocity, and the velocity of the balls are fixed at zero ($x(0) = y(0) = \dot{x}(0) = \dot{y}(0) = \dot{\phi}_1(0) = \dot{\phi}_2(0) = \dot{\phi}_3(0) = \dot{\phi}_4(0) = 0$) in all the panels. The initial position of the balls are fixed at $\phi_1(0) = \pi/2$, $\phi_2(0) = -\pi/2$, $\phi_3(0) = \pi$ and $\phi_4(0) = 0$ in panels (a1)-(a2), $\phi_1(0) = \pi/4$, $\phi_2(0) = -\pi/4$, $\phi_3(0) = \pi$ and $\phi_4(0) = \pi$ in (b1)-(b2), $\phi_1(0) = 3\pi/4$, $\phi_2(0) = -3\pi/4$, $\phi_3(0) = 0$ and $\phi_4(0) = 0$ in (c1)-(c2), and $\phi_1(0) = \pi/4$, $\phi_2(0) = -\pi/4$, $\phi_3(0) = 3\pi/4$ and $\phi_4(0) = -3\pi/4$ in (d1)-(d2). Both the amplitude of the radial vibration $r = \sqrt{x^2 + y^2}$ (panels (a1), (b1), (c1) and (d1)) and the position of the balls $\phi_1$, $\phi_2$, $\phi_3$ and $\phi_4$ (panels (a2), (b2), (c2) and (d2)) are plotted against the dimensionless time $t$.

better in an ADB with four balls. For that, we will comment Figure 5.9, in which the maximum amplitude of the radial vibration $r_{max}$ is plotted against the initial position of the first ball $\phi_1(0)$, while the other balls start from different positions. In Figs.5.9(a1), (a2), and (a3), the second ball start at opposite side that the first one, such that the line joining them is orthogonal to the '$x$'-axis ($\phi_2(0) = -\phi_1(0)$). When the third and fourth balls start from $\phi_3(0) = \phi_4(0) = 0$, we can see in Fig.5.9(a1) that $r_{max}$ always decreases as the first and second balls coming away from the unbalanced side, that is, as $\phi_1(0)$ increases. In that case, there is not any position in which $r_{max}$ takes a zero value because the third and fourth balls start from the unbalanced side ($\phi_3(0) = \phi_4(0) = 0$), and there exist no initial position of the other two balls to reach the balance. When the third and fourth balls start from $\phi_3(0) = \phi_4(0) = \pi$ (panel (a2)), and from $\phi_3(0) = 0$ and $\phi_4(0) = \pi$ (panel (a3)), $r_{max}$ has a zero value, around which it becomes larger. This initial position corresponds to a balanced equilibrium position which satisfies the equilibrium conditions in (3.6) for $n = 4$ ($\phi_1 = -\phi_2 = 0.45102681179626$, $\phi_3 = \phi_4 = \pi$ in the panel (a2), and $\phi_1 = -\phi_2 = 1.67096374795646$, $\phi_3 = 0$, $\phi_4 = \pi$ in the panel (a3)). In these Figs.5.9(a1), (a2) and (a3) we can see some initial positions of the balls for which there is no balance after the transient. These points correspond to three limit cycles (for $\phi_1(0) = \phi_2(0) = \phi_3(0) = \phi_4(0) = 0$ in (a1), for $\phi_1(0) = -\phi_2(0) = 0.72986495992490$, $\phi_3(0) = \phi_4(0) = 0$ in (a1), and for $\phi_1(0) = -\phi_2(0) = 2.63386050755508$, $\phi_3(0) = \phi_4(0) = \pi$ in (a2)), an unbalanced coincident equilibrium **2-** (for $\phi_1(0) = \phi_2(0) = \phi_3(0) = \phi_4(0) = \pi$ in (a2)), and an unbalanced in-line equilibrium **3(4-3)-** (for $\phi_1(0) = \phi_2(0) = \phi_3(0) = 0$, $\phi_4(0) = \pi$ in (a3)).

In Figs.5.9(b1), (b2), and (b3) the second ball starts at opposite side from the first ball, and in line with the centre of rotation ($\phi_2(0) = \phi_1(0) + \pi$) , while the initial position of the third and fourth balls are fixed at $\phi_3(0) = \phi_4(0) = 0$ in (b1),at $\phi_3(0) = \phi_4(0) = \pi$ in (b2), and at $\phi_3(0) = 0$, $\phi_4(0) = \pi$ in (b3). In these cases, $r_{max}$ values varies only a little with $\phi_1(0)$ value. In panel (b3), the $r_{max}$ values have a less order of magnitude than in panels (b1) and (b2) ( 0.05 against 0.5). In this panel (b3), the system always attains the balance, while in (b1) and (b2) there are three initial positions of the balls in which the system stops at unbalanced equilibria. For $\phi_1(0) = \phi_3(0) = \phi_4(0) = 0$, $\phi_2(0) = \pi$ in (b1) the system goes to the in-line steady state **3(4-3)-**, and for $\phi_1(0) = 0$, $\phi_2(0) = \phi_3(0) = \phi_4(0) = \pi$ and $\phi_1(0) = \pi$, $\phi_2(0) = 2\pi$, $\phi_3(0) = \phi_4(0) = \pi$ in (b2), the system reaches the in-lines equilibrium **3(4-1)+**. In an ADB mechanism with four balls, we can study many more configurations for the initial positions of the balls, besides $\phi_2(0) = -\phi_1(0)$ and $\phi_2(0) = \phi_1(0) + \pi$.

In Fig.5.9(c), the four balls start from an equidistant initial relative position, that is, $\phi_1(0) = \phi_2(0) - \pi/2 = \phi_3(0) - \pi = \phi_4(0) - 3\pi/2$. In this case, we can observe that $r_{max}$ is practically constant with $\phi_1(0)$, and its value is approximately equal to 0.045, what is a advantage with respect to the other studied cases. Besides that, the balance of the system is achieved for all $\phi_1(0)$ values, that is, there exists no limit cycle nor unbalance equilibrium. In Fig.5.9(d), the balls are initially positioned symmetrically with respect both '$x$'-axis and '$y$'-axis, that is, $\phi_1(0) = -\phi_2(0) = -\phi_3(0) + \pi = \phi_4(0) + \pi$. In this panel (d) we can observe similar characteristics than in (c), but with a little more variation of $r_{max}$ values with the initial positions of the balls. Comparing the different initial positions of the balls we have seen in Fig.5.9, we could say that, to try to obtain the best transient response, we would have to avoid two or more balls starting from a coincident position. As we have just seen, this situation might take the system to an unbalance equilibrium or to a limit

cycle in a few situations, and in several cases, the $r_{max}$ would reach high values during the transient. Therefore, we can conclude that, in practical applications of the ADB mechanism with four balls, the best configurations for the initial positions of the balls would be equidistant separation (panel (c)), or double in-line position, that is $\phi_2(0) = \phi_1(0) + \pi$ and $\phi_4(0) = \phi_3(0) + \pi$ (panels (b3) and (d)). These affirmations can be confirmed, if we remember that in Fig.5.8, the lowest $r_{max}$ values were found in (a1) and (d1), in which the balls started from equidistant initial positions, and in (b1) and (c1) (in which the third and the fourth balls started from a coincident position), the obtained $r_{max}$ were larger.

We have seen that the response of the ADB system with two, three, and four balls is very sensitive to the initial positions of the balls. In fact, the stability of the balanced steady state, whereas which specific balanced equilibrium is achieved for three and four balls, depends on $\phi_i(0)$ values. After analysing some different configurations for the initial positions of the balls, we conclude that the best results are obtained when the balls start equidistantly. In that case, the balance was found to be always stable, and the transient response was quite softer, with short decay time, and small maximum amplitude of the radial vibration. Moreover, we saw in Figs.5.5(b), 5.7(c), and 5.9(c) that $r_{max}$ was almost constant with $\phi_1(0)$. That is a very important factor, in the sense that in practical applications of the ADB mechanism, we we will not know the position of the unbalance. For that, in practice, we cannot use initial positions of the balls in which we need to know the absolute positions of the balls (for example when the two balls are symmetrically opposite such as the line joining them is orthogonal to the '$x$'-axis). Therefore, in the following we will always consider equidistant initial positions of the balls. Comparing the results we obtained for ADB with two balls, for ADB with three balls, and for ADB with four balls, we note that they are very similar. For example, the $r_{max}$ values for equidistant initial positions of the balls are almost the same in the three cases ( 0.045). The only mentionable difference between the systems which we found was that, for the used initial positions of the balls, the ADB with two balls showed more cases in which the system undergoes a limit cycle (see Fig.5.5(a)). However, we cannot get any conclusion with this single fact. We will try to do a deeper comparison between the different systems in the next section.

### 5.1.3 Initial velocity of the balls

Until now, we have obtained the response of the ADB system when the balls start from a stationary position within the rotating frame, that is, $\dot{\phi}_i(0) = 0$, $\forall i$. Let us see how the initial velocity of the balls affect the system behaviour. We will make some runs considering the balls are initially stationary within the fixed frame, that is, the balls will start with an initial velocity within the rotating frame to equal $-\Omega$. We choose this configuration because it could be easily realizable in practical situations. Really, we could keep the balls fixed at a position within an external fixed frame, while the rotor is rotating until it achieves a stationary dimensionless velocity $\Omega$, and suddenly leave the balls free, so they would start with $\dot{\phi}_i(0) = -\Omega$, $\forall i$. In Figure 5.10 we depict the response of the system with two balls (panels (a1)-(a2)), with three balls (panels (b1)-(b2)), and with four balls (panels (c1)-(c2)), for the parameter set (5.1). The initial positions of the balls are chosen equidistantly: $\phi_1(0) = \pi/2$, and $\phi_2(0) = -\pi/2$ for two balls, $\phi_1(0) = \pi/3$, $\phi_2(0) = \pi$, and $\phi_3(0) = -\pi/3$ for three balls, and $\phi_1(0) = \pi/2$, $\phi_2(0) = -\pi/2$, $\phi_3(0) = \pi$, and $\phi_4(0) = 0$ for four balls. We can see that all the systems (with two, three and four balls) do not reach any equilibrium and they undergo a limit cycle behaviour. In Fig.5.10 (b2), the three

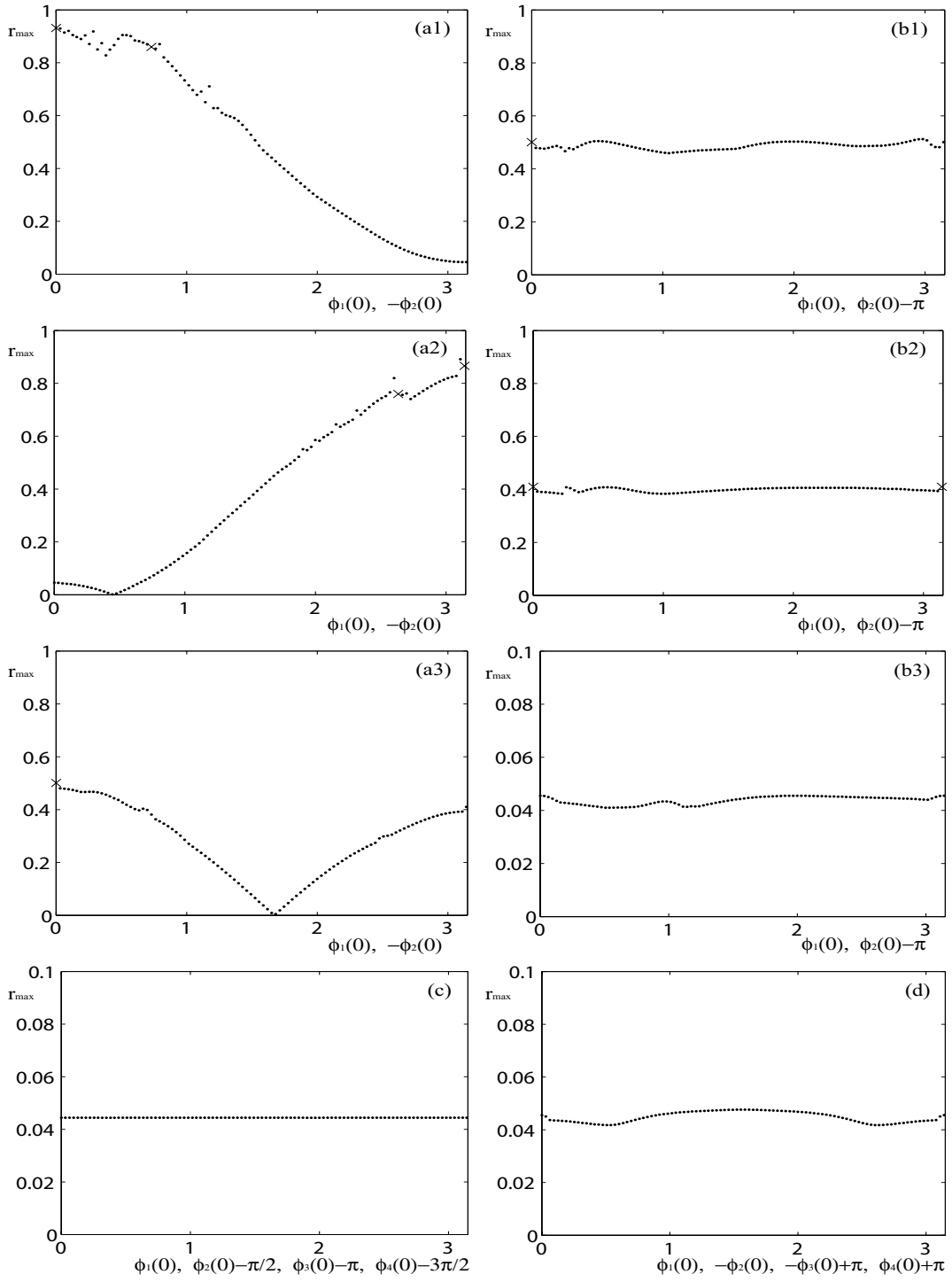


Figure 5.9: Maximum amplitude of the radial vibration $r_{max}$ against $\phi_1(0)$, while $\phi_2(0) = -\phi_1(0)$ in panels (a1), (a2) and (a3), and $\phi_2(0) = \phi_1(0) + \pi$ in panels (b1), (b2) and (b3), for the ADB system with four balls. The third and fourth balls were fixed at $\phi_3(0) = \phi_4(0) = 0$ in panels (a1) and (b1), $\phi_3(0) = \phi_4(0) = \pi$ in panels (a2) and (b2), and $\phi_3(0) = 0$ and $\phi_4(0) = \pi$ in (a3) and (b3). In panels (c) and (d) all the balls follow a correlation with respect $\phi_1(0)$: $\phi_2(0) = \phi_1(0) + \pi/2$, $\phi_3(0) = \phi_1(0) + \pi$ and $\phi_4(0) = \phi_1(0) + 3\pi/2$ in panel (c), and $\phi_2(0) = -\phi_1(0)$, $\phi_3(0) = \pi - \phi_1(0)$ and $\phi_4(0) = \phi_1(0) - \pi$ in panel (d). The rest of the initial conditions in all the panels are chosen to equal zero ($x(0) = y(0) = \dot{x}(0) = \dot{y}(0) = \dot{\phi}_1(0) = \dot{\phi}_2(0) = \dot{\phi}_3(0) = \dot{\phi}_4(0) = 0$), and the taken parameter set is $\Omega = 4$, $\zeta = \beta = \delta = 0.01$ and $\mu = 0.05$. The points marked by '$\cdot$' refers to balanced states, and points marked by '$\times$' refers to cases in which the balance is not achieved.

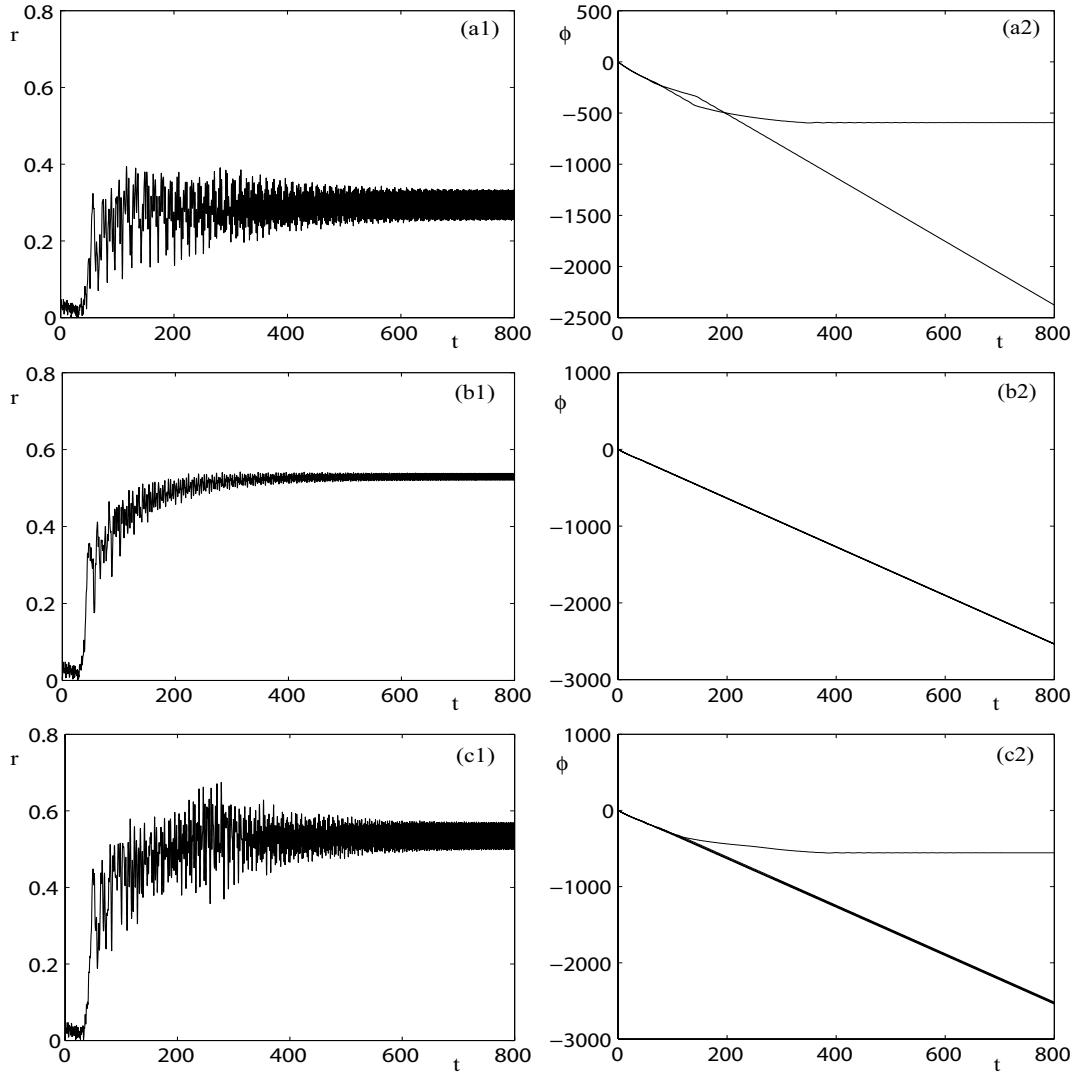


Figure 5.10: Numerical simulations of the ADB systems with two balls (panels (a1)-(a2)), three balls (panels (b1)-(b2)), and four balls (panels (c1)-(c2)), for the parameter set $\Omega = 4.0$, $\zeta = 0.01$, $\beta = 0.01$, $\delta = 0.01$, and $\mu = 0.05$. The initial position of the centre of rotation and its velocity are fixed at zero ($x(0) = y(0) = \dot{x}(0) = \dot{y}(0) = \doteq 0$), and the velocity of the balls are fixed at $\dot{\phi}_i = -\Omega, \quad \forall i$ in all the panels. The initial positions of the balls are chosen equidistantly, and are fixed at $\phi_1(0) = \pi/2$ and $\phi_2(0) = -\pi/2$ in panels (a1)-(a2), $\phi_1(0) = \pi/3$, $\phi_2(0) = \pi$ and $\phi_3(0) = -\pi/3$ in (b1)-(b2), and $\phi_1(0) = \pi/2$, $\phi_2(0) = -\pi/2$, $\phi_3(0) = \pi$ and $\phi_4(0) = 0$ in (c1)-(c2). Both the amplitude of the radial vibration $r = \sqrt{x^2 + y^2}$ (panels (a1), (b1), and (c1)) and the position of the balls $\phi_i$ (panels (a2), (b2), and (c2)) are plotted against the dimensionless time $t$.

balls of the ADB system keep going over the rotor indefinitely. However, in Figs.5.10 (a2), and (c2), one of the balls stops giving laps to the rotor, and it oscillates around a specific position. The lowest $r_{max}$ value is shown in panel (a1), and the lowest oscillation amplitude is in panel (b1). In every case, the order of magnitude of the amplitude of the oscillation is quite large ( 0.5). Thus, these responses are highly undesirable, and we should avoid them. We will check that when the balls start with initial velocity to equal $-\Omega$, the system always reaches a limit cycle, or unlike, there exist some cases in which the balance is achieved.

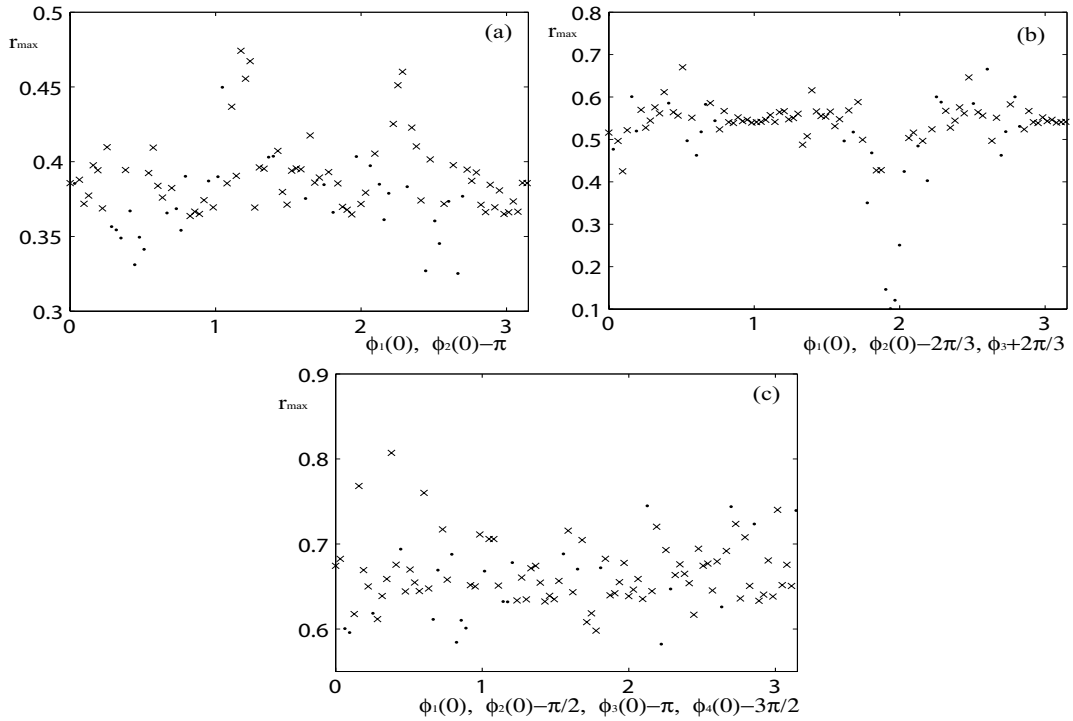


Figure 5.11: Maximum amplitude of the radial vibration $r_{max}$ against $\phi_1(0)$, when the balls start with a initial velocity $\dot{\phi}_i(0) = -\Omega, \quad i = 1 \ldots n$, and the initial position of the centre of rotation and its velocity are zero ($x(0) = y(0) = \dot{x}(0) = \dot{y}(0) = 0$), for the taken parameter set $\Omega = 4$, $\zeta = \beta = \delta = 0.01$ and $\mu = 0.05$. The initial positions of the balls are chosen equidistantly: $\phi_2(0) = \phi_1(0) + \pi$ for the ADB system with two balls (panel (a)), $\phi_2(0) = \phi_1(0) + 2\pi/3$, $\phi_3(0) = \phi_1(0) - 2\pi/3$ for the ADB system with three balls (panel (b)), and $\phi_2(0) = \phi_1(0) + \pi/2$, $\phi_3(0) = \phi_1(0) + \pi$ and $\phi_4(0) = \phi_1(0) + 3\pi/2$ for the ADB system with four balls (panel (c)). The points marked by '$\cdot$' refer to balanced states, and points marked by '$\times$' refer to cases in which the system goes to a limit cycle.

In Fig.5.11, the $r_{max}$ values are plotted against $\phi_1(0)$ when the balls start with a initial velocity $\dot{\phi}_i(0) = -\Omega$, $i = 1, \ldots, n$, for the ADB system with two balls (panel (a)), for the ADB system with three balls (panel (b)), and for the ADB system with four balls (panel (c)). The chosen parameter set is (5.1) and the initial position of the centre of rotation and its velocity are fixed at zero ($x(0) = y(0) = \dot{x}(0) = \dot{y}(0) = 0$). We chose equidistant initial positions of the balls, that is, $\phi_2(0) = \phi_1(0) + \pi$ for two balls, $\phi_2(0) = \phi_1(0) + 2\pi/3$ and $\phi_3(0) = \phi_1(0) - 2\pi/3$ for three balls, and $\phi_2(0) = \phi_1(0) + \pi/2$, $\phi_3(0) = \phi_1(0) + \pi$ and $\phi_4(0) = \phi_1(0) + 3\pi/2$ for four balls. We can see that there exist some $\phi_1(0)$ values

for which the balance is achieved when the balls start with an initial velocity to equal $-\Omega$. This cases are marked in Fig.5.11 by '$\cdot$'. For the one hundred different solved initial positions, the ADB with two balls reaches the balance in 32 cases, the ADB with three balls 28 times, and the ADB with four balls 24 times. This balance has high $r_{max}$ values that grows with the number of balls. The reason could be that the $\mu$ parameter was chosen the same for the three systems, which means that the total mass of the balls is larger as bigger number of balls. Hence the kinetic energy of the system is larger as bigger number of balls, so it would be necessary more time to dissipate the energy of the system to reach an equilibrium. As conclusion, we can say that the initially stationary positions of the balls within the fixed frame do no give good results, in the sense that it is difficult to reach the balance, and when it is achieved, the radial vibration during the transient is large.

## 5.2 Effects of the parameters

In Chapter 4 we performed a bifurcation analysis to investigate the effect that a variation of the dimensionless parameters has on the dynamics of the ADB. Now in this section, we use numerical simulation to confirm the results obtained by bifurcation theory, and to study further the effect of the parameters on the response of the ADB system with two, three, and four balls. In all subsequent runs, we will take zero initial position and velocity of the centre of rotation ($x(0) = y(0) = \dot{x}(0) = \dot{y}(0) = 0$), and zero initial velocity of the balls ($\dot{\phi}_i(0) = 0$, for $i = 1, \ldots, n$). The initial positions of the balls will be

$$\phi_1(0) = \pi/2, \quad \phi_2(0) = -\pi/2, \tag{5.3}$$

for the ADB system with two balls,

$$\phi_1(0) = \pi/3, \quad \phi_2(0) = -\pi/3, \quad \phi_3(0) = \pi, \tag{5.4}$$

for the ADB system with three balls, and

$$\phi_1(0) = \pi/2, \quad \phi_2(0) = -\pi/2, \quad \phi_3(0) = \pi, \quad \phi_4(0) = 0, \tag{5.5}$$

for the ADB system with four balls. That is, we choose an equidistant initial position of the ball for each system.

### 5.2.1 Exploration in $(\Omega, \mu)$-diagram

Figures 5.12, 5.13, and 5.14 explore the dynamics of different regions of the bifurcation diagrams in the $(\Omega, \mu)$-plane shown in Figs.4.1, 4.5, and 4.10 for the ADB with two, three and four balls, respectively. Panels (a) in Figures 5.12, 5.13, and 5.14, show the case for $\Omega = 0.5$ and $\mu = 0.05$. Eventually, and for the three cases (ADB with two, three and four balls) the transient of the rotor with the ADB (shown in black) becomes attracted to the stable coincident state **2-**, and the values of $\phi_i$, for $i = 1, \ldots, n$ (not depicted), are indeed observed to converge. However, in the three cases, for these parameter values, this steady state results in a much greater radial vibration $r$ than would be the case without the ADB (shown in gray). The highest $r$ values are for ADB with four balls, ADB with three balls, and ADB with two balls, respectively, that is, $r$ becomes larger as the number of balls

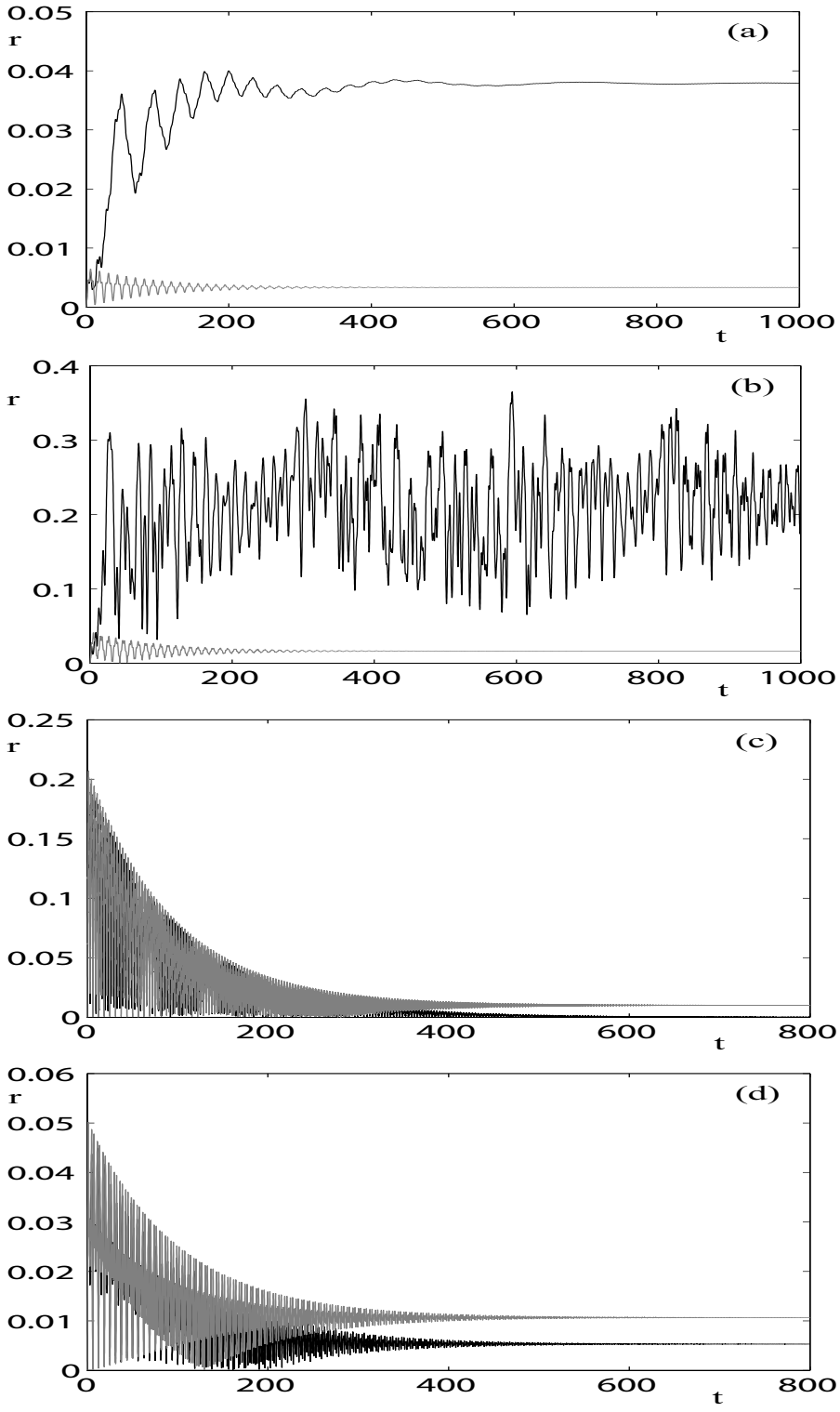


Figure 5.12: Numerical simulations of the ADB system with two balls for the parameter set $\zeta = 0.01$, $\beta = 0.01$, and $\delta = 0.01$. Initial conditions were fixed at $x(0) = y(0) = \dot{x}(0) = \dot{y}(0) = \dot{\phi}_1(0) = \dot{\phi}_2(0) = 0$, $\phi_1(0) = \pi/2$, and $\phi_2(0) = -\pi/2$. Values of $\Omega$ and $\mu$ varied as $(\Omega, \mu) = (0.5, 0.05)$ (a), $(\Omega, \mu) = (1.6, 0.05)$ (b), $(\Omega, \mu) = (20, 0.05)$ (c), and $(\Omega, \mu) = (4, 0.0025)$ (d).

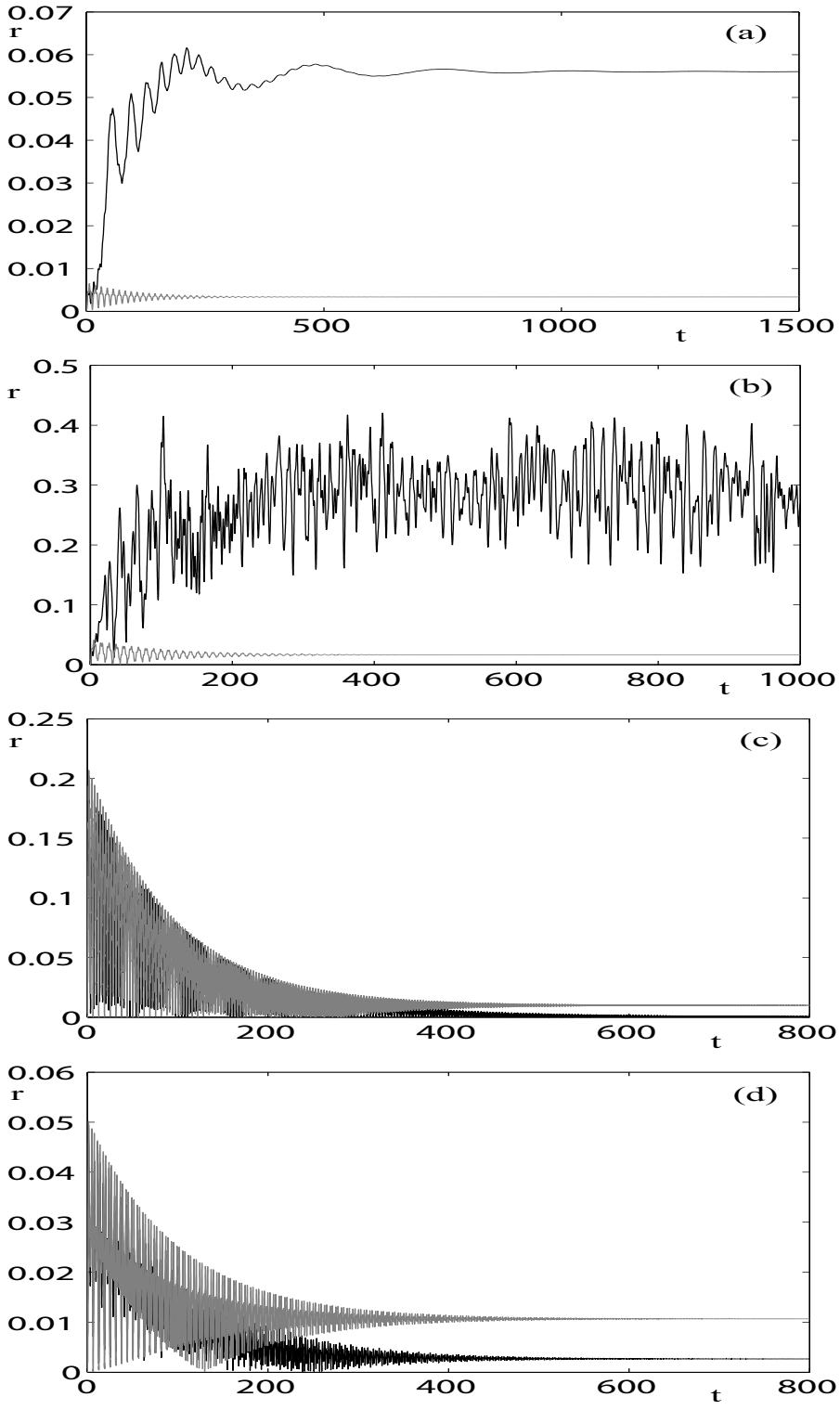


Figure 5.13: Numerical simulations of the ADB system with three balls for the parameter set $\zeta = 0.01$, $\beta = 0.01$, and $\delta = 0.01$. Initial conditions were fixed at $x(0) = y(0) = \dot{x}(0) = \dot{y}(0) = \dot{\phi}_1(0) = \dot{\phi}_2(0) = \dot{\phi}_3(0) = 0$, $\phi_1(0) = \pi/3$, $\phi_2(0) = -\pi/3$, and $\phi_3(0) = \pi$. Values of $\Omega$ and $\mu$ varied as $(\Omega, \mu) = (0.5, 0.05)$ (a), $(\Omega, \mu) = (1.6, 0.05)$ (b), $(\Omega, \mu) = (20, 0.05)$ (c), and $(\Omega, \mu) = (4, 0.0025)$ (d).

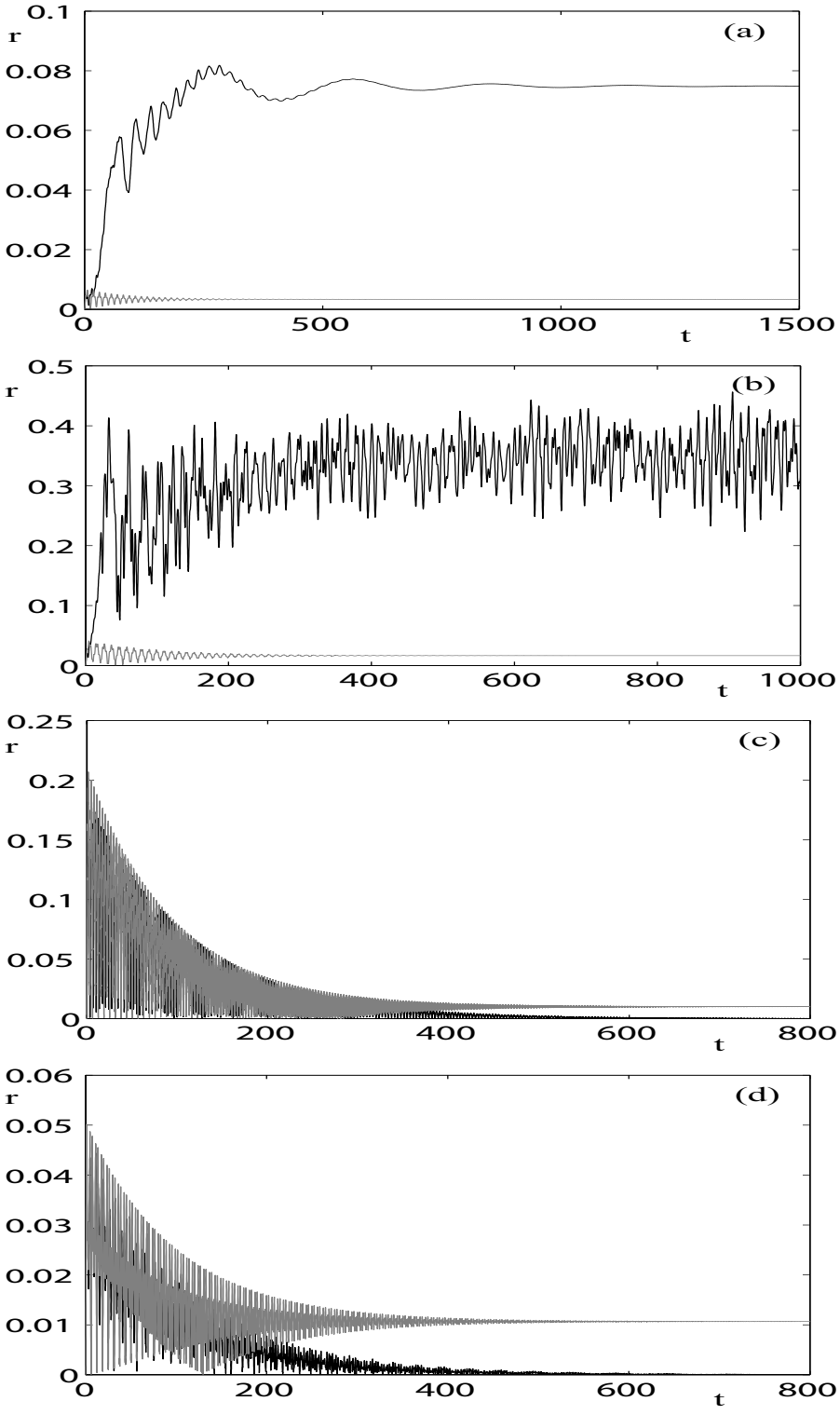


Figure 5.14: Numerical simulations of the ADB system with four balls for the parameter set $\zeta = 0.01$, $\beta = 0.01$, and $\delta = 0.01$. Initial conditions were fixed at $x(0) = y(0) = \dot{x}(0) = \dot{y}(0) = \dot{\phi}_1(0) = \dot{\phi}_2(0) = \dot{\phi}_3(0) = \dot{\phi}_4(0) = 0$, $\phi_1(0) = \pi/2$, $\phi_2(0) = -\pi/2$, $\phi_3(0) = \pi$, and $\phi_4(0) = 0$. Values of $\Omega$ and $\mu$ varied as $(\Omega, \mu) = (0.5, 0.05)$ (a), $(\Omega, \mu) = (1.6, 0.05)$ (b), $(\Omega, \mu) = (20, 0.05)$ (c), and $(\Omega, \mu) = (4, 0.0025)$ (d).

increases. Panels (b) depict the case for $\Omega = 0.16$ and $\mu = 0.05$. Here the bifurcation analysis finds no stable equilibria (or limit cycles) (see Figs.4.1, 4.5, and 4.10). The rotor with the ADB (shown in black) in the three cases, appears now to exhibit chaotic motion, again reaching much larger values of radial vibration $r$ than the rotor without the ADB mechanism. This case deserves further study. In the three systems, $r$ reaches approximately similar high values around 0.4. Figures 5.12, 5.13, and 5.14, depict in their panels (c) a high-rotation speed $\Omega = 20.0$, and $\mu = 0.05$, this is well to the right of the stability boundary H1 for the balanced state **1** (see Figs.4.1, 4.5, and 4.10). Balance is eventually achieved, albeit at the expense of a large transient response. The $r_{max}$ values are 0.1940, 0.1903, and 0.1855 for two, three, and four balls, respectively. Considering the transient is finished when $r < 10^{-3}$, the $t_{dec}$ values would be 567.89, 722.13, and 603.44, respectively. As we have checked out, the transient response is very similar in each case, although we can emphasize that the transient length for two balls is the shortest, and for three balls is the longest.

Panels (d) of Figs.5.12-5.14 show a case with a small mass ratio $\mu = 0.0025$ and $\Omega = 4.0$. This does not satisfy the balance conditions (3.14) for the given eccentricity $\delta$ when $n = 2$ and $n = 3$. Hence, for two and three balls (see Figs.5.12(d) and 5.13(d)), the system does not achieve the balance, but reaches the coincident equilibria **2-**, which, as it is shown in Figs.4.1 and 4.5, is stable for $\Omega = 4$ and $\mu = 0.0025$, in both cases $n = 2$ and $n = 3$. In contrast to Figs.5.12(a) and 5.13(a), this coincident equilibrium is preferable to the final state obtained without the ADB. In fact, as we can see in Figs. 4.2, 4.6, and 4.11, the balls in the coincident state **2-** are situated on the same side of the rotor as the imbalance for low $\Omega$, thus causing a much greater radial vibration than when the rotor does not have the ADB mechanism (compare black and gray curves in panels (a)). Furthermore, if the number of balls were bigger, the whole unbalanced mass would be greater, so the vibration would be increased (compare $r$ values in Fig.5.12(a) ($n = 2$ balls), with 5.13(a) ($n = 3$ balls), and with 5.14(a) ($n = 4$ balls)). However, as $\Omega$ is increased, the coincident state moves the balls to the other side of the rotor, opposite to the imbalance, and a reduction in the radial vibration is observed (proportional to the number of balls), that is, $r$ would be smaller with the ADB system than in the rotor without it (compare black and gray curves in Figs.5.12(d) and 5.13(d)). Now the $r$ value of the coincident state **2-** for the ADB with three balls is smaller than the one for the ADB with two balls, in contrast with the one of panel (a). For the ADB with four balls, Fig.5.14(d) shows that the balance is achieved, but for this balanced state the balls are in the same position. That means, as we said in Chapter 3, that the balanced state **1** and the coincident state **2-** are the same when $\mu = \mu_c := \delta/n$ (for this parameter set, $\delta/n = 0.01/4 = 0.0025 = \mu$). It corresponds to a pitchfork bifurcation, as we can see in Fig.4.10(a).

### 5.2.2 Effect of the damping $\beta$ and $\zeta$

Figures 5.15, 5.16, and 5.17 show the effects of both increasing the damping ratio of the suspension of the rotor (governed by the dimensionless parameter $\zeta$) and the viscous damping of the motion of the balls (governed by the dimensionless parameter $\beta$), for the ADB system with two, three, and four balls, respectively. In these Figures, $\delta$ and $\mu$ are fixed at 0.01 and 0.05, respectively. These results should be compared with the two-parameter bifurcation diagrams in the $(\Omega, \zeta)$-plane shown in Figs.4.4(b), 4.8(b), and 4.13(b), and in the

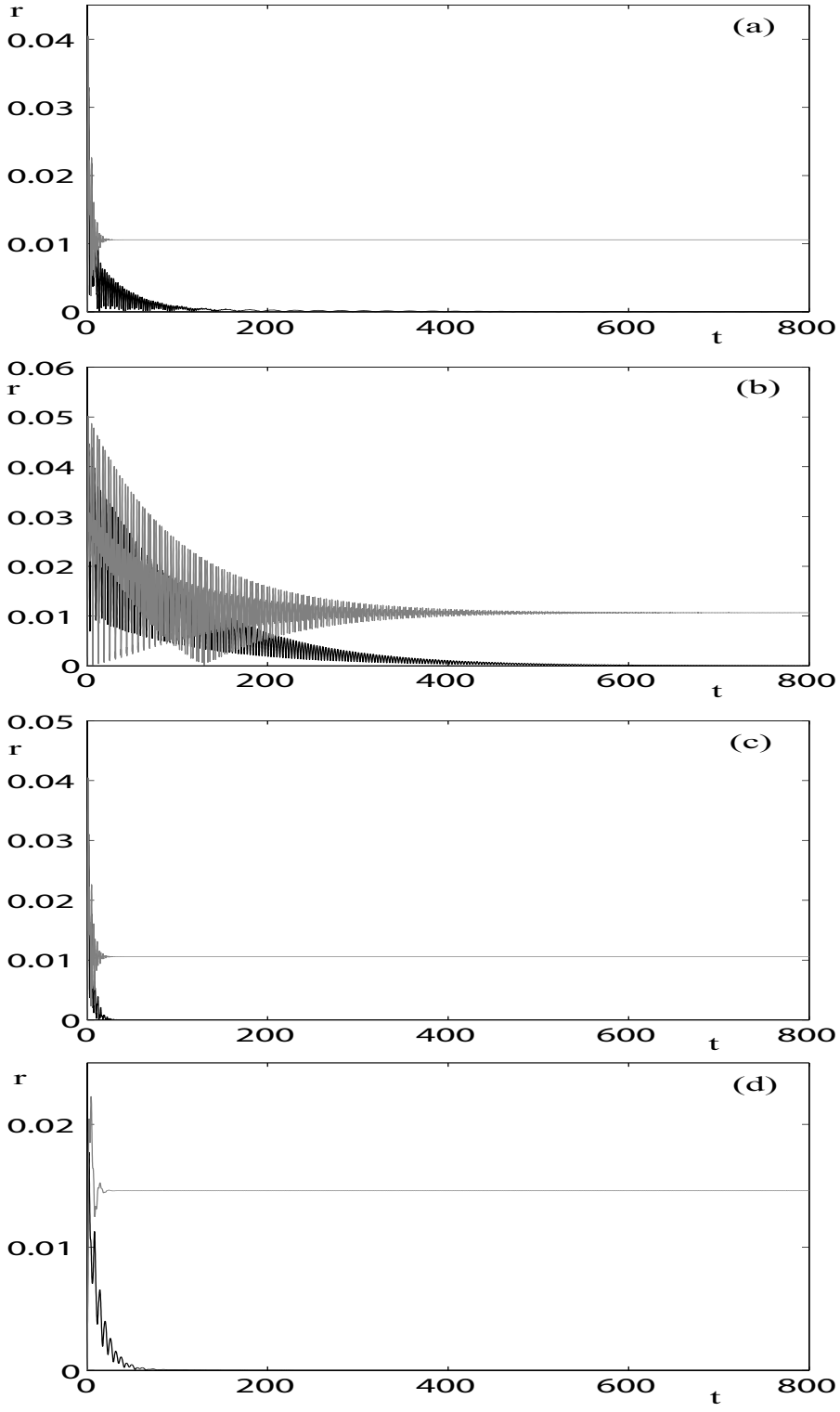


Figure 5.15: Numerical simulations of the ADB system with two balls for the parameter set $\delta = 0.01$, and $\mu = 0.05$. Initial conditions were fixed at $x(0) = y(0) = \dot{x}(0) = \dot{y}(0) = \dot{\phi}_1(0) = \dot{\phi}_2(0) = 0$, $\phi_1(0) = \pi/2$, and $\phi_2(0) = -\pi/2$. Values of $\Omega$, $\zeta$ and $\beta$ varied as $(\Omega, \zeta, \beta) = (4, 0.25, 0.01)$ (a), $(\Omega, \zeta, \beta) = (4, 0.01, 0.25)$ (b), $(\Omega, \zeta, \beta) = (4, 0.25, 0.25)$ (c), and $(\Omega, \zeta, \beta) = (1.6, 0.25, 0.25)$ (d).

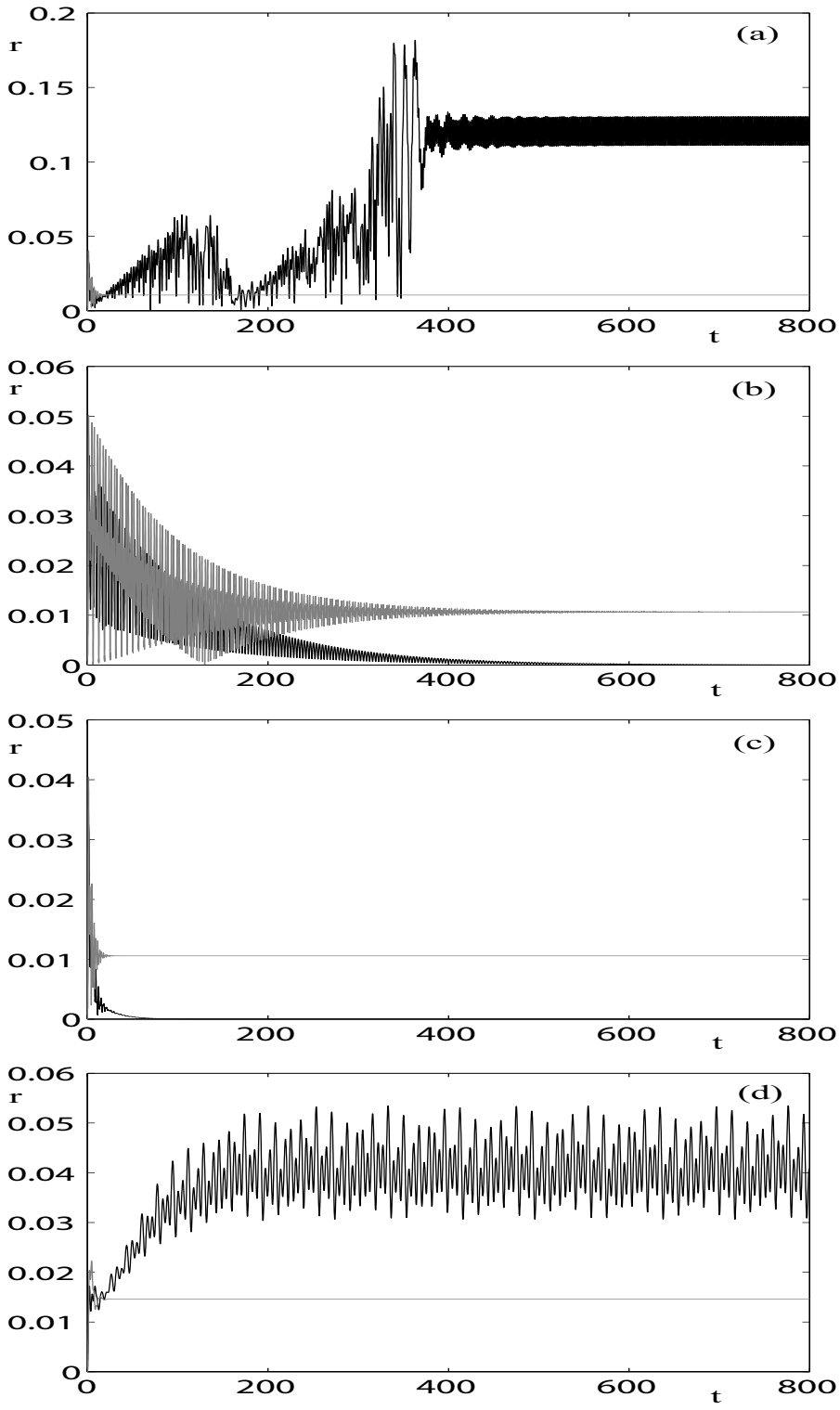


Figure 5.16: Numerical simulations of the ADB system with three balls for the parameter set $\delta = 0.01$, and $\mu = 0.05$. Initial conditions were fixed at $x(0) = y(0) = \dot{x}(0) = \dot{y}(0) = \dot{\phi}_1(0) = \dot{\phi}_2(0) = \dot{\phi}_3(0) = 0$, $\phi_1(0) = \pi/3$, $\phi_2(0) = -\pi/3$, and $\phi_3(0) = \pi$. Values of $\Omega$, $\zeta$ and $\beta$ varied as $(\Omega, \zeta, \beta) = (4, 0.25, 0.01)$ (a), $(\Omega, \zeta, \beta) = (4, 0.01, 0.25)$ (b), $(\Omega, \zeta, \beta) = (4, 0.25, 0.25)$ (c), and $(\Omega, \zeta, \beta) = (1.6, 0.25, 0.25)$ (d).

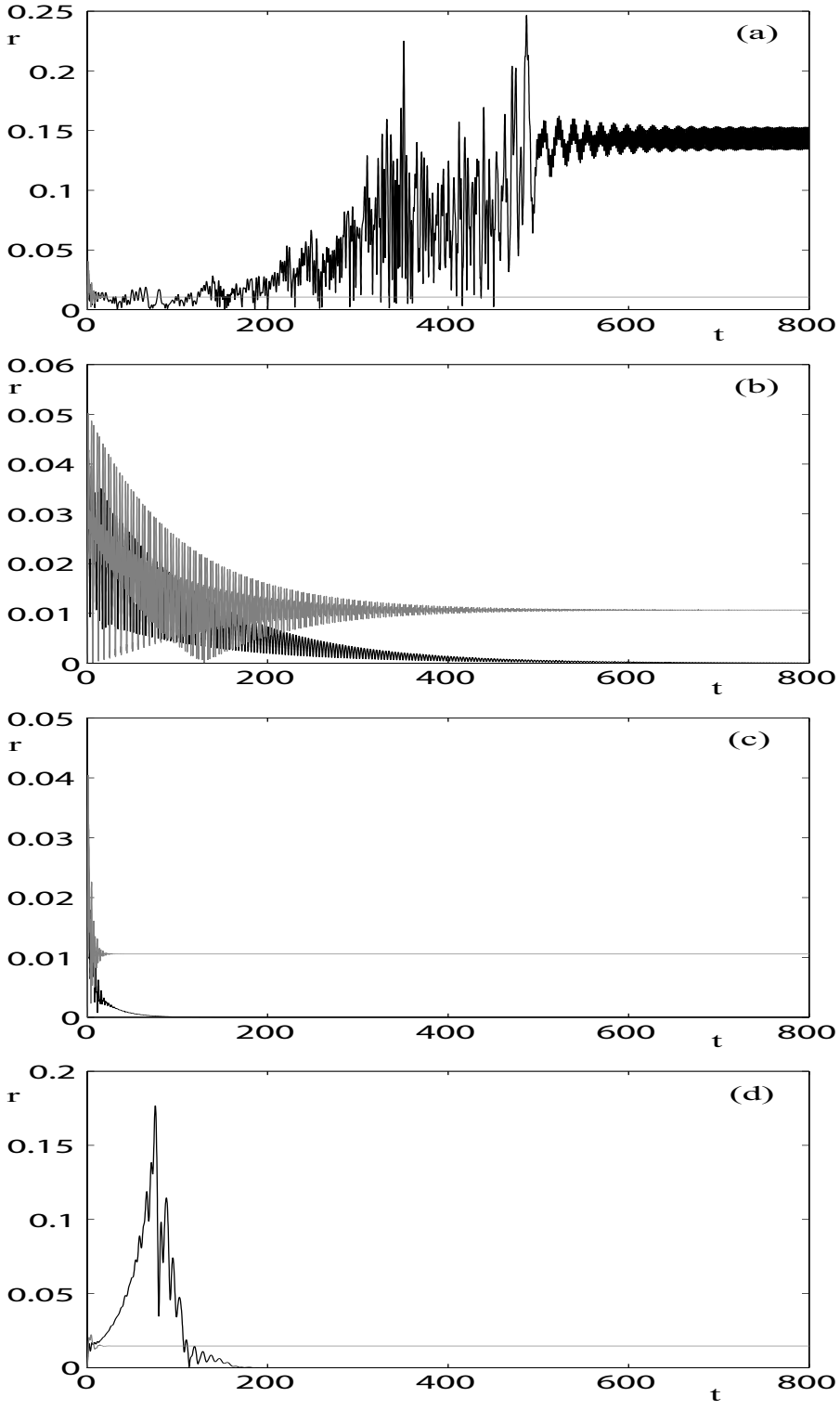


Figure 5.17: Numerical simulations of the ADB system with four balls for the parameter set $\delta = 0.01$, and $\mu = 0.05$. Initial conditions were fixed at $x(0) = y(0) = \dot{x}(0) = \dot{y}(0) = \dot{\phi}_1(0) = \dot{\phi}_2(0) = \dot{\phi}_3(0) = \dot{\phi}_4(0) = 0$, $\phi_1(0) = \pi/2$, $\phi_2(0) = -\pi/2$, $\phi_3(0) = \pi$, and $\phi_4(0) = 0$. Values of $\Omega$, $\zeta$ and $\beta$ varied as $(\Omega, \zeta, \beta) = (4, 0.25, 0.01)$ (a), $(\Omega, \zeta, \beta) = (4, 0.01, 0.25)$ (b), $(\Omega, \zeta, \beta) = (4, 0.25, 0.25)$ (c), and $(\Omega, \zeta, \beta) = (1.6, 0.25, 0.25)$ (d).

$(\Omega, \beta)$-plane shown in Figs.4.4(c), 4.8(c), and 4.13(c), in which the parameters $(\delta, \mu)$ are also fixed at $(0.01, 0.05)$. Figure 5.15(a) shows for the ADB with two balls, that for an increased damping ratio of the rotor $\zeta = 0.25$, while keeping the ball damping fixed at $\beta = 0.01$, a balanced state with lower $r$ values during the transient, as well as a shorter decay time than for $\zeta = 0.01$ (see Fig.5.4(a1)) is obtained. However, Figs.5.16(a) and 5.17(a) show that for ADB with three and four balls, the balance loses its stability, and the system reaches a limit cycle with $r$ values around 0.1 and 0.15. This result agrees with the bifurcation digram in the $(\Omega, \zeta)$-plane for ADB with three balls (Fig.4.8(b)) and for ADB with four balls (Fig.4.13(b)), in which we can see that the balanced state loses the stability for high $\Omega$ values when $\zeta$ is increased. Approximately, for $\Omega = 4$, the bifurcation analysis shows that the balanced state is only stable for $\zeta < 0.02$ in the ADB with three balls, and for $\zeta < 0.1$ in the ADB with four balls.

Figs.5.15(b), 5.16(b), and 5.17(b) show that increasing the damping of the balls to $\beta = 0.25$, while keeping the damping ratio of the rotor fixed at $\zeta = 0.01$ results in convergence to the balanced state **1** after a long transient, for all the ADB systems with two, three and four balls. Now, the transient oscillations are much smoother than for $\beta = 0.01$. The transient response for each system is again very similar. Thus, the ($r_{max}$, $t_{dec}$) values are (0.0447, 406.21), (0.0421, 421.82), and (0.0429, 437.60) for two, three, and four balls respectively. Figures 5.15(c), 5.16(c), and 5.17(c) show that an increase in damping of both the rotor $\zeta = 0.25$ and the balls $\beta = 0.25$ seems to have a highly desirable effect; convergence to the balanced state **1** is very rapid. The three system has very similar transient response again, although the transient length is a bit longer as the number of balls increases: $t_{dec} = 15.76$ for two balls, $t_{dec} = 32.47$ for three balls, and $t_{dec} = 41.42$ for four balls. We can also note in this case that, besides a shorter transient, the $r_{max}$ values are a bit smaller than in last panels (b): $r_{max} = 0.0315$ for two balls, $r_{max} = 0.0325$ for three balls, and $r_{max} = 0.0323$ for four balls.

Finally, Figs.5.15(d), and 5.17(d) show that increasing both damping parameters to $\zeta = \beta = 0.25$ can stabilise the chaotic dynamics shown in Figs.5.12(b), and 5.14(b) for ADB with two and four balls, respectively. Again, stability is achieved in a very short time, and with a very low $r_{max}$ value in the case with two balls. However, the ADB system with four balls takes more time to reach the balance, and the amplitude of the radial vibration $r$ reaches high values during the transient ($r_{max} \approx 0.17$). The ADB with three balls seems to be attracted to a limit cycle, and although the balance is not achieved, the $r$ values for this limit cycle are much smaller than the values reached during the chaotic motion for $\zeta = \beta = 0.01$ in Fig.5.13(b). Further numerical experiments using the values $\beta = \zeta = 0.25$, show a far greater robustness than those for $\beta = \zeta = 0.01$. It would appear that a far greater range of initial conditions is attracted to the balanced state **1** and that the transient is as rapid as in Figs.5.15(c), 5.16(c), 5.17(c). We will confirm these results in the next paragraph.

Let us continue studying the effects of the damping of both the ball $\beta$ and the rotor $\zeta$. We have already seen that an increased damping of the rotor $\zeta$, while keeping the ball damping fixed at $\beta = 0.01$, produces a loss of stability of the balanced state for the cases $n = 3$ and $n = 4$ balls. We will see that this effect is also experimented by the ADB with two balls.

Figure 5.18 shows the basins of attraction of the balanced steady state for varying initial positions of the balls $\phi_1(0)$ and $\phi_2(0)$, for the ADB system with two balls. Internal damping

was fixed at $\beta = 0.01$, while external damping ratio $\zeta$ was varied from panel to panel. The regions with the plotted points ' $\cdot$ ' correspond to initial conditions from which the balanced state is attracting, the light regions to initial conditions from which unbalanced steady states, periodic or more complex dynamics are observed. Note that all plots are symmetric about the line $\phi_1(0) = \phi_2(0)$, due to the two balls are assumed to be identical. Fig.5.18(a) shows that, for $\zeta = 0.01$, the basin of attraction of the balanced state is accessible from most initial ball positions. Exceptions being when the balls are launched from the same position, $\phi_1(0) = \phi_2(0)$, or from a small number of positions about this line, and others few positions around $\phi_{1,2}(0) = 0.5$, $\phi_{2,1}(0) = 5$. As the external damping ratio $\zeta$ is increased, Fig.5.18(b) for $\zeta = 0.1$ shows that the basin of attraction decreases. One observes regions with complex boundaries about the line $\phi_1(0) = \phi_2(0)$ and also when the balls are launched close to the imbalance $\phi_{1,2}(0) = 0$, $\phi_{2,1}(0) = \phi_{1,2}(0) + 2\pi$. Fig.5.18(c) shows that for $\zeta = 0.2$ these regions, outside the basin of attraction, become broader and their edges become smoother; correspondingly, the shaded region defining the basin of attraction is seen to decrease in size. Finally, Fig.5.18(d) for $\zeta = 0.25$ shows a little smaller basin of attraction of the balanced state, very similar to the one shown one in panel (c). We can see that these shaded regions for $\zeta = 0.2$ and $\zeta = 0.25$ correspond with points around the lines $\phi_2(0) = \phi_1(0) + \pi$ and $\phi_2(0) = \phi_1(0) - \pi$, that is, in-line initial positions of the balls. That confirms what we saw in Fig.5.5(b), that when $\phi_2(0) = \phi_1(0) + \pi$ for ADB with two balls, the balanced is achieved easier than with any other initial position of the balls. Note that the balanced state is, of course, contained within this 'tear-drop' shaped basin of attraction (as it is within each shaded region of Fig.5.18).

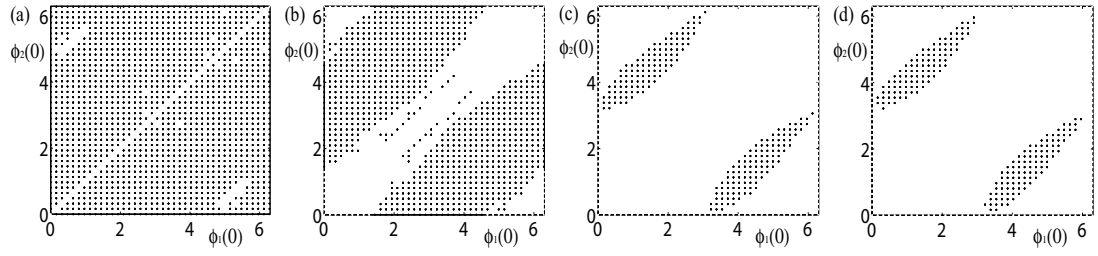


Figure 5.18: Basins of attraction of the balanced state for varying initial positions of the balls $\phi_1(0)$ and $\phi_2(0)$, for the ADB system with two balls. All other initial conditions were set to zero. Parameters were fixed at $\Omega = 4$, $\beta = 0.01$, $\delta = 0.01$, $\mu = 0.05$. From (a) to (d), the external damping ratio $\zeta$ was given values 0.01, 0.1, 0.2 and 0.25. The regions with the plotted points ' $\cdot$ ' correspond to initial conditions from which the balanced state is attracting, the light regions to initial conditions from which unbalanced steady states, periodic or more complex dynamics are observed.

We made similar numerical experiments for the ADB system with three balls, in which $\phi_1(0)$ and $\phi_2(0)$ were varied from 0 to $\pi$, and the initial position of the third ball was fixed at opposite side than the first ball, and in line with the centre of rotation ($\phi_3(0) = \phi_1(0) + \pi$). While keeping ball damping fixed at $\beta = 0.01$, we solved problems for $\zeta = 0.01$, 0.1, 0.2, and 0.25, for forty different equidistant values of $\phi_1(0)$ and $\phi_2(0)$. For $\zeta = 0.01$ it was observed that the system reached the balance for all different initial positions of the balls, except when $\phi_1(0) = \phi_2(0)$. However, when we solved the problem for $\zeta = 0.1$, it was observed that the balance was achieved only twice of the 1600 different initial positions of the balls for which the problem was solved, that is, practically for all initial positions of the balls the

balance was not attracting. Again, for $\zeta = 0.2$ and $\zeta = 0.25$ there was no initial position from which the system reached the balance. This fact agrees with the bifurcation diagram shown in Fig.4.8(b), that is, the balance for the ADB system with three balls loses its whole stability when $\zeta$ is over a determinated value depending on $\Omega$ value.

In the case of the ADB with four balls, we made the same numerical experiments keeping the third and fourth balls at opposite side of the first and the second balls, respectively, and in line with the centre of rotation ($\phi_3(0) = \phi_1(0) + \pi$, and $\phi_4(0) = \phi_2(0) + \pi$). The results are shown in Figure 5.19. In panel (a) we can see that when $\zeta = 0.01$, the system reaches the balance from all the initial positions of the balls, including $\phi_1(0) = \phi_2(0)$. In Fig.5.19(b) we observe that, for $\zeta = 0.1$, there are some irregularly distributed points from which the balance state is not attracting. For $\zeta = 0.2$ and $\zeta = 0.25$, Figs.5.19(c) and (d) show that the stability of the balanced state is reduced to the line $\phi_1(0) = \phi_2(0)$, and to four small regions around $\phi_{1,2}(0) = \pi/2$ and $\phi_{1,2}(0) = 3\pi/2$. Although it could seem strange that, in contrast to what we had seen for two and tree balls, now the balance state is attracting for $\phi_1(0) = \phi_2(0)$, it has an explanation. In this case, $\phi_1(0) = \phi_2(0)$ implies that there are two balls in a coincident initial position ($\phi_1(0) = \phi_2(0)$), and the other two in another coincident position at the opposite side and in line with the centre of rotation ($\phi_3(0) = \phi_4(0) = \phi_1(0) + \pi$). This situation would be equivalent to an ADB with two balls, in which they start from an in line position, that is, $\phi_2(0) = \phi_1(0) + \pi$. As we saw in Fig.5.18 for the ADB with two balls, for this initial relative positions of the balls, the balance is very attracting. In fact, it was found that in the line $\phi_1(0) = \phi_2(0) = \phi_3(0) - \pi = \phi_4(0) - \pi$ the ADB system with four balls behaves as an ADB with two balls, that is, the starting together coincident balls never separate each other. Furthermore, the response of the system with four balls is identical to the response of an ADB with two balls with double $\mu$ value ($\mu = 0.1$). Hence, we note that there exists some equivalence relationship between the system with different number of balls. Finally, the four shade regions from which the balance is reached, correspond to points around the initial positions $\phi_{1,2} = \pi/2$ and $\phi_{1,2} = 3\pi/2$. That means two balls starting near the position $\phi_1 = \pi/2$, and the other two near $\phi = 3\pi/2$.

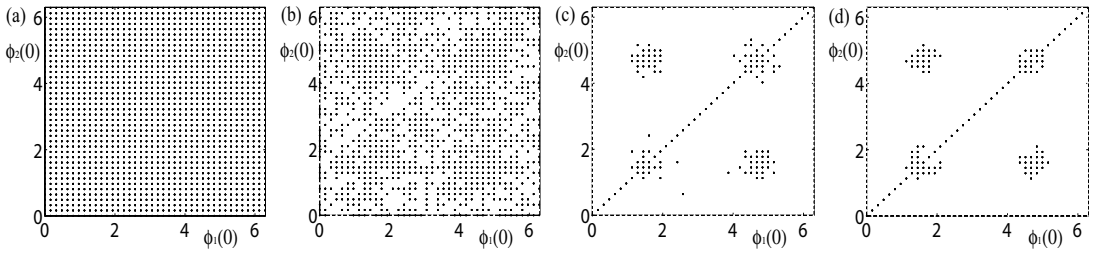


Figure 5.19: Basins of attraction of the balanced state for varying initial positions of the balls $\phi_1(0)$ and $\phi_2(0)$, for the ADB system with four balls. The initial positions of the third and fourth balls were varied as $\phi_3(0) = \phi_1(0) + \pi$ and $\phi_4(0) = \phi_2(0) + \pi$. All other initial conditions were set to zero. Parameters were fixed at $\Omega = 4$, $\beta = 0.01$, $\delta = 0.01$, $\mu = 0.05$. From (a) to (d), the external damping ratio $\zeta$ was given values 0.01, 0.1, 0.2 and 0.25. The regions with the plotted points ' $\cdot$ ' correspond to initial conditions from which the balanced state is attracting, the light regions to initial conditions from which unbalanced steady states, periodic or more complex dynamics are observed.

In addition to what we have already commented, we note that an investigation of a

variation of the internal damping $\beta$ was shown to increase the basin of attraction of the balanced state. In fact, keeping ball damping fixed at $\beta = 0.25$, for varying rotor damping $\zeta = 0.01$, 0.1, 0.2, and 0.25, the only initial conditions which did not converge to the balanced state were the ones along the line $\phi_1(0) = \phi_2(0)$ for the ADB with two and three balls. For the ADB system with four balls, the balance was shown to be attracting even in the line $\phi_1(0) = \phi_2(0)$, for the reason explained in last paragraph.

We have just studied the basins of attraction of the balanced steady state for a varying rotor damping $\zeta$, while the ball damping $\beta$ is fixed. Figure 5.20 shows the basins of attraction for varying both $\zeta$ and $\beta$, with equidistant initial position of the balls. We can see in panel (a) that, for the ADB with two balls, the balance is attracting for the whole area $[\zeta, \beta] \in [[0.01, 0.25] \times [0.01, 0.25]]$. Panel (b) shows that, for the ADB with three balls, the balanced equilibrium loses its stability in a large region inside the area $[\zeta, \beta] \in [[0.01, 0.25] \times [0.01, 0.25]]$. Thus, for low $\beta$ values, the balance is only stable in a $\zeta$ values range from 0.01 to a specific value, which is higher while $\beta$ increases. This result agrees again with the bifurcation diagram in the $(\Omega, \zeta)$-plane for ADB with three balls (see Fig.4.8(b)). The ADB with four balls shows more stability for the balance than the ADB with three balls. In panel (c) we can see that for four balls, the system does not achieve the balance only for a few $\zeta$ values, when $\beta$ is very small.

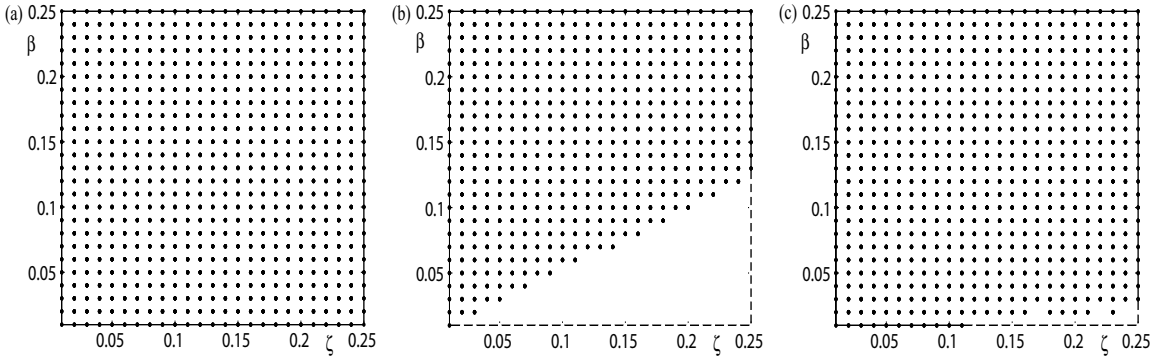


Figure 5.20: Basins of attraction of the balanced state for varying rotor damping $\zeta$ and varying ball damping $\beta$. The other parameters were fixed at $\Omega = 4$, $\delta = 0.01$ and $\mu = 0.05$. The initial positions of the balls were $\phi_1(0) = \pi/2$, and $\phi_2(0) = -\pi/2$ for the ADB system with two balls (a); $\phi_1(0) = \pi/3$, $\phi_2(0) = -\pi/3$, and $\phi_3(0) = \pi$ for the ADB system with three balls (b); $\phi_1(0) = \pi/2$, $\phi_2(0) = -\pi/2$, $\phi_3(0) = \pi$, and $\phi_4(0) = 0$ for the ADB system with four balls (d). All other initial conditions were set to zero. The regions with the plotted points '$\cdot$' correspond to ($\zeta$, $\beta$) values for which the balanced state is attracting, the light regions to ($\zeta$, $\beta$) values for which unbalanced steady states, periodic or more complex dynamics are observed.

Let us see how the transient response changes for varying both $\zeta$ and $\beta$. Figure 5.21 depicts the maximum amplitude of the radial vibration during the transient $r_{max}$, against both the balls and rotor damping ($\beta$ and $\zeta$). We chose equidistant initial positions of the balls for all the systems, with two balls (panel (a)), with three balls (panel (b)), and with four balls (panel (c)). In general, we can see that $r_{max}$ grows when $\zeta$ and $\beta$ decrease. We can also observe that $r_{max}$ is more sensitivity to $\zeta$ than to $\beta$. In fact, the variation of $r_{max}$ with $\beta$ is almost imperceptible if we compare with its variation with $\zeta$. However, the $\beta$

parameter affects the transient response in the sense that for low values, the balance becomes non attracting for increased $\zeta$, as we saw in Fig.5.20. Thus, the highest $r_{max}$ values in Figs.5.21(b) and (c), correspond to unstable balance for ADB with three and four balls, respectively. In other points in which the balance is attracting, specially for low $\zeta$ and $\beta$ values, the $r_{max}$ values are a bit lower for ADB with three and four balls than for ADB with two balls.

In Figure 5.22, the transient length $t_{dec}$ is plotted against $\zeta$ and $\beta$, also for equidistant initial positions of the balls. In panel (a), we can see that, for the ADB with two balls, the transient length $t_{dec}$ always becomes shorter when $\zeta$ and $\beta$ increases. Effectively, while the damping of the suspension $\zeta$ and the damping of the balancing system $\beta$ are larger, it would take less time to dissipate the kinetic energy, and the equilibrium would be achieved faster. However, we can see in panels (b) and (c), that for three and four balls, there is a region of $(\zeta, \beta)$ values in which $t_{dec}$ becomes larger while $\zeta$ increases. This is due to the fact that, for those damping values, the balance is not attracting. Thus, for low $\beta$ and high $\zeta$ values, we can see that $t_{dec}$ reaches the highest values. This confirms what we have already said, that is, the ADB system with three and four balls loses the balance stability for large $\zeta$, when $\beta$ keeps small. We can observe again that this effect is harder in the ADB with three balls than in the ADB with four balls. Unlike, for high $\beta$ values, $t_{dec}$ always decreases with $\zeta$ and $\beta$. This variation of $t_{dec}$ is harder for low $\zeta$ values. Thus, for $\zeta > 0.1$, $t_{dec}$ keeps almost constant with $\zeta$, whenever the balance is attracting, that is, when $\beta$ is large enough.

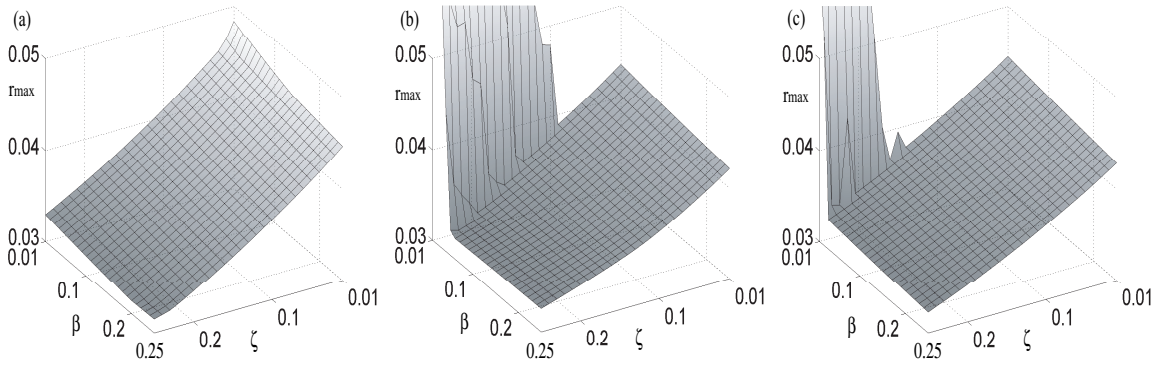


Figure 5.21: Maximum amplitude of the radial vibration $r_{max}$ for varying rotor damping $\zeta$ and varying ball damping $\beta$. The other parameters were fixed at $\Omega = 4$, $\delta = 0.01$ and $\mu = 0.05$. The initial positions of the balls were $\phi_1(0) = \pi/2$, and $\phi_2(0) = -\pi/2$ for the ADB system with two balls (a); $\phi_1(0) = \pi/3$, $\phi_2(0) = -\pi/3$, and $\phi_3(0) = \pi$ for the ADB system with three balls (b); $\phi_1(0) = \pi/2$, $\phi_2(0) = -\pi/2$, $\phi_3(0) = \pi$, and $\phi_4(0) = 0$ for the ADB system with four balls (d). All other initial conditions were set to zero.

### 5.2.3 Simulation for $\Omega$ and $\delta$ ranges

In Figure 5.23 we depict the maximum amplitude of the radial vibration $r_{max}$ and the transient length $t_{dec}$ against a $\Omega$ values range, from 0 to 20. We use equidistant initial positions of the balls for the ADB systems with two, three, and four balls. In practical situations we will not know the absolute initial positions of the balls within the rotation

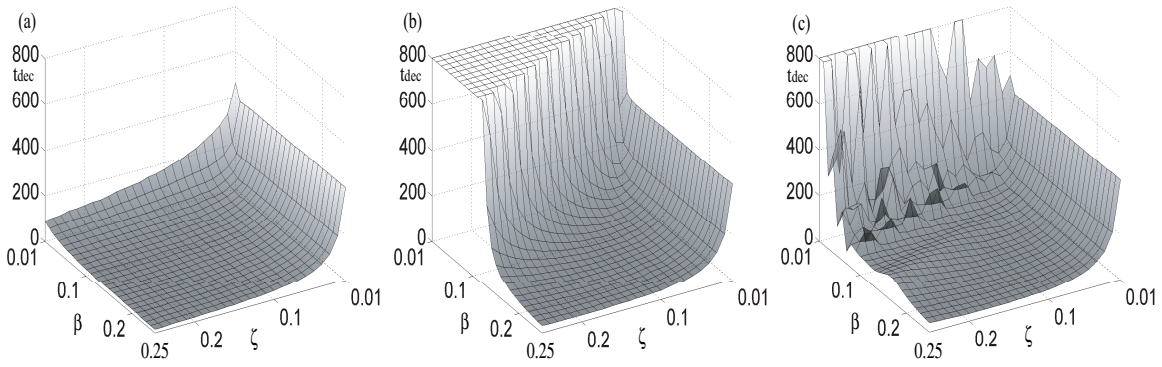


Figure 5.22: Transient decay time $t_{dec}$ for varying rotor damping $\zeta$ and varying ball damping $\beta$. The other parameters were fixed at $\Omega = 4$, $\delta = 0.01$ and $\mu = 0.05$. The initial positions of the balls were $\phi_1(0) = \pi/2$, and $\phi_2(0) = -\pi/2$ for the ADB system with two balls (a); $\phi_1(0) = \pi/3$, $\phi_2(0) = -\pi/3$, and $\phi_3(0) = \pi$ for the ADB system with three balls (b); $\phi_1(0) = \pi/2$, $\phi_2(0) = -\pi/2$, $\phi_3(0) = \pi$, and $\phi_4(0) = 0$ for the ADB system with four balls (d). All other initial conditions were set to zero.

frame, since we do not actually know where the centre of mass of the rotor is positioned. Therefore, we study which $r_{max}$ and $t_{dec}$ values range will be obtained in practical applications of the ADB. For that, we solve the equations of motion for ten random absolute equidistant initial positions of the balls for each $\Omega$ value. The $\mu$ parameter value it is chosen such that the whole balls mass is $\widetilde{m} := n\mu = 6\delta = 0.06$. Thus, $\mu = 0.03$ for ADB with two balls, $\mu = 0.02$ for ADB with three balls, and $\mu = 0.015$ for ADB with four balls. In this way, we are comparing if it is better to share the balance mass between two, between three, or between four balls. Figs.5.23 (a1), (b1), and (c1) show that $r_{max}$ grows linearly while $\Omega$ increases. The $r_{max}$ values for two balls in (a1), for three balls in (b1), and for four balls in (c1) are very similar. For each $\Omega$, we obtain very similar $r_{max}$ values for the ten different absolute initial positions of the balls. For $\Omega < 2.04$, $r_{max}$ takes very high values since in these cases the balance is not stable, and the system would undergo limit cycles or other more complex dynamic behaviours. In Figs.5.23 (a2), (b2), and (c2) we can see the transient length $t_{dec}$ for two, three, and four balls, respectively. The variation of $t_{dec}$ with $\Omega$ is softer than the variation of $r_{max}$. Now, there are more differences in the obtained results for the ten different absolute initial positions of the balls. Thus, we can observe that for a specific $\Omega$, the $t_{dec}$ values range is quite wide. The transient length is in general similar for the different numbers of balls, but we can observe that the $t_{dec}$ range is a bit smaller for four balls. Furthermore, for ADB with four balls, $t_{dec}$ values are a bit lower.

To sum up, we can assert that the transient response becomes worse while the rotor increases its angular velocity. We also conclude that the only difference between sharing the balance mass in two, three, or four balls, is that the ADB with four balls shows a bit lower $t_{dec}$ values, and that it is more constant with different initial positions of the balls (when they are equidistantly positioned).

Let us study how the parameter $\delta$ affects the transient response in the cases in which the balance is achieved. Thus, Figure 5.24 depicts $r_{max}$ and $t_{dec}$ against a $\delta$ values range from 0 to $\widetilde{m} := n\mu = 0.03$. In fact, for $\delta > \widetilde{m}$, the balls mass are not big enough to

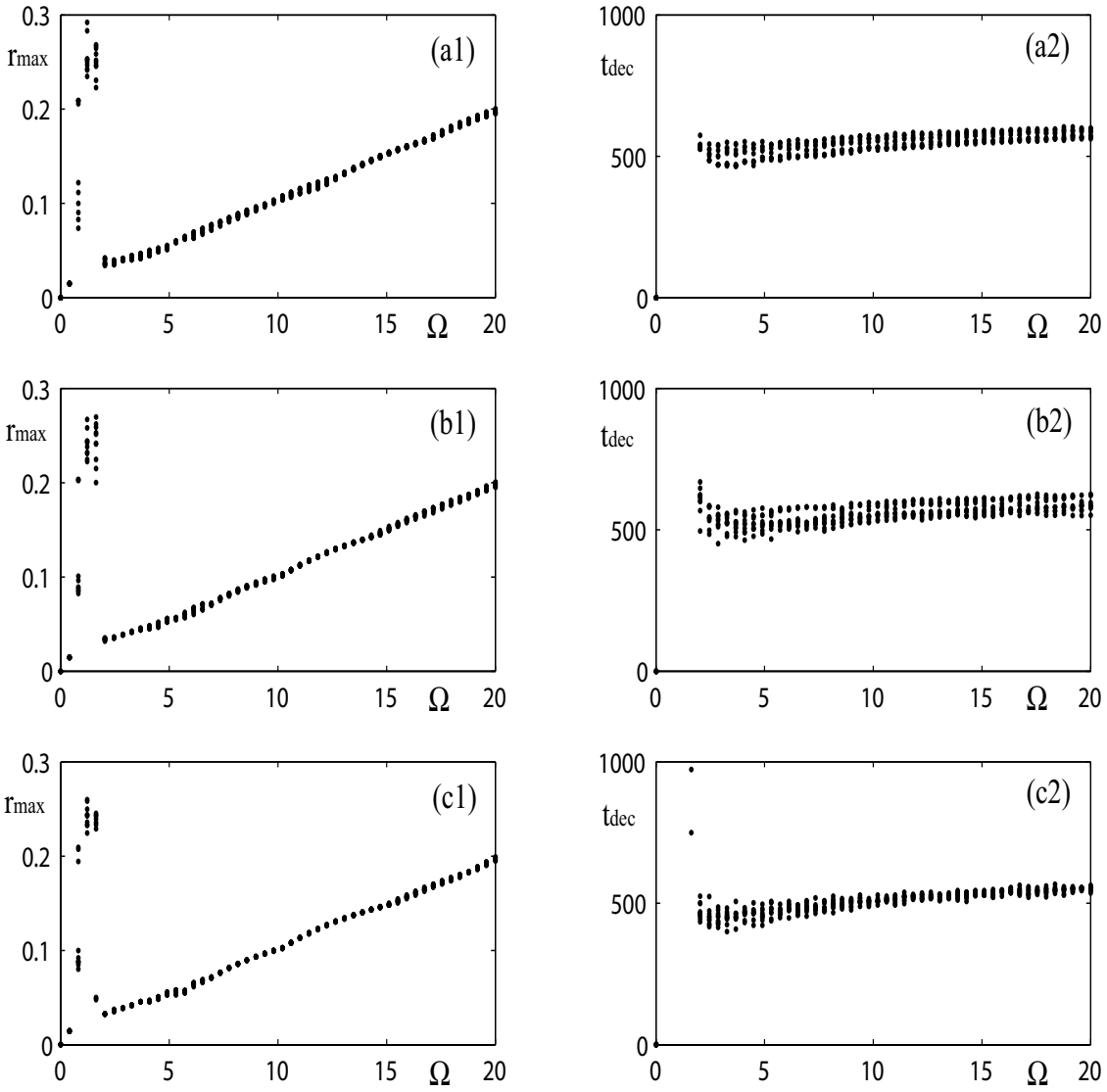


Figure 5.23: Simulations of the ADB system with two, three, and four balls, for the range $\Omega \in [0, 20]$. The other parameters are $\zeta = \beta = \delta = 0.01$, and $\mu = 6\mu_c$ (where $\mu_c := \delta/n$, and $n$ is the number of balls); that is, $\mu = 0.03$ for ADB with two balls (panels (a1)-(a2)), $\mu = 0.02$ for ADB with three balls (panels (b1)-(b2)), and $\mu = 0.015$ for ADB with four balls (panels (c1)-(c2)). The equations of motion was solved for ten random equidistant initial positions of the balls for each $\Omega$ value: $\phi_2(0) = \phi_1(0) + \pi$, with $\phi_1(0) \in [0, \pi]$ for two balls; $\phi_2(0) = \phi_1(0) + 2\pi/3$, and $\phi_3(0) = \phi_1(0) - 2\pi/3$, with $\phi_1(0) \in [0, 2\pi/3]$ for three balls; and $\phi_2(0) = \phi_1(0) + \pi/2$, $\phi_3(0) = \phi_1(0) + \pi$, and $\phi_4(0) = \phi_1(0) - \pi/2$, with $\phi_1(0) \in [0, \pi/2]$ for four balls. The rest of initial conditions are fixed at zero value. The maximum amplitude of the radial vibration during the transient $r_{max}$ is plotted against $\Omega$ in panels (a1), (b1), and (c1) for two, three, and four balls, respectively; the transient length $t_{dec}$ is plotted against $\Omega$ in panels (a2), (b2), and (c2) for two, three, and four balls, respectively.

balance the eccentricity of the rotor. For each $\delta$ value, we solve the equations of motions of the system for ten different random equidistant initial positions of the balls. We can observe in Fig.5.24 that the results dispersion is bigger when $\delta$ becomes larger. Unlike, for small $\delta$, $r_{max}$ and $t_{dec}$ are proximately the same for the different $\phi_1(0)$ values for which the equations were solved. We can also see in Fig.5.24 that the transient response is harder while $\delta$ increases. Really, since the eccentricity of the rotor is larger, the vibration due to the rotation would be greater, and hence, it would be more difficult to balance the system. Thus, panels (a1) for two balls, (b1) for three balls, and (c1) for four balls, show that $r_{max}$ grows linearly with $\delta$. In panels (a2), (b2), and (c2) we can see that $t_{dec}$ varies sharper for small $\delta$. For high $\delta$ values, the transient length variation is softer, but is more sensitivity to $\phi_1(0)$, that is, there is more difference for the different initial positions of the balls within the rotating frame. Thus, we can see that the points range for each $\delta$ is wider as $\delta$ increases. Comparing the obtained results for the different numbers of balls (panels (a1)-(a2) for two balls, (b1)-(b2) for three balls, and (c1)-(c2) for four balls), we note that the ADB system with four balls shows less sensitivity to $\phi_1(0)$ than the ADB with two balls, and than the ADB with three balls. For example, in panel (c1), the $r_{max}$ values for the different initial positions of the balls are proximately represented in the same points. In contrast, in (a1), we can observe different $r_{max}$ values for a same $\delta$. In Figure 5.25, we depict the same results than in Fig.5.24, but with a higher total ball mass: $\widetilde{m} = 0.12$. Now, the $\delta$ range is bigger, since the balls are able to reach the balance for a larger eccentricity $\delta$. The results shown in Fig.5.25 are very similar to the ones in Fig.5.24. Thus, the dispersion grows as $\delta$ increases, and the $r_{max}$ and $t_{dec}$ values in the range $\delta \in [0, 0.03]$, are the same than for $\widetilde{m} = 0.03$.

Therefore, we can conclude that, bigger balls do not affect badly the transient response of the system. Moreover, with a higher $\mu$ value, it would be possible to reach the balance for a larger $\delta$ range. Hence, in practical applications of the ADB it would be recommendable to use as bigger balls as possible. Finally, looking at Figs.5.25 (a2), (b2), and (c2), it is possible to confirm that when the total ball mass $\widetilde{m}$ is distributed between four balls, instead of between two balls, we obtain much less dispersion of the results. Hence, we reassert that the transient response of the system would be less sensitivity to the initial positions of the balls as the number of balls increases. Therefore, it would be better in practical applications to use the ADB mechanism with four balls, instead of the ADB mechanism with two balls, since we would obtain more similar results for different experiments, in which the initial positions of the balls are different. We must remember that this conclusion is valid only for equidistant initial positions of the balls, for which we have obtained the numerical results. Again, further investigation should be undertaken to get more general results.

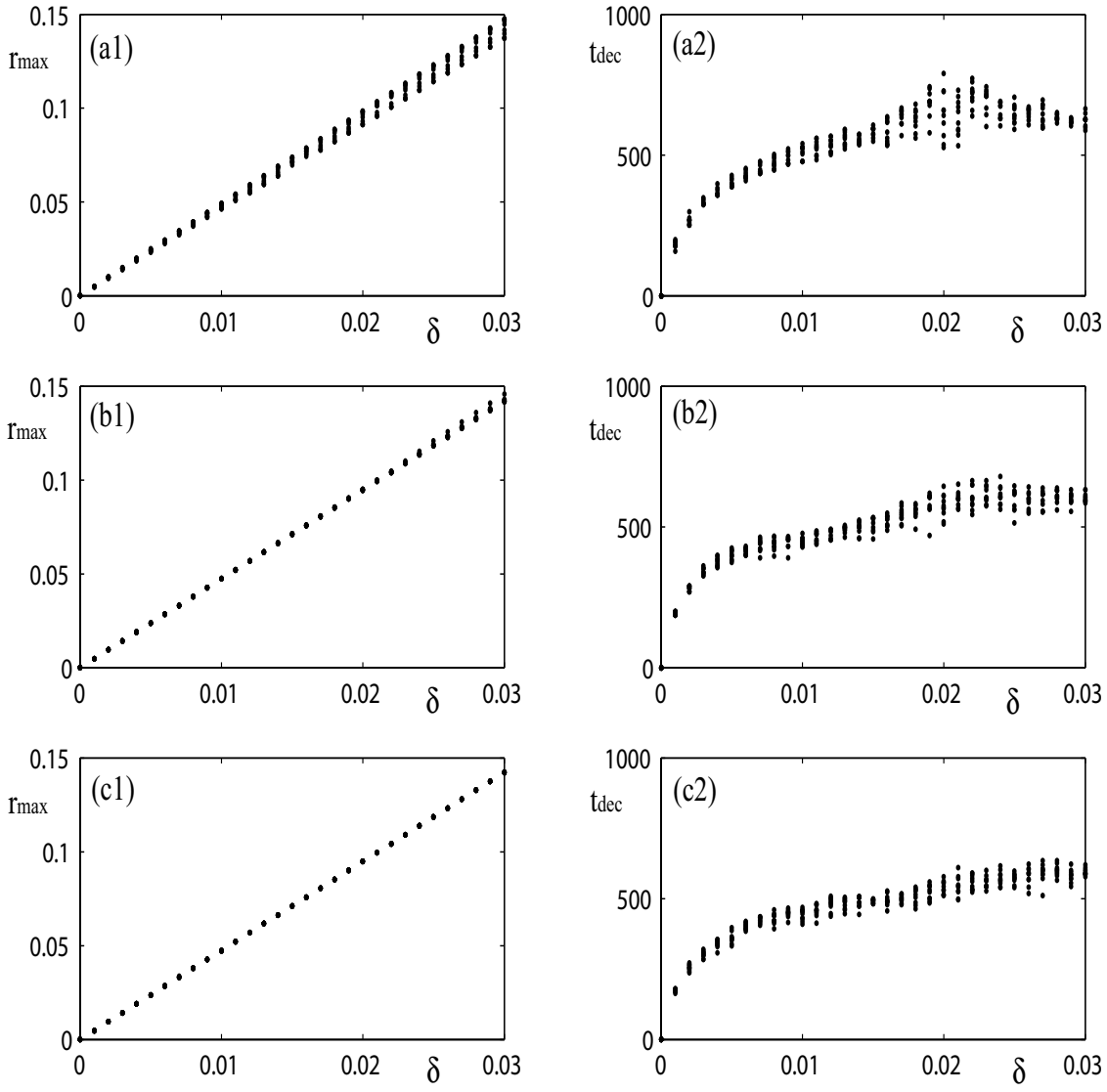


Figure 5.24: Simulations of the ADB system with two, three, and four balls, for the range $\delta \in [0, \widetilde{m}]$, with $\widetilde{m} = 0.03$. The other parameters are $\Omega = 4$, $\zeta = \beta = 0.01$, and $\mu = \widetilde{m}/n$; that is, $\mu = 0.015$ for ADB with two balls (panels (a1)-(a2)), $\mu = 0.01$ for ADB with three balls (panels (b1)-(b2)), and $\mu = 0.0075$ for ADB with four balls (panels (c1)-(c2)). The equations of motion was solved for ten random equidistant initial positions of the balls for each $\delta$ value: $\phi_2(0) = \phi_1(0)+\pi$, with $\phi_1(0) \in [0, \pi]$ for two balls; $\phi_2(0) = \phi_1(0) + 2\pi/3$, and $\phi_3(0) = \phi_1(0) - 2\pi/3$, with $\phi_1(0) \in [0, 2\pi/3]$ for three balls; and $\phi_2(0) = \phi_1(0) + \pi/2$, $\phi_3(0) = \phi_1(0) + \pi$, and $\phi_4(0) = \phi_1(0) - \pi/2$, with $\phi_1(0) \in [0, \pi/2]$ for four balls. The rest of initial conditions are fixed at zero value. The maximum amplitude of the radial vibration during the transient $r_{max}$ is plotted against $\delta$ in panels (a1), (b1), and (c1) for two, three, and four balls, respectively; the transient length $t_{dec}$ is plotted against $\delta$ in panels (a2), (b2), and (c2) for two, three, and four balls, respectively.

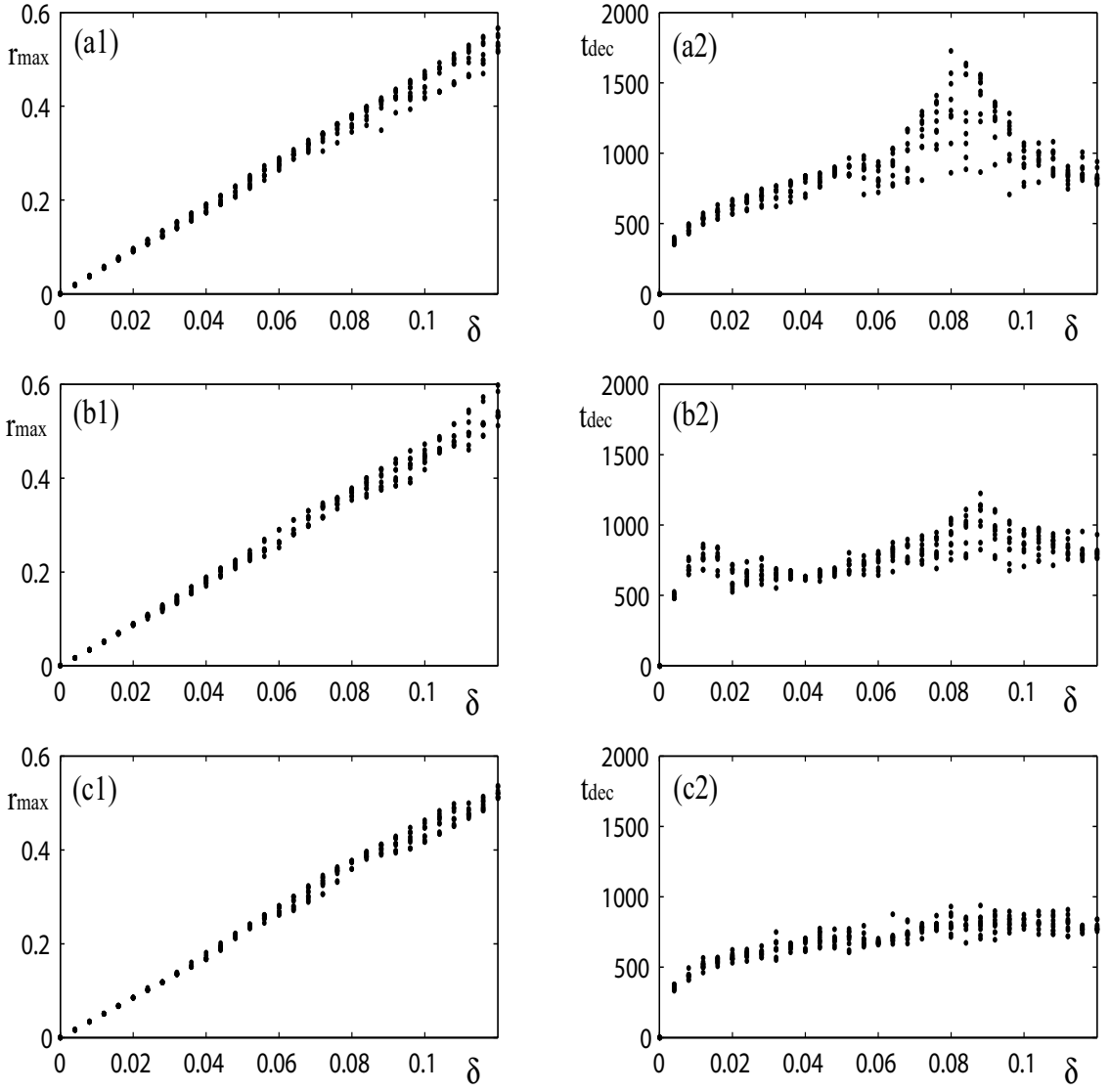


Figure 5.25: Simulations of the ADB system with two, three, and four balls, for the range $\delta \in [0, \widetilde{m}]$, with $\widetilde{m} = 0.12$. The other parameters are $\Omega = 4$, $\zeta = \beta = 0.01$, and $\mu = \widetilde{m}/n$; that is, $\mu = 0.06$ for ADB with two balls (panels (a1)-(a2)), $\mu = 0.04$ for ADB with three balls (panels (b1)-(b2)), and $\mu = 0.03$ for ADB with four balls (panels (c1)-(c2)). The equations of motion was solved for ten random equidistant initial positions of the balls for each $\delta$ value: $\phi_2(0) = \phi_1(0)+\pi$, with $\phi_1(0) \in [0, \pi]$ for two balls; $\phi_2(0) = \phi_1(0) + 2\pi/3$, and $\phi_3(0) = \phi_1(0) - 2\pi/3$, with $\phi_1(0) \in [0, 2\pi/3]$ for three balls; and $\phi_2(0) = \phi_1(0) + \pi/2$, $\phi_3(0) = \phi_1(0) + \pi$, and $\phi_4(0) = \phi_1(0) - \pi/2$, with $\phi_1(0) \in [0, \pi/2]$ for four balls. The rest of initial conditions are fixed at zero value. The maximum amplitude of the radial vibration during the transient $r_{max}$ is plotted against $\delta$ in panels (a1), (b1), and (c1) for two, three, and four balls, respectively; the transient length $t_{dec}$ is plotted against $\delta$ in panels (a2), (b2), and (c2) for two, three, and four balls, respectively.

# Chapter 6

# Conclusions

The analysis of the automatic dynamic balancer for eccentric rotors, which we have performed in this project, is useful to better understand the behaviour of these mechanisms. For example, the obtained results show how the ADB mechanism changes its response under variation of the parameter set and initial conditions. We also provide necessary conditions to reach balance of the system with two, three, and four balls, and reveal differences and similarities between the three studied cases.

The numerical bifurcation analysis carried out in Chapter 4 showed that the balance of the system is possible when the balancing balls are large enough to offset the imbalance. Specifically, if the ratio between the ball mass and the mass of the rotor system is larger than the dimensionless eccentricity divided by the number of balls ($\mu > \delta/n$), then dynamic balance can in principle be achieved. This means that, for similar correction masses, an ADB with more balls can counteract a larger eccentricity $\delta$. The balanced equilibrium was shown to be stable for sufficiently high values of the rotation speed $\Omega$. We saw that the region of stable balance is delimited by a Hopf bifurcation for large $\Omega$. When the balance condition is not satisfied, that is $\mu < \delta/n$, another equilibrium in which all the balls are coincident was found to be stable for almost all $\Omega$ values. Simulations showed that for large $\Omega$, this coincident state presents improvements in the response of the system comparing with the rotor without the ADB.

The main difference revealed between the ADB with two, three, and four balls in the bifurcation analysis was that, with more balls the balance loses its stability for a large damping ratio of the rotor $\zeta$; see panel (b) of Figs.4.8 and 4.13. This effect is more noticeable in the ADB with three balls than for four balls. It was found that this stability can be recovered if the viscous damping of the balls $\beta$ takes a high value; see Figs.4.9 and 4.14. Simulation results ratified these facts, and showed that when $\zeta$ is increased, the balance is attained for a smaller number of initial position of the balls; see Figs.5.18 and 5.19. However, in Figs.5.21 and 5.22 we saw that the transient response becomes better (that is, both the maximum amplitude of the radial vibration and the transient length decrease) with higher values of the damping parameters $\zeta$ and $\beta$.

Simulation results were used to study the effects of the initial conditions on the performance of the ADB mechanism. In general, it was shown that the response of the system is relatively insensitive to the initial position and velocity of the axis of the rotor. In contrast,

the initial position of the balls and their initial velocity have a strong influence on their behaviour. Thus, the way in which the balls are launched determines the dynamic attraction to the balanced state, and the transient response of the system. For example, it was shown in Fig.5.10 that even for a parameter set for which the bifurcation analysis predicts stability of the balanced state, when balls are released with an initial velocity within the rotating frame equal to $-\Omega$, the balance is not reached, and the long term motion system is a limit cycle. Therefore, there is coexistence between the balanced state and another dynamic behaviour, and the dynamic attraction is determined by the initial conditions of the balls. After several numerical runs, an optimal initial position of the balls was found, consisting of releasing them equidistantly and initially stationary within the rotating frame. For this configuration, the balance is reached almost always, and the transient is found to be optimal (small radial amplitude and short transient length) and to have little sensitivity to the absolute position of the balls within the rotor. Moreover, the numerical results for all three cases were found to be qualitatively similar when the balls are launched with this equidistant configuration.

A comparison between the ADB mechanisms with a differing number of balls, but with the same total ball mass $n\mu$, showed that the system with four balls is the most insensitive to the initial position of the balls within the rotating frame, when they are released equidistantly. Moreover, the maximum radial vibration is in general a bit smaller for the ADB with four balls, and the transient length a little shorter. These effects were found to be more pronounced for larger values of $\Omega$ and $\delta$. The results obtained for different ball masses were similar, but the balance is reached for a larger eccentricity when the value $n\mu$ is higher. Hence there is no disadvantage in taking big correction masses other than the extra inertial mass to be overcome by the motor.

The conclusions obtained in this project are useful to give some recommendations for practical applications of the ADB:

- It is advisable to keep the balls equidistantly spaced within the plane of the rotor until it reaches stationary rotation speed, and after that to release them. In that way, since it is not possible to know the location of the eccentricity, we can obtain optimal response because of the insensitivity to the absolute initial position of the balls for this equidistant configuration.

- Since a large ball mass has no disadvantage on the transient response of the system, it is recommendable to use as big balls as possible. In that way we can make sure of being able to offset the imbalance produced by great eccentricity of the rotor.

- In case of using ADB with three or four balls, which have been shown to have a marginally better transient response, we must be sure that the rotor damping is sufficiently small for the balance equilibrium to be stable.

- Since a large viscous ball damping provides a smooth transient response, and makes the balance more attractive, it is recommended to take a high $\beta$ value.

- Generally the higher the number of balls, the better.

Finally, we must comment on future work that with `MATCONT` it is possible to obtain bifurcation diagrams with high precision, but it has the inconvenience of working slowly in

comparison with AUTO. Thus, we have not undertaken continuation of limit cycles from the Hopf bifurcation curves, due to time constraints. Hence, a future work could be to obtain limit cycles with AUTO for the ADB with three and four balls. Since in this project we are supposing that the balls travel around different races, further work would be to make a model assuming impacts between balls, and to find how this interaction between the balls affects on the behaviour of the ADB mechanisms. We can also encourage a deeper study for a larger number of balls than four, to prove if the advantages found for the ADB with three and four balls are accentuated with a larger number of balls. More work would be required, using the methods presented in this project, in order to reach an optimal design for a particular physical application. This would clearly need to be tested against experiment.

# Appendix A

# Equations in MATLAB

`Matlab` has been used to compute numerical bifurcation diagrams and to integer the equations of motion of the ADB system in order to obtain the evolution of the coordinates with the time. To write the equations of motion (2.25)-(2.26) in `Matlab`, it is necessary to transform them into a first order differential equations system. For that, we define the following new variables,

$$\begin{aligned} u &= \dot{x}, \\ v &= \dot{y}, \\ \theta_i &= \dot{\phi}_i, \end{aligned} \tag{A.1}$$

so we can define the vector of coordinates of the system as

$$q = \begin{pmatrix} x \\ u \\ y \\ v \\ \phi_1 \\ \theta_1 \\ \phi_2 \\ \theta_2 \\ ... \\ \phi_n \\ \theta_n \end{pmatrix}. \tag{A.2}$$

After substituting (A.1) in equations (2.25) and (2.26), we obtain the following $2+n$ equations,

$$(1+n\mu)\dot{u} + 2\zeta u - 2\Omega(1+n\mu)v + kx - 2\Omega\zeta y = \delta\Omega^2 + \tag{A.3}$$
$$\mu\sum_{i=1}^{n}(\Omega+\theta_i)^2\cos\phi_i + \mu\sum_{i=1}^{n}\dot{\theta}_i\sin\phi_i,$$

$$(1+n\mu)\dot{v} + 2\Omega(1+n\mu)u + 2\zeta v + 2\Omega\zeta x + ky = -\mu\sum_{i=1}^{n}\dot{\theta}_i\cos\phi_i + \tag{A.4}$$
$$\mu\sum_{i=1}^{n}(\Omega+\theta_i)^2\sin\phi_i,$$

$$\dot{\theta}_i + \beta\theta_i = (\dot{u} - \Omega^2 x - 2\Omega v)\sin\phi_i - (\dot{v} - \Omega^2 y + 2\Omega u)\cos\phi_i, \tag{A.5}$$

where $i = 1 \ldots n$.

Removing (A.5), it is possible to write $\dot{\theta}_i$ as an expression in terms of the coordinates vector $q$, and $\dot{u}$ and $\dot{v}$. Thus, we have,

$$\dot{\theta}_i = -\beta\theta_i + (\dot{u} - \Omega^2 x - 2\Omega v)\sin\phi_i - (\dot{v} - \Omega^2 y + 2\Omega u)\cos\phi_i = G_{2+i}(q). \tag{A.6}$$

After substituting the expression (A.6) into (A.3) and (A.4), we can write expressions for $\dot{u}$ and $\dot{v}$ in terms of the coordinates vector $q$. Therefore, we obtain,

$$\dot{u} = \frac{b(q)g(q) - c(q)f(q)}{b(q)^2 - a(q)c(q)} = G_1(q), \tag{A.7}$$

$$\dot{v} = \frac{b(q)f(q) - a(q)g(q)}{b(q)^2 - a(q)c(q)} = G_2(q), \tag{A.8}$$

where $a, b, c, f$ and $g$ are the following expressions in terms of $q$,

$$a = (1 + n\mu) - \mu\sum_{i=1}^{n}(\sin\phi_i)^2, \tag{A.9}$$

$$b = \mu\sum_{i=1}^{n}\sin\phi_i\cos\phi_i, \tag{A.10}$$

$$c = (1 + n\mu) - \mu\sum_{i=1}^{n}(\cos\phi_i)^2, \tag{A.11}$$

$$\begin{aligned} f = {} & -2\zeta u + 2\Omega(1 + n\mu)v - kx + 2\Omega\zeta y + \delta\Omega^2 + \\ & \mu\sum_{i=1}^{n}(\Omega + \theta_i)^2\cos\phi_i - \mu\beta\sum_{i=1}^{n}\theta_i\sin\phi_i + \\ & \mu(-\Omega^2 x - 2\Omega v)\sum_{i=1}^{n}(\sin\phi_i)^2 - \mu(-\Omega^2 y + 2\Omega u)\sum_{i=1}^{n}(\sin\phi_i\cos\phi_i), \end{aligned} \tag{A.12}$$

$$\begin{aligned} g = {} & -2\Omega(1 + n\mu)u - 2\zeta v - 2\Omega\zeta x - ky + \\ & \mu\beta\sum_{i=1}^{n}\theta_i\cos\phi_i - \mu(-\Omega^2 x - 2\Omega v)\sum_{i=1}^{n}\sin\phi_i\cos\phi_i + \\ & \mu(-\Omega^2 y + 2\Omega u)\sum_{i=1}^{n}(\cos\phi_i)^2 + \mu\sum_{i=1}^{n}(\Omega + \theta_i)^2\sin\phi_i. \end{aligned} \tag{A.13}$$

In summary, we have been able to write the equation of motion as a first order differential equations system,

$$\dot{q} = F(q) = \begin{pmatrix} \dot{x} \\ \dot{u} \\ \dot{y} \\ \dot{v} \\ \dot{\phi}_i \\ \dot{\theta}_i \end{pmatrix} = \begin{pmatrix} u \\ G_1(q) \\ v \\ G_2(q) \\ \theta_i \\ G_{2+i}(q) \end{pmatrix}, \tag{A.14}$$

which is the way in what the equations of motion have been written in `Matlab`.

# Bibliography


[1] J. Adolfsson. *Passive Control of Mechanical Systems: Bipedal Walking and Autobalancing*. PhD thesis, Royal Institute of Technology, Stockholm, 2001.

[2] J. D. Alexander. An Automatic Dynamic Balancer. *Proceeding, 2nd Southeastern Conference*, 415-426, 1964

[3] P. Bövik and C. Högfors. Autobalancing of rotors. *Journal of Sound and Vibration*, 111(3):429-440, 1986.

[4] J. W. Cade. Self-Compensating Balancing in Rotating Mechanisms. *Design News*, 234-239, 1965.

[5] P. C. P. Chao, Y.-D Huang, and C.-K. Sung. Non-planar dynamic modeling for the optical disk drive spindles equipped with an automatic balancer.*Mechanism and Machine Theory*, 38:1289-1305, 2003.

[6] J. Chung and I. Jang. Dynamic response and stability analysis of an automatic ball balancer for a flexible rotor. *Journal of Sound and Vibration*, 259(1):31-43, 2003.

[7] J. Chung and D.S.Ro. Dynamic analysis of an automatic dynamic balancer for rotating mechanisms. *Journal of Sound and Vibration*, 228(5):1035-1056, 1999.

[8] A. Dhooge, W. Govaerts, Yu.A. Kuznetsov, W. Mestrom, and A.M. Riet. MATCONT: A continuation toolbox in Matlab, 2004. http://allserv.UGent.be/ ãdhooge/.

[9] K. Green, A. R. Champneys, and N. J. Lieven. Bifurcation analysis of an automatic dynamic balancing mechanism for eccentric rotors. Preprint: Bristol Laboratory for Advanced Dynamic Engineering, University of Bristol, Bristol, 2004.

[10] K. Green, A. R. Champneys, and M. I. Friswell. Analysis of transient response of an automatic dynamic balancer for eccentric rotors. Preprint: Bristol Laboratory for Advanced Dynamic Engineering, University of Bristol, Bristol, 2004.

[11] J. P. Den Hartog. *Mechanical Vibrations*, Dover, New York, 225-281, 1956.

[12] Health and Safety Executive. *Hand-arm Vibration*, volume HS(G)88. HSE Books, Sudbury, 1994. ISBN 0-7176-0743-7.

[13] W.-Y. Huang, C.-P. Chao, J.-R. Kang, and C.-K. Sung. The application of balltype balancers for radial vibration reduction of high-speed optic drives. *Journal of Sound and Vibration*, 250(3):415-430, 2002.

[14] C.-H. Hwang and J. Chung. Dynamic analysis of an automatic ball balancer with double races. *JSME International Journal: Series C*, 42(2):265-272, 1999.

[15] H. H. Jeffcott. The lateral vibration of loaded shafts in the neighbourhood of a whirling speed - The effect of want of balance. *Philos. Mag. Ser. 6*, 37:304-314, 1919.

[16] W. Kim and J. Chung. Performance of automatic ball balancers on optical disc drives. *Proc Instn Mech Engrs Part C: J Mechanical Engineering Science*, 216(1071-1080), 2002.

[17] Y. A. Kuznetsov. *Elements of Applied Bifurcation Theory*. Springer, Berlin, 1995.

[18] J. Lee and W. K. Van Moorhem. Analytical and experimental analysis of a self-compensating dynamic balancer in a rotating mechanism. *Transactions of ASME*, 118:468-475, 1996.

[19] T. Majewski. Synchronous vibration eliminator for an object having one degree of freedom. *Journal of Sound and Vibration*, 112(3):401-413, 1987.

[20] R. Rajalingham and S. Rakheja. Whirl suppression in hand-held power tool rotors using guided rolling balancers. *Journal of Sound and Vibration*, 217(3):453-466, 1998.

[21] R. S. Sharp. An analysis of a self-balancing system for rigid rotors. *J. Mech. Engng. Sci.*, 17(4):186-189, 1975.

[22] S. H. Strogatz. *Nonlinear Dynamics and Chaos, with Applications in Physics, Biology, Chemistry, and Engineering Studies in Nonlinearity*. Addison-Wesley, 1994.

[23] SKF Autobalance Systems. Dynaspin. http://dynaspin.skf.com.

[24] E. L. Thearle. A New Type of Dynamic-Balancing Machine. *Transactions of ASME*, 54(APM-54-12):131-141, 1932.

[25] N. van de Wouw, M. N. van den Heuvel, J. A. van Rooij, and H. Nijmeijer. Performance of an automatic ball balancer with dry friction. Preprint: Eindhoven University of Technology, The Netherlands.